Benefits and pitfalls in the longitudinal assessment of the somatosensory cortex post-stroke using EEG

Kalogianni, Konstantina

DOI
10.4233/uuid:2dceae5b-145f-41fd-9b08-200d1e4781af

Publication date
2018

Document Version
Final published version

Citation (APA)
Kalogianni, K. (2018). *Benefits and pitfalls in the longitudinal assessment of the somatosensory cortex post-stroke using EEG*. [Dissertation (TU Delft), Delft University of Technology]. https://doi.org/10.4233/uuid:2dceae5b-145f-41fd-9b08-200d1e4781af

Important note
To cite this publication, please use the final published version (if applicable).
Please check the document version above.

Benefits and pitfalls in the longitudinal assessment of the somatosensory cortex post-stroke using EEG

Konstantina KALOGIANNI

Design: Konstantina Kalogianni, Gildeprint
Cover Design: Sofia Vini, Gildeprint
Printing: Gildeprint

ISBN: 978-94-6233-950-7

The 4D-EEG Project:
This research was funded by the European Research Council under the European Union's Seventh Framework Programme (FP/2007-2013) ERC Grant Agreement n. 291339, project 4D-EEG: A new tool to investigate the spatial and temporal activity patterns in the brain.

European Research Council
Established by the European Commission

Benefits and pitfalls in the longitudinal assessment of the somatosensory cortex post-stroke using EEG

Dissertation

for the purpose of obtaining the degree of doctor
at Delft University of Technology
by the authority of the Rector Magnificus Prof.dr.ir. T.H.J.J. van der Hagen*;*
Chair of the Board for Doctorates
to be defended publicly on

Wednesday 9th May 2018 at
12:30 o'clock

by
Konstantina KALOGIANNI

Master of Science in Medical Informatics, Aristotle University
born in Thessaloniki, Greece

This dissertation has been approved by the promotors.

Composition of the doctoral committee:

Rector Magnificus	chairperson
Prof.dr. F.C.T. van Der Helm	Delft University of Technology, promotor
Prof.dr. A. Daffertshofer	Vrije Universiteit Amsterdam, promotor
Dr. J.C. de Munck	VU Univ. Medical Center, Amsterdam, copromotor
Dr.ir. A.C. Schouten	Delft University of Technology, copromotor

Independent members

Prof.dr.ir. M.J.A.M van Putten	University of Twente
Dr. P.P.W Ossenblok	Technische Universiteit Eindhoven
Dr. F. Tecchio	National Research Council of Italy
Prof.dr.ir. W.A. Serdijn	Delft University of Technology
Prof.dr.ir. J. Harlaar	Delft University of Technology
Prof.dr.ir. H.E.J. Veeger	Delft University of Technology (reserve member)

Table of Contents

Chapter 1

Introduction

ΕΑΝ ΜΗ ΕΛΠΗΤΑΙ ΑΝΕΛΠΙΣΤΟΝ ΟΥΚ ΕΞΕΥΡΗΣΕΙ
Εάν δεν ελπίζεις στο ανέλπιστο δεν θα το βρεις
Ηράκλειτος

"If you do not hope for the unexpected you will not find it"
Heraclitus

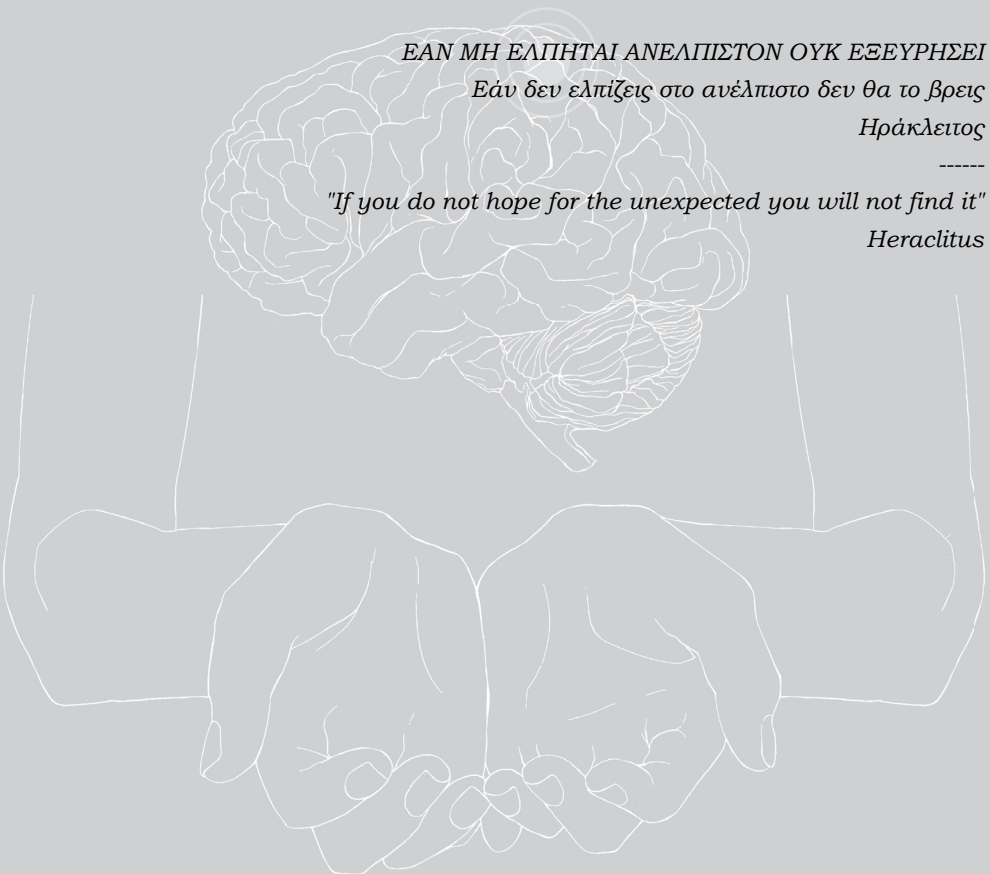

1.1 Impact of stroke

Stroke is a leading cause of long-term impairment (WHO World Health Organization. Geneva Switzerland, 2003). It is caused by a reduction of the blood flow to a part or parts of the brain, that leads to neuro-structural damage. As a consequence, one can observe a functional deficit. According to the American stroke association, there are two types of stroke: (i) ischemic stroke caused by an obstruction within a supplying blood vessel; (ii) hemorrhagic stroke that occurs after a rupture of a blood vessel, in the case of a transient ischemic accident (TIA), the first one may be temporary. This is also referred to as “mini-stroke” and is caused by a temporary clot. “Worldwide in 2010, an estimated 11 569 538 events of incident ischaemic stroke took place (63% in low-income and middle-income countries), and 5 324 997 events of incident haemorrhagic stroke (80% in low-income and middle-income countries); furthermore, 2,835,419 individuals died from ischaemic stroke (57% in low-income and middle-income countries) and 3,038,763 from haemorrhagic stroke (84% in low-income and middle-income countries” (page e260, Krishnamurthi et al., 2013).

In the present thesis, I addressed consequences of ischemic stroke, in particular motor and sensory impairments in the upper extremities, which have a prevalence of approximately 87% in all stroke survivors, immediately after stroke onset (Parker et al., 1986). Kwakkel and co-workers, (2006) reported that 16-42% of the spontaneous motor recovery occurs at six to ten weeks after stroke onset. The maximum possible recovery based on functional assessment might even be higher as formulated in the so-called proportional recovery rule formulated by Prabhakaran et al. (2008); see also below. Given this early time window, it appears that clinical decision about therapy requires likewise timely patient stratification for their potential neurobiological recovery. The earlier stroke severity can be assessed, e.g., by measuring motor impairment, the sooner patient characteristics may be stratified (Winters et al., 2016a). For instance, shoulder abduction and finger extension (the SAFE model) measured in the acute phase, i.e. within the first 72 hours after stroke, are strongly associated with recovery of upper limb function six months post-stroke, i.e. in the chronic phase (Nijland et al., 2010b).

Physical therapists and neurologists can assess functional impairment and, thus, stroke severity and indicate possible recovery based on various clinical tests. One example is the Fugl-Meyer test (Fugl-Meyer et al., 1975), which is considered one of the most reliable and valid clinical measures of motor recovery post stroke (Duncan et al., 1983; Gladstone et al., 2002). The probability of upper limb recovery has a largely linear relationship with the Fugl-Meyer scores, when recorded from the acute to the chronic phase post stroke. As mentioned above, recovery after stoke is proportional: on average patients will recover about 70% of their functional deficit (Prabhakaran et al., 2008). Unfortunately, this proportional rule comes with exceptions and not all patients can be properly stratified, especially those with a low Fugl-Meyer scores in the acute phase (Winters et al., 2015). Prognosis remains difficult, and models need to be improved when searching for better stratification and patient-specific strategies for stroke rehabilitation.

One way of doing might be supplementing these prediction models with information about the neurophysiological mechanisms involved in stroke recovery. Neuroimaging modalities can indeed provide important information (Boyd et al., 2017). Blood-oxygen-level-dependent functional magnetic resonance imaging (BOLD-fMRI) can help to understand longitudinal metabolic changes after stroke onset on group (Ward et al., 2003) and on patient-specific level (Ward et al., 2006). The interpretation of BOLD, however, relies on an intact neurovascular coupling, which cannot be guaranteed in a large portion of patients (Ward, 2017). Diffusion tensor imaging (DTI) can reveal the integrity of large white matter tracts after stroke onset (Schulz et al., 2015), which is interesting but thus far less informative about functional connections (Ward, 2017). As an alternative to these MRI-based imaging techniques, electroencephalography (EEG) might be a suitable modality to study ischemic stroke as it is a very sensitive to altered cortical functioning resulting from ischemia (van Putten and Hofmeijer, 2016).

1.2 What is recorded with EEG?

In 1929, Berger was the first to record human EEG signals. After almost a century of his discovery, EEG has become an ambulant and easy-to-use neuroimaging method that provides a very high temporal resolution (milliseconds scale). EEG is an excellent tool for research and the clinic – it is instrumental in the diagnoses of neurological diseases, in particular epilepsy (Niedermeyer and da Silva, 2004).

EEG measures potential differences as a function of time between electrodes placed on the scalp. It maps cortical activity in a non-invasive manner (Michel and Murray, 2012). Due to space limitations, EEG employs a fairly limited number of electrodes, ranging from 32 to 256. The small voltage differences measured at the scalp are a result of excitatory and inhibitory postsynaptic potentials (Kirschstein and Kohling, 2009) at the apical dendritic tree of the pyramidal cells located in the cerebral cortex. During the formation of an action potential, the potential difference between extracellular space and cell soma and the basal dendrite yields a current from the non-excited membrane of the soma and the basal dendrites to the apical dendritic tree. That current causes an electric field and a potential field inside the human head. It flows through the volume conductor, i.e. the cerebrospinal fluid, the skull and the scalp (also referred to a ‘leadfield’; see below), and reaches the EEG electrodes. Pyramidal cells of the gray matter are thought to be the generators of the EEG because the axes of their dendritic tree are spatially aligned and perpendicular to the surface of the cortex (Hallez et al., 2007). When numerous cortical pyramidal neurons are synchronously active, the electrical activity is sufficiently large to be measurable by the EEG; an EEG signal recorded from a healthy individual is about 10 to 100 μV in amplitude. Roughly, the electrical activity measured by EEG can be modelled by an equivalent current dipole (ECD, de Munck et al., 1988).

1.3 EEG as an imaging modality

EEG is not often referred to as an imaging modality (Michel and Murray, 2012), in contrast to, e.g., fMRI. A primary reason for this lack of notion might be the very limited spatial resolution of EEG. EEG measures the activity on the scalp surface,

whereas in imaging one is interested in the activity inside the brain, i.e. in the location at which pyramidal cortical neurons fire synchronously.

Using EEG source reconstruction techniques, one can estimate the activity inside the cortex. In brief, a so-called 'forward model' predicts how the current flows from the dipolar sources in the brain to the surface electrodes on the scalp. Such a model relies on conventional electro-statics by means of the Poisson's equation which allows for determining potentials on the scalp for any given dipole configuration. One can use these forward models to approximate what is called 'the inverse problem'. That is, one can infer the strength and location of active dipoles or, in brief, sources in the brain that match the recorded activity. This process will from here-on referred to as source localization. Due to the large number of possible dipoles within the brain volume and the small number of electrodes on the scalp surface, the inverse problem is ill-posed (von Helmholtz, 1853). As a consequence, the inverse problem does not have a unique solution. To generate uniqueness, additional assumptions must be made. Over the last decades, numerous approaches have been proposed to solve this. Depending on the type of assumptions incorporated, three main groups of inverse methods can be distinguished: dipole fitting methods, scanning methods, and imaging methods (Darvas et al., 2004). Dipole fitting methods assume a limited number of active sources and the inverse problem is often addressed by means of least squares fitting. Scanning methods use a fine grid to search by brute force for optimal dipole positions throughout the source space. EEG imaging methods usually tackle the inverse problem in a constrained representation of the cortex and compute a unique solution by introducing some regularization methods or priors of the solution (Baillet et al., 2001).

1.4 Event-related potentials, EEG data model, and signal-to-noise-ratio

Estimating the brain activity of interest from raw and continuous EEG data is not trivial because EEG represents a mixture of a plenitude of neural sources (Hämäläinen et al., 1993). Moreover, EEG is contaminated with physiological noise including eye-blink artifacts, muscle artifacts and pulsation artifacts caused by

electrodes placed on top of an artery. Fortunately, there are several ways to extract responses associated with specific neural processing, especially in the vicinity of isolated events. In 1954, Dawson proposed averaging time-locked segments of EEG data to a specific event or stimulus (Dawson, 1954). Ever since so-called event-related potentials (ERPs) are a common approach to study sensory, motor, and cognitive processing as a response to transient stimuli.

Experimentally, ERPs are typically obtained using a repetitive presentation of stimuli. Think of visual-evoked potentials that can be observed over occipital areas when stimulating the visual field. To obtain an ERP, data are typically filtered before segmenting them around the consecutive events. This yields time-locked epochs from which those with too strong artifacts are removed. Over the remaining epochs the data are averaged. ERPs are meaningful under the proviso that whenever a specific stimulus is presented, the brain responds in the same manner and that the omnipresent noise averages to zero.

An ERP consists of positive or negative voltage deflections or peaks. Studying ERPs hence involves measuring the latencies and amplitudes of these peaks. The peaks are categorized in ERP-components where the letters P and N are used to indicate positive or negative deflections, respectively. The number in the ERP-component refers to the latency in (integer) milliseconds and is used to signify in which time instant after the presentation of the stimulus the peak appeared (Luck, 2005). A well-known ERP component is the P300 component elicited when the subject is presented with an unexpected visual or auditory stimulus.

This approach assumes that event-related potentials contain all the ‘relevant’ information to describe the response to a stimulus and that the residual activity is ‘irrelevant’ background noise, which cancels out in the course of the averaging procedure. Transferring this to the generating neural sources, the background noise should be caused by randomly distributed sources that are not related with the sources generating the ERP, i.e. the source of interest (De Munck et al. 1992). Background noise is not white and Gaussian but typically correlated in time and space with a skewed distribution. It also might differ in every repetition of the stimulus (de Munck et al., 2002). Modeling the relationship among the sensor recordings, the underlying sources, and specifying the background noise can

facilitate the afore-discussed inverse modeling. As an extend it may reveal the 'true' sources of the recorded activity. Let $b_{n,k}(t)$ be the EEG signal at recording channel $n = 1, \dots, N$ during the k^{th} repetition of the stimulus. This might be modeled by

$$b_{n,k}(t) = \sum_{m} L_{nm} j_m(t) + \varepsilon_{n,k}(t) \tag{1.1}$$

where L_{nm} is the so-called leadfield matrix, which is a bio-physically motivated (see above) linear matrix mapping source activities j_m, with $m = 1, \dots, M$ to channel $b_{n,k}(t)$; note that $M \gg N$. $\varepsilon_{n,k}(t)$ denotes background noise picked up at that channel during recording k. Under the ERP assumption, repetitive activation will improve the signal-to-noise ratio (SNR) of the averaged EEG recording $\overline{b_{n,k}}(t)$ as the strength of $j_m(t)$ stays constant while $\overline{\varepsilon_{n,k}}(t)$ tends to zero – here the over-line indicates the average over repetitions k. In turn, the higher the SNR the better the estimation of the underlying sources $j_m(t)$.

1.5 Somatosensory evoked potentials

Somatosensory-evoked potentials (SEPs) are a common way to study the somatosensory cortex, especially in patients with somatosensory or motor-related deficits. Stimulating the limbs via mechanical or electrical perturbations elicits SEPs in the hemisphere contralateral to the stimulation. In my thesis, I employed electrical stimulation of the fingers and of the median nerve. The resulting time-locked responses can be represented by the global field power, i.e. the root mean squared across all electrodes, which is a global measure of the electrical field at the scalp (Lehmann and Skrandies, 1980). Median nerve SEPs are dominated mainly by four ERP-components, the P20 or N20, P50, P100, N120 and a later peak after 100 ms P140; cf. Fig. 1.1. Note that the peak around 20 ms is referred in the literature as N20 or N20/P25 or as P/N20 but here we will use the term P20. The first two peaks are believed to originate from the contralateral S1 cortex and the later peaks to correspond to activity in S2 (Hari and Forss, 1999). When fingers are stimulated, the peaks arrive some milliseconds later at the cortex.

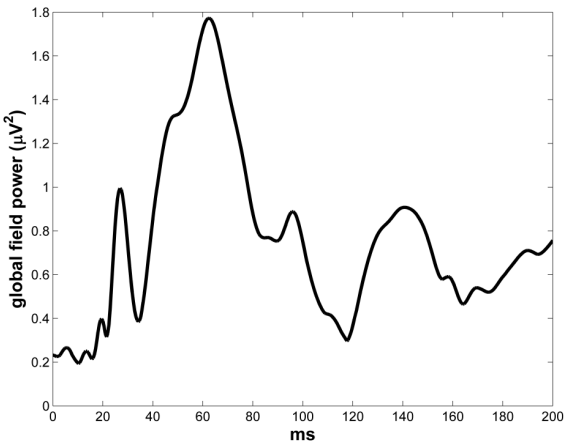

Fig. 1.1 Global field power of the SEP response after electrical stimulation of the median nerve.

1.6 Evoked responses recorded with EEG and their relevance for stroke rehabilitation monitoring

Currently, stroke recovery assessment is realized in the clinic by use of different clinical tests. As mentioned in Section 1.1, the prognostic value of these clinical tests come with limitations. EEG is starting to gain popularity as a monitoring tool for stroke recovery (Finnigan and van Putten, 2013; Sheorajpanday et al., 2011, 2009; de Vos et al., 2008). Since EEG measures extracellular currents resulting from the postsynaptic potentials of the cortical pyramidal cells, it is very sensitive to detect cerebral ischemia that manifests itself as abnormalities in the EEG signal (Jordan, 2004). Early after ischemic stroke onset, finger extension and shoulder abduction are considered indicative for proper recovery (Nijland et al., 2010b). The involvement of the somatosensory area in these motor behaviors is commonly agreed on (Bolognini et al., 2016). Hence, looking for EEG abnormalities in contralesional SEPs is expected to add information to the mere observation of motor capacities for the prospect of recovery.

There are a few studies using SEPs and a wealth of studies using somatosensory evoked fields (SEFs) that are recorded with the magnetic counterpart of EEG, the magneto-encephalogram (MEG). All these studies argue that components at the

window from 20 to 200 ms post stimulus, and the characteristics of their underlying sources may indicate neural reorganization after stroke in the somatosensory area. Changes of SEP or SEF responses at a few weeks post-stroke compared to the acute stage are in fact correlated with recovery (Laaksonen et al., 2013). Small SEF amplitudes or absence of early SEF responses (20-30 ms) correlate with a more severe impairment (Feys et al., 2000; Huang et al., 2004; Keren et al., 1993; Oliviero et al., 2004; Tecchio et al., 2007a; Tecchio et al., 2006; Tzvetanov and Rousseff, 2003; Wikström et al., 2000, 1999). Interhemispheric latency differences of the early peaks correlate with a high level of impairment (Oliviero et al., 2004; Tecchio et al., 2001). Hyper-excitability of the unaffected hemisphere can reflect changes in the affected hand (Oliviero et al., 2004) associated with physiological mechanisms during recovery. The literature disagrees on the causes of dipole displacements early post-stroke. Are they due to reorganization, i.e. neuroplasticity, (Druschky et al., 2002; Huang et al., 2004) or due to tissue swelling (Oliviero et al., 2004; Tecchio et al., 2006; Wikström et al., 2000, 1999)? Recovery based on neural reorganization appears evident primarily in the chronic phase as spatial shifts of generator sources (Altamura et al., 2007; Huang et al., 2004; Rossini et al., 2001, 1998a, 1998b, Tecchio et al., 2007a, 2006) and increased hand representations (Oliviero et al., 2004; Roiha et al., 2011; Rossini et al., 2001, 1998a, 1998b). Tecchio et al., (2007) show that the absence of P20 components is associated with reduced recovery of hand function. In general, there are indicators that SEPs or SEFs can be used for subject-specific prediction of recovery after stroke. Yet, their use as biomarkers is lacking from clinical trials (Boyd et al., 2017).

1.7 Problem statement

Do SEP responses contain subject-specific prognostic information about stroke recovery? To answer this question, one has to realize that the changes in the brain related to somato-sensation within the first few weeks' time after stroke are confined to a very small area: S1 and S2. This confined location offers the opportunity to test whether SEP responses induced by electrical stimulation of the

median nerve or the fingers are in fact a proper means to detect and analyze those changes as one 'knows' where to look at. By proper mean I refer to testing for reproducible measurements and increased spatial resolution.
Studying SEP and SEF responses of chronic or acute stroke patients have already been addressed in the literature at group level. As of yet, however, it is an open question to what extent the analysis of these signals provides meaningful information at the subject level. There is need for well reproducible EEG measurements with high enough SNR in order to ensure that the expectedly subtle changes are not caused by noise but are due to stroke recovery or physiological processes involved with the disease. Additionally, increased spatial resolution is required to track expectedly subtle changes in the somatosensory cortex. All this requires longitudinal SEP studies with large numbers of EEG channels that explore stroke recovery in a substantial number of patients.

1.8 Aim of this thesis

Longitudinal changes occurring within the S1 area of the somatosensory cortex are the main focus of my thesis. For studying this a high spatial resolution and repeatable measurements are required. My goal was to develop a methodology for tracking longitudinal changes after stroke within the somatosensory cortex using SEP, with the ultimate aim to test for the validity of SEP as a biomarker in the clinical assessment of stroke.

1.9 Research questions

The overarching objective of this thesis was to investigate to what extent longitudinal changes in the brain that occur post-stroke can be monitored using comparably simple electro-physiological measurements. I approached this from experimental, analytical, numerical, and clinical perspectives. Along these lines, the following specific questions have been addressed:

- Is finger stimulation a valid approach for investigating S1?
    - Are SEPs and their topographical distribution induced by stimulation of the fingers reproducible?
    - Can we disentangle the activity of adjacent fingers on the somatosensory cortex with the use of EEG?
    - Can we set some thresholds and limitations for the community?
- How can we define EEG's spatial resolution and what is the resolution?
    - Which is the optimal inverse method to disentangle simultaneously activated dipoles in close proximity?
    - How is source localization accuracy affected by realistic EEG noise, as opposed to synthetic white noise?
    - Is pre-whitening beneficial for the realistic case scenario?
- Can SEP parameters, early or a few weeks after stroke, be used to improve the prediction of the rehabilitation curve of stroke patients?
    - Can we set some guidelines on how to use SEP parameters for monitoring stroke recovery?
- Can SEPs induced by finger stimulation provide useful insights about chronic stroke patients?
    - Are there other ways of extracting useful information from SEPs apart from looking at ERPs?

1.10 Outline

In **Chapter 2**, the spatial accuracy of EEG was studied using electrical stimulation of the fingers with limited success. This called for defining the EEG's 'spatial resolution' in **Chapter 3** using a simulation study. Subsequently, I applied the resulting methodology to ischemic stroke patients both in the acute phase (**Chapter 4**) and in the chronic phase, six months after stroke (**Chapter 5)**. Finally, in **Chapter 6**, the outcomes of this thesis have been discussed including recommendations for future research.

Chapter 2

Disentangling somatosensory evoked potentials of the fingers: limitations and clinical potential[1]

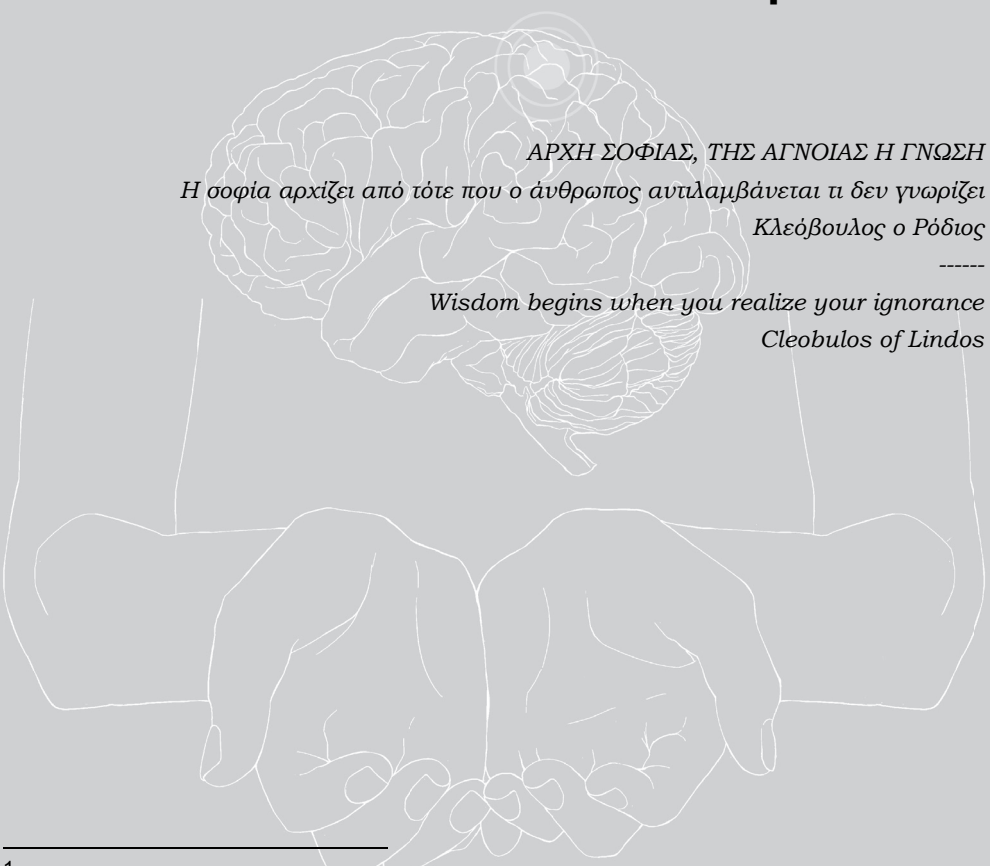

ΑΡΧΗ ΣΟΦΙΑΣ, ΤΗΣ ΑΓΝΟΙΑΣ Η ΓΝΩΣΗ
Η σοφία αρχίζει από τότε που ο άνθρωπος αντιλαμβάνεται τι δεν γνωρίζει
Κλεόβουλος ο Ρόδιος

Wisdom begins when you realize your ignorance
Cleobulos of Lindos

[1] This chapter is published in BRAIN TOPOGRAPHY, Minor style and word changes have been made to facilitate integration in this thesis: Konstantina Kalogianni, Andreas Daffertshofer, Frans C.T. van der Helm, Alfred C. Schouten, Jan C. de Munck, on behalf of the 4D-EEG consortium. *Disentangling somatosensory evoked potentials of the fingers: limitations and clinical potential*. Brain Topography 2018;31(3):498-512.

ABSTRACT

In searching for predictors for recovery of upper limb function post stroke we studied reproducibility of somatosensory potentials (SEP) evoked by finger stimulation in healthy subjects. SEPs induced by electrical stimulation and especially after median nerve stimulation is a method widely used in the literature. It is unclear, however, if EEG recordings after finger stimulation are reproducible within the same subject. Therefore, we assessed different stimulation amplitudes and durations. Using the stimulation with the maximum response, we tested in 5 healthy subjects the consistency and reproducibility of responses through bootstrapping as well as test-retest recordings. We further evaluated the possibility to discriminate activity of different fingers both at electrode and at source level. The lack of consistency and reproducibility suggest responses to finger stimulation to be unreliable, even with reasonably high signal-to-noise ratio (SNR) and adequate number of trials. At sources level, somatotopic arrangement of the fingers representation was only found in one of the subjects. Although finding distinct locations of the different fingers activation was possible, our optimized protocol did not allow for non-overlapping dipole representations of the fingers. We conclude that despite its theoretical advantages we cannot recommend the use of somatosensory potentials evoked by finger stimulation to extract clinical biomarkers, such as predictors of upper limb recovery post stroke.

2.1 Introduction

Somatosensory impairment is highly associated with stroke severity (Connel et al., 2008; Meyer et al., 2016). More specifically, regaining individual finger function is considered a good predictor for recovery of upper limb function post stroke (Nijland et al., 2010b). Whether this marks recovery of efferent or afferent connections from motor or somatosensory areas is a matter of dispute. In the current study, we focused on the latter and asked whether electric stimulation of the fingers may yield reliable responses in sensory areas as assessed by electro-encephalography (EEG). We tested for the candidate capacity of responses to finger stimulation as a clinical biomarker in general and more specifically for stroke recovery.

Somatosensory evoked potentials and fields (SEPs and SEFs, respectively) induced by electrical or mechanical stimulation on the median nerve is a well-established approach to investigate the electrophysiological phenomena linked to impaired somatosensation occurring, for example, while recovering from a stroke (Al-Rawi et al., 2009; Feys et al., 2000; Hari and Forss, 1999; Huang et al., 2004; Keren et al., 1993; Oliviero et al., 2004; Péréon et al., 1995; Rossini et al., 2001, 1998a, Tecchio et al., 2007b, 2006, 2007a; Timmerhuis et al., 1996; Tzvetanov and Rousseff, 2003; Wikström et al., 2000, 1999). Early components of median nerve SEPs may indicate whether afferent connections arrive at the contralateral primary somatosensory cortex (S1). By stimulating directly at the median nerve, however, both cutaneous muscle and joint afferents are stimulated and potentially efferent fibers intervening (muscles) (Dawson, 1956; Kuiken et al., 2007; Mauguiere, 1999). Dependent on the intensity of the stimulus, finger stimulation will excite primarily Aβ fibers (Dowman, 1997), followed by Aδ, followed by C fibers (Kandel et al., 2000; McAllister et al., 1995) while median nerve stimulation includes additionally sensory and motor fibers of larger diameter and partially the ulnar nerve. In view of our interest on hand representation, we hence focused on activity induced by stimulation of the digits, as assuming this to elicit responses at a more specified area at the somatosensory cortex.

Somatotopic arrangement and discrete representation of the fingers in the human cortex is well studied in the literature; Penfield and Boldrey (1937) already showed

a systematic arrangement of representation of the human fingers on the cortex using intraoperative electrocorticography (ECoG), which was later confirmed by Penfield and Rasmussen (Penfield and Rasmussen, 1950). Studies using local field potential recordings in animals revealed the refined spatial representation differentiating the input from different fingers (Kaas, 1983), in particular in area 3b of SI. Over the last decade or so, high-resolution fMRI studies confirmed the somatotopic arrangement in area BA 3b reporting inter-digit distances that varied from 3.7 mm to 15.5 mm (Martuzzi et al., 2014; Pfannmöller et al., 2015; van Westen et al., 2004). M/EEG studies concentrated mainly on the representation of 1st and 5th digit. Using EEG, Baumgartner et al. (1993) revealed a distance of 12.5 mm between representations of thumb and little finger. Buchner et al. (1994) reported a somatotopic arrangement for two of three subjects tested. Barbati et al. (2006) found statistically significantly different representations for 1st and 5th finger with MEG that Houzé et al. (2011) confirmed with EEG, and the differences between ulnar and median nerve representation were found more significant. In the MEG studies of Rossini et al. (2001) and Rossini et al. (1998a) discrimination of the 1st and 5th digit was shown possible both for healthy controls and stroke patients, where enlargement of the hand area occurred.

Although the somatotopy of evoked responses has been addressed in various studies, it is still unclear how reliable and reproducible those responses are within and across subjects, both at sensor and at source level. In particular, it is unknown whether somatotopy of all the fingers can be demonstrated with EEG in individual subjects and in a reproducible way. The heterogeneity in stimulus protocols and the lack of datasets where all fingers are stimulated render the findings described in the literature difficult to judge. Using a pneumatic stimulation protocol, Schaefer et al. (2002) sketched test-rest reliability and reported a mean Euclidean distance of 7.42 mm between sources activations revealed by EEG measurements separated 1 month in time. However, this study did not address the possibility to discriminate non-overlapping representation of all the fingers in the somatosensory cortex with the use of EEG. We consider such a discrimination crucial when interested in using finger SEPs as potential biomarker.

In the present study, we assessed the test-retest variability of the responses. We also tested for the number of trials needed to obtain robust topographies and examined the possibility of discriminating different fingers at the cortex. Ultimate goal was to examine the possibility of using EEG and SEP on the finger as a subject-specific biomarker.

2.2 Materials and methods

2.2.1 Participants

Five healthy volunteers participated in the study (1 left handed; mean±SD age: 34±12; 3 male: 39±13 years; and 2 female: 26±3 years). Measurements were scheduled in four consecutive working days. The subjects had no previous or current neurological/motor deficits. They provided written informed consent, prior to the start of the experiment. The experimental protocol was in compliance with the declaration of Helsinki and approved by the institutional ethics committee of the Faculty of Human Movement Science, Vrije Universiteit Amsterdam, The Netherlands (ECB 2014-72). We note here, that this is an exploratory study and therefore we included a rather small sample size of five healthy volunteers. In order to suggest SEP induced by electrical stimulation of the finger as a relevant patient-specific biomarker, reproducible SEP responses and discrimination of finger representations should be possible in all five healthy participants tested.

2.2.2 Experiment

Experimental setup

During the experiment, participants were sitting comfortably with their dominant hand and forearm positioned on their lap with the fingers on top (supine position). Between forearm and lap a pillow was placed to secure a stable position and comfort, as depicted in Fig. 2.1. The experiment was performed within a NEN1010 approved measurement van, which was equipped with high-density EEG located at the VU University Medical Center (Amsterdam, The Netherlands).

Data were recorded with a 64-channel EEG system (TMSi, Netherlands) with ground electrode placed at the left mastoid and referenced to the common average

during recording. Sampling rate was 1024 Hz and apart from anti-aliasing filters no other filters were applied online. Positions of the EEG electrodes for every subject were measured with the ANT Neuro Xensor system (ANT Neuro, Enschede, Netherlands).

Electric stimuli were delivered to the fingers with a bipolar battery-powered electrical stimulator by Micromed (Brain quick) in order to record the somatosensory evoked potentials (SEPs) with EEG. Two electrodes (bipolar stimulation) were applied to all the fingers. The anodal stimulation was placed at the most distal phalange of the finger and the cathode at the second most distal phalange of the finger with an inter-electrode distance of approximately 1 cm. A monophasic anodic rectangular electrical pulse of 400 μs width and a stimulation intensity of two times the sensation threshold was chosen. The sensation threshold was defined as the level at which the subject was able to sense half of the 10 pulses given. To define the aforementioned parameters, we reviewed the literature and we tested for effects of the electrical pulse's width and intensity on the amplitude and reproducibility of the SEP responses on one participant prior to conducting the experiment; more information can be found in the Appendix. The chosen stimulation did not cause any inconvenience to the participants.

Experimental protocol

Participants were instructed to relax neck, shoulder, and face muscles, to blink normally, to avoid talking or swallowing, and to fixate their gaze at a cross at a computer screen about 60 cm in front of them. All fingers of the dominant hand were electrically stimulated in random order.

The five conditions of the experiment (corresponding to the five different fingers) were repeated in two blocks, with approximately 10-15 minutes difference between the two blocks. Each condition consisted of 500 trials (repetitions of stimuli). Different (random) orders of stimulation were used in both blocks of the experiment. The inter-stimulus interval (ISI) was chosen from 250 to 330 ms (varied randomly), as the later responses at the somatosensory area are expected up to 110 ms (Hämäläinen et al., 1990) and ISIs larger than 150 ms do not affect the deflections of P35 and P60 (Wikström et al., 1996). Between every finger's

stimulation there was a break of at least 1 min but not longer than 3 min according to participant's needs.

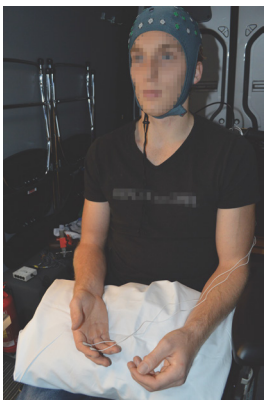

Fig. 2.1 Experimental setup. One participant is seated on a wheelchair inside the experimental van with his dominant hand on a supine position, placed on a pillow. Here, the electrodes are attached on his index finger.

2.2.3 Pre-processing of the data

The data were pre-processed offline using Matlab (R2013b; The Mathworks, Natick, MA) with the Fieldtrip (Oostenveld et al., 2011) and EEGlab toolboxes (Delorme and Makeig, 2004). After linear interpolation of the stimulation artefact (lasting for approximately 6 ms after stimulus onset), data were band-pass filtered between 1 and 250 Hz using a bi-directional 4th order Butterworth filter. The data were segmented in 250 ms stimulus-locked epochs including a 50-ms pre-stimulus interval. Noisy epochs and channels were identified visually and discarded. Artifact-free data consisted of about 780 trials (78% of the total number of trials) and about 50 channels (78% of the total number of channels). After re-referencing to the average of the remaining channels, the SEPs were computed for each dataset.

2.2.4 Signal-to-noise ratio (SNR)

The SNR per channel and sample was calculated via:

$$SNR(c) = \sqrt{\frac{\sum_{t=1}^{T} \overline{x(c,t)^2}}{\sum_{t=1}^{T} var_n(x(n,c,t))}} . N \qquad (2.1)$$

where x is a 3-way data matrix consisting of n trials, c channels, t time samples. N is the total number of trials. The power of the averaged signal $\bar{x}$ over trials was calculated by taking the sum of squares of all samples T over a specific time window (20 to 120 ms after stimulus onset) and then divided by the sum of the variance over trials var_n. This ratio was multiplied by the total number of trials and the square root of this portion served as measure of SNR.
The SNR was averaged over all the channels resulting in one SNR value for every subject and every finger.

2.2.5 Dipole fitting

A dipole fit for all the subjects and conditions of the experiment was computed with a current dipole algorithm as described by De Munck et al. (2001). The current dipole algorithm splits the inverse problem into the linear and non-linear part and then performs a global search based on a fixed grid with mesh size of 1 cm, followed by a full nonlinear search. A concentric three-sphere head model was determined by fitting a sphere on the subject-specific electrode positions. For the inner and outer radii of the skull fixed ratios with respect to the fitted head radius were used. The dipole fit was applied to the P50 peak that was identified for every subject and for every condition after computing the global field power (μV^2) at the BIAP software (http://www.demunck.info/software/index.html). By this, individual differences were accounted for.

2.2.6 Statistics

Spatio-temporal reproducibility

The spatio-temporal reproducibility of the SEPs was quantified as the correlation coefficient *r* between two averages A_{ct} and B_{ct}, where A_{ct} and B_{ct} represent two averaged responses and *c* refers to channel and *t* to sample. Here *t* is varied over a specific time window corresponding to the signal's peak. The correlation coefficient was calculated similar to Goszczynska et al. (2014) and it is as follows:

$$r = \frac{\sum_c \sum_t (A(c,t) - \bar{A})(B(c,t) - \bar{B})}{\sqrt{(\sum_c \sum_t (A(c,t) - \bar{A})^2)(\sum_c \sum_t (B(c,t) - \bar{B})^2)}} \quad (2.2)$$

Here $\overline{A}$ and $\overline{B}$ are determined by averaging the SEPs over channels and time samples. With the use of *r* the whole spatiotemporal pattern of the responses is taken into account. *r* is used to quantify the similarity of the SEPs belonging to the same experimental condition but consisting of different subset of trials. The values of *r* range between -1 and +1, where +1 defines full correlation and -1 full negative correlation. As proposed by (Goszczynska et al., 2014) a value of *r* = 0.9 identifies similar EEG spatiotemporal patterns.

Bootstrapping

We used a resampling bootstrapping technique in order to set confident regions of the responses at electrodes and sources level (Darvas et al., 2005). By randomly drawing a specific number of trials out of the total number of trials (780 ± 50) a bootstrap of the average response was constructed for a specific number of trials. We took 100 random subsets of a certain percentage of the trials and for each subset we computed the averaged SEP response. The percentages of trials were varied in steps of 10% from 10 to 90%, in order to determine the requested number of trials for a reproducible response.

For every bootstrapped-based average, a dipole was computed, resulting in 100 dipoles for every condition. Each dipole is represented in 3D space in (*x*,*y*,*z*)-coordinates. Nasion, left pre-auricular point (LPA), and right pre-auricular point (RPA) coordinates were used, with +*x* pointing to the nose, +*y* pointing to the left ear and +*z* pointing to the top of the head. To quantify the findings, we computed for every condition the mean location *m* of the cloud of 100 dipoles and the position covariance matrix C. Parameter variations of the reconstructed dipole locations are illustrated with an ellipse centered at the m dipole position. The axes of the ellipsoids are oriented according to the principal axes of variation of each cloud of dipoles. The principal axes are computed as the eigenvectors of the C. For specifying the overlap of the ellipsoids corresponding to the bootstrapped-based representation of the fingers i and j we computed the pre-whitened distance between the cluster's centroids i and j. Assuming that the ellipsoids have independent Gaussian distributions with covariances C_i and C_j, then the distribution of their difference is Gaussian, with mean $m_i - m_j$ and covariance $C_i + C_j$. If W_{ij} is

a pre-whitening matrix, such that $W_{ij}W_{ij}^{T} = \left(C_i + C_j\right)^{inv}$,the possible separability of the two ellipsoids is defined by the length of the vector z

$$z = W_{ij}\left(m_i - m_j\right) \tag{2.3}$$

The (dimensionless) measure of separability S_{ij} of the two ellipsoids is defined as

$$S_{ij} = \sqrt{z_x^2 + z_y^2 + z_y^2} \tag{2.4}$$

When S_{ij} is larger than 2 the ellipses corresponding to the dipoles representations are considered as not overlapping and when S_{ij} is smaller than 2 the ellipses overlap.

2.3 Results

2.3.1 Global field power of the SEP responses

The global field power (GFP) computed in μV^2 (Brunet et al., 2011) for different fingers is plotted for participant 5 in Fig. 2.2. The GFP was used to identify peaks in the event-related signal (Michel and Murray, 2012). Although the peaks varied between participants and fingers, typically three peaks could be observed in the SEP: one peak around 30 ms, one peak around 50 ms (P50 peak) and one peak around 100 ms. Since we were particularly interested in the early responses that correspond to S1 activation, a window of 25 to 65 ms after stimulus onset was selected for further analysis. The P50 was always present in the SEPs of all subjects in contrast to the P30. We thus selected P50 as the candidate peak for source localization.

2.3.3 Signal-to-Noise ratio

The SNR was determined as explained in Section 2.2.6 for the time window 25 to 65 ms post-stimulus. It was found to be (SNR±SD): 2.6±0.8 for subject 1, 3.4±0.5 for subject 2, 3.8±0.5 for subject 3, 2.4 ±0.6 for subject 4, and 3.3±0.5 for subject 5. Here, standard deviations (SD) were computed over fingers. Accordingly, the SNR for the pre-stimulus window -40 ms to 0 ms was found to be (SNR±SD):

1.7±0.5 for subject 1, 1±0.1 for subject 2, 1±0.1 for subject 3, 1.5 ±0.3 for subject 4, and 1±0.2 for subject 5.

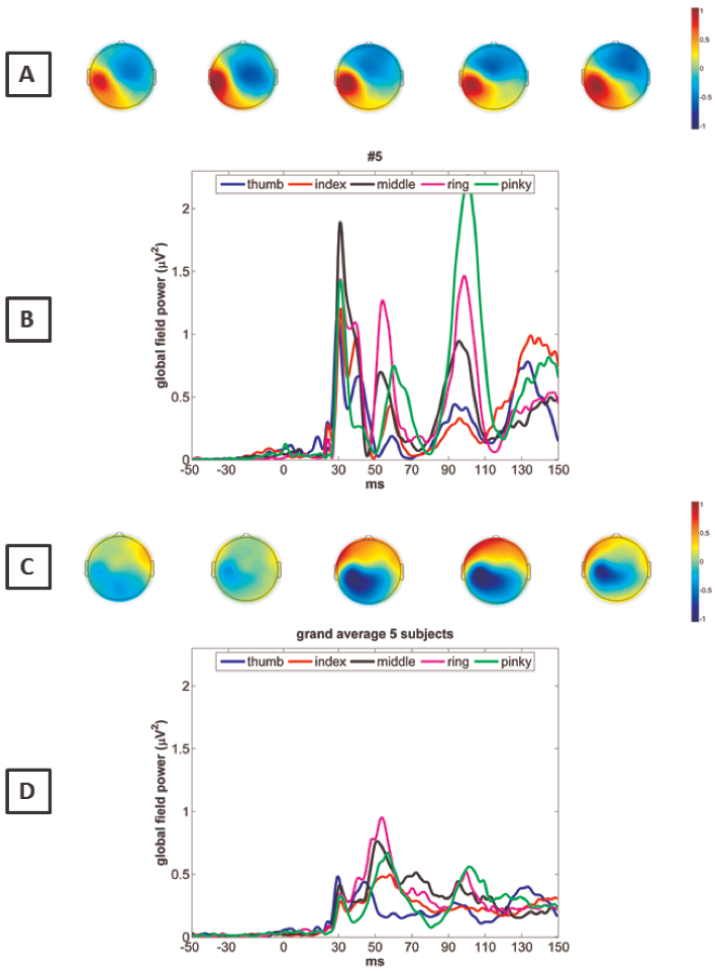

Fig. 2.2 (A) topographical distribution of the P30 peak. (B) GFPs of SEP responses after stimulation of the individual fingers of subject 5. Different colors represent different fingers. (C) topographical distribution of the P50 peak. (D) GFP of grand average of SEP responses of 5 subjects.

2.3.4 Reproducibility of SEP responses

Test-retest reproducibility

The correlation coefficients for the two experimental runs over a time window 25 to 65 ms are shown in Fig. 2.3. We selected a window that most probably contains 2 peaks, because we want to test the reproducibility of the topographical distribution, generated after electrical stimulation. The mean correlation coefficient was 0.77±0.14 and the mean correlation coefficients per finger were, thumb: 0.74±0.20, index: 0.77±0.06, middle: 0.86±0.02, ring: 0.85±0.05, pinky: 0.70±0.30, where standard deviations indicate inter-subject variability. This indicates that the middle finger yielded the most reproducible response. To address the habituation effects that might occur at the second experimental run, we constructed two datasets containing randomly selected non-overlapping subsets of trials (50 % of the trials in each dataset) and then the correlation coefficient was computed as shown in Fig. 2.3. Small differences were present in the correlation coefficient of the two runs, however they had a similar pattern.

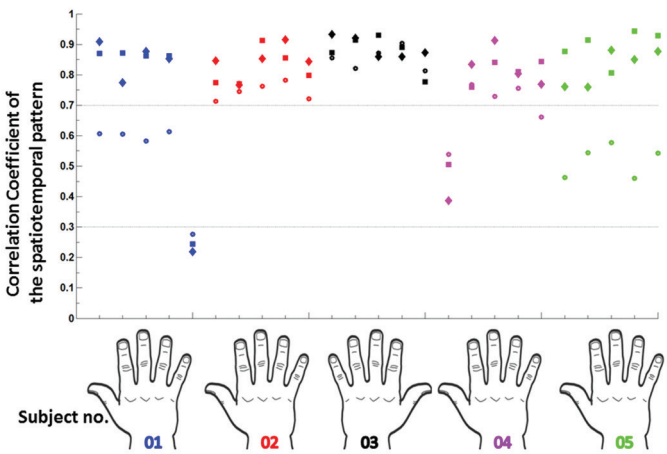

Fig. 2.3 Reproducibility of the SEP. The spatiotemporal correlation coefficient was computed for the window of 25-65 ms after stimulus onset. The diamond markers represent the correlation between the 2 experimental repetitions of the same finger, the 'o' markers represent the correlation of one finger with all the others and the square markers refers to the correlation coefficient of 2 randomly selected subsets after stimulation of the same finger. Each subject is associated with a specific color and the correlation coefficients of every finger are plotted above the fingers of the hand representation. Subject 3 was left handed.

The computation of the correlation coefficient between the SEP responses of all combinations of fingers shows that the spatiotemporal patterns of all the fingers did not differ significantly (mean correlation coefficient 0.67 ±0.15) from the patterns of all the other fingers, as also supported from Wang et al. (2004) for index-pinky spatiotemporal correlation coefficient In Fig. 2.3 this is indicated per subject with the “o” markers. This finding suggests that at least at sensor level there was no large distinct spatiotemporal pattern per finger.

Number of trials needed for reproducible responses:

A bootstrapping-resampling technique served to assess the effect of the number of trials on the reconstruction of the spatial-temporal responses patterns determined from the total number of trials. The quality of this reconstruction was quantified by computing the correlation coefficient between the SEP response computed with the total number of trials and a subset of a certain percentage of the trials. The mean and standard deviations of these correlations were computed over 100 random subsets, and displayed as a function of the percentage of trials in Fig. 2.4. Computations were conducted separately for all five fingers and five subjects. One observes that after including in the dataset 30% of the total number of trials it was possible to reproduce the original dataset by 85% (except two outliers).

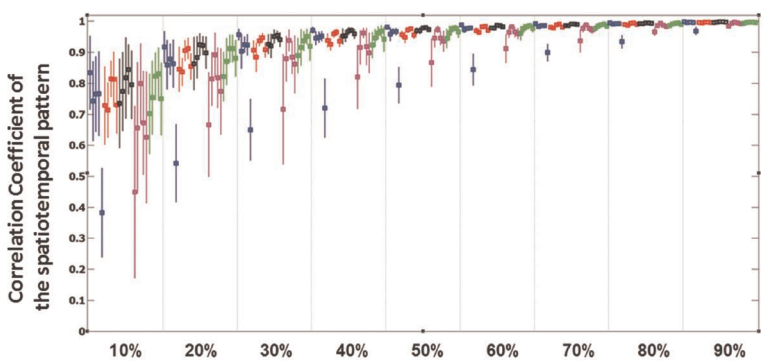

Fig. 2.4 Correlation coefficient of X % trials averaged pattern and true averaged pattern (100% of trials). The mean and standard deviation of the correlation coefficient is shown, computed from 100 randomly selected time windows from 25 to 65ms. Every percentage block shows means and standard deviations for all subjects and fingers. The same color code for the different fingers is used as in Fig. 2.3.

By including 50% of the trials (390 trials) a correlation coefficient of 95% was achieved on average. Specifically, after including 390 trials in the SEP response, the topographical distribution showed similarity to the response after including all trials and was: 0.93 for the thumb, 0.96 for the index, 0.97 for the thumb 0.94 for the ring and 0.96 for the pinky, as shown in Table 2.1.Those values exceeded the threshold 0.9 as indicated by (Goszczynska et al., 2014) and therefore the responses after including 50% of the trials (390) and 100% of the trials showed similarity.

Table 2.1 Mean and standard deviation (mean±std) of the spatio-temporal correlation coefficient of the averaged response after including 30% and 50% of the total number of trials and of the averaged response after including the total number of trials.

	%30 of the total number of trials					***%50 of the total number of trials***				
	#1	*#2*	*#3*	*#4*	*#5*	*#1*	*#2*	*#3*	*#4*	*#5*
thumb	0.96 ±0.02	0.89 ±0.03	0.92 ±0.04	0.72 ±0.16	0.88 ±0.05	0.98 ±0.01	0.95 ±0.01	0.96 ±0.01	0.87 ±0.07	0.94 ±0.03
index	0.90 ±0.05	0.88 ±0.04	0.92 ±0.04	0.88 ±0.06	0.90 ±0.06	0.96 ±0.02	0.95 ±0.02	0.97 ±0.01	0.95 ±0.03	0.96 ±0.02
middle	0.92 ±0.02	0.92 ±0.02	0.95 ±0.02	0.94 ±0.03	0.93 ±0.03	0.97 ±0.01	0.97 ±0.01	0.98 ±0.01	0.97 ±0.01	0.97 ±0.01
ring	0.92 ±0.03	0.94 ±0.02	0.95 ±0.02	0.89 ±0.05	0.94 ±0.03	0.97 ±0.01	0.97 ±0.01	0.98 ±0.01	0.95 ±0.02	0.97 ±0.01
pinky	0.67 ±0.09	0.90 ±0.03	0.94 ±0.02	0.86 ±0.08	0.92 ±0.04	0.81 ±0.05	0.95 ±0.01	0.97 ±0.01	0.94 ±0.03	0.96 ±0.02

2.3.5 Representation of different fingers on the sources level

Location of the centroids of the bootstrapped- based dipoles

In Fig. 2.5 the mean location per finger over the 100 permutations is shown as the cluster of the centroid (with a bold dot) and around this a sphere is plotted with the radius as defined in Section 2.2.6.

For the two subjects whose data are displayed in Fig. 2.5 (subject 2 and 5) we observed no systematic order of the representation of the fingers while the

estimated representations of fingers were strongly overlapping. In order to have a proper somatotopic arrangement, the values of *y*-coordinates should have had an ascending order from thumb to pinky. This arrangement could only be confirmed to some extent for subject 2 (see Table 2.2), although the radii of the representation ellipsoids (while being the smallest over subjects) did not allow for a complete separation of the representation of the fingers. The other four subjects did not show such somatotopic arrangement.

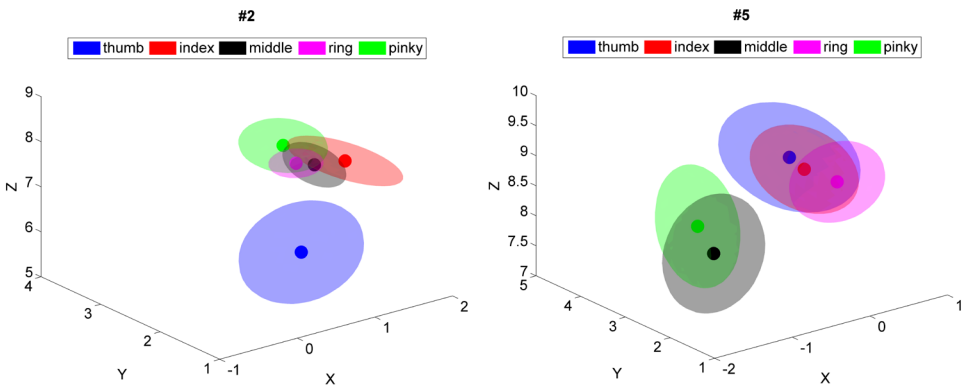

Fig. 2.5 The mean dipole locations of the P50 components, estimated over 100 random subsets of trials are plotted for different fingers with filled dot. The ellipses around them represent the radius of confidence. Blue = thumb, red = index finger, black = middle finger, purple =ring finger and green = pinky. The half axes of the ellipsoids are two times the standard deviation of the spatial variation of the 100 bootstrapped based locations. The orientation of the ellipsoids is given by the eigenvectors of the covariance matrix of the dipole locations of each cloud of points. Dipole coordinates are represented in Nasion-Ear coordinates, in cm. On the left results of subject 2 are shown and on the right those of subject 5.

Overlap of the fingers' representation

To illustrate the general overlap of the finger representations, we show in Table 2.3 the minimum and maximum separability measure over all subjects. For example, the separability index between middle and ring fingers amounts to 7.10 in the "best" subject, indicating that there was no substantial overlap between the bootstrapped-based representations for this subject. However, for the same combination of fingers, we found a subject in whom the separability was only 0.96

implying an almost complete overlap of the bootstrapped-based clusters. Since the figures represented in Table 2.3 are not caused by a single good or poor performing subject, we have to conclude that there was no pair of fingers for which good separability exists for all subjects. Specifically, the minimum part of the table shows there was no pair of fingers for which the separability was higher than 0.68 for all the subjects.

Table 2.2 Mean location and confidence radius of the dipoles estimated over 100 random subsets. Dipoles are computed for the P50 peak. Note that subject 3 is left-handed thus stimulated at left hand so location refers to right hemisphere. All values are in cm and nasion-ears coordinates are used.

	finger	x	y	z	radius
Subject 1	Thumb	4.16	1.51	5,32	1.67
	Index	3.90	2.07	2.98	2.54
	Middle	4.4	1.01	3.42	2.00
	Ring	6.07	-0.33	1.58	2.39
	Pinkie	2.89	4.98	3.18	4.18
Subject 2	Thumb	0.60	1.71	6.19	0.83
	Index	1.44	2.07	7.61	0.54
	Middle	1.14	2.20	7.58	0.40
	Ring	0.89	2.18	7.74	0.32
	Pinkie	1.07	2.63	7.78	0.51
Subject 3	Thumb	1.01	-3.82	6.99	1.44
	Index	0.47	-3.49	6.73	1.63
	Middle	-0.10	-3.72	7.76	1.01
	Ring	-0.92	-4.00	8.42	0.63
	Pinkie	0.38	-2.49	6.52	1.71
Subject 4	Thumb	2.50	4.83	9.01	1.62
	Index	2.64	1.75	6.81	1.31
	Middle	3.69	3.11	6.55	1.30
	Ring	2.36	4.18	9.55	1.17
	Pinkie	2.25	3.59	8.32	1.35
Subject 5	Thumb	0.19	3.14	8.84	0.90
	Index	0.87	2.62	8.85	0.70
	Middle	-1.06	2.65	7.85	0.84
	Ring	0.39	2.41	8.61	0.60
	Pinkie	-0.83	3.42	7.95	0.83

Table 2.3 The maximum and minimum separability over all subjects are shown for all finger combinations

Digit number	1	2	3	4	5	
1	-	3.65	3.50	3.96	3.90	
2	0.74	-	2.55	6.52	3.36	MAX
3	1.69	0.68	-	7.10	3.45	
4	0.87	0.85	0.96	-	4.17	
5	1.33	1.13	1.42	1.37	-	
	MIN					

2.4 Discussion

In the present study, we evaluated the use of somatosensory evoked potentials induced by finger stimulation, as a potential biomarker tool for post-stroke recovery. We were especially interested in testing the robustness of such a biomarker as a lack of consistency would make it impossible to track longitudinal changes at a subject-specific level. The large overlap of the dipole representations for different fingers and the relatively low reproducibility of the test-retest design indicate the difficulty of separating the representations of different fingers as determined by EEG and electrical finger stimulation. Moreover, the somatotopic representation of the fingers could only be confirmed in one of the five subjects, whereas for the others it was not so consistent. We emphasize that these results were found in the 'ideal' condition in which an optimal stimulation protocol was used and reproducibility measure was not compromised by detaching and re-attaching the EEG cap.

Parts of these admittedly discouraging results are consistent with other studies. We found one or two peaks from 25 to 65 ms (Baumgartner et al., 1993; Bourguignon et al., 2013; Buchner et al., 1994; Hari and Forss, 1999; Houzé et al., 2011; Nierula et al., 2013; Schubert et al., 2008; Wang et al., 2004) and a later peak around 100 ms (Hämäläinen et al., 1990). Note that the early peaks are often referred to as N20 and P27 in the literature in accordance with peaks found after median nerve stimulation, the latencies found after finger stimulation do not agree with 20 or 27 ms (Wang et al., 2004). In order to assess the test-retest repeatability of the responses and the number of trials needed for reproducible responses, we

selected a window from 25 to 65 ms, since only a few studies referred to the later peaks. The early peak appears to correspond to activity in S1 (Forss et al., 1994b). Even at the convenient setup of not removing the EEG cap, correlation coefficients were at mean (± SD) of 0.8±0.16. The fairly low reproducibility was not affected by habituation effects in the test re-test design because the correlation coefficients of the random subset of trials are in the same range. Seeking to eliminate all parameters that may lead to irreproducible responses, we estimated the SNR with a similar way as Darvas et al. (2005) and the minimum number of trials needed in order to have repeatable spatiotemporal patterns. With an SNR of 2.9 (2.8 found in a MEG study, (Darvas et al., 2005)) we believe that our pre-processed signal was accurate. We found a minimum number of 230 trials to be needed for reproducing topographies that can be achieved with the total number of 780 trials. An indication about the variations at the brain responses is given by Darvas et al. (2005). We also observed a higher correlation coefficient for the middle finger and a lower correlation coefficient for the pinky, in accordance with small amplitudes, poor SNR and difficulty in source localization for the fifth digit reported in other studies (Baumgartner et al., 1993; Buchner et al., 1994; Houzé et al., 2011).

Although many studies applied electrical stimulation on the fingers to evoke SEPs or SEFs, as of yet there is no consensus on stimulus characteristics, nor explanation on the design of the chosen experimental protocol. To the best of our knowledge all studies used a monophasic anodic rectangular pulse of various pulse widths and intensities. MEG studies used a pulse width of 0.2 ms and an intensity of two times the sensory threshold or a pulse width of 1 ms and an intensity below the pain threshold (Darvas et al., 2005; Kristeva-Feige et al., 1995; Xiang et al., 1997). Stimulation protocols among EEG studies were even more inconsistent. The width of electrical pulse found was 0.2, 0.3, 0.4 ms and the intensities varied as well as 1.5, 2, 3 times the sensory threshold, maximum comfortable level or below the pain threshold (Baumgartner et al., 1993; Buchner et al., 1994; Houzé et al., 2011; Nierula et al., 2013; Schubert et al., 2008; Yao and Dewald, 2005). Inconsistency of stimulation protocols led us to test several stimulation parameters and their ability to produce reproducible responses (see Appendix). A more detailed test protocol with smaller steps between the pulse

widths will be helpful in revealing the effect of the pulse width to the responses. However, this is not the purpose of the present study.

With a high SNR, a number of trials adequate for resulting in reproducible responses and a stimulation protocol optimal for finger stimulation, we further tested the representation of the fingers at the sources level. Although there is evidence for discrimination of the activation related to different fingers and mainly of thumb and pinky using EEG (Baumgartner et al., 1993; Buchner et al., 1994; Houzé et al., 2011; Nierula et al., 2013) or MEG (Barbati et al., 2006; Buchner et al., 1994; Rossini et al., 2001, 1998a) it was still unclear if this discrete representation of the fingers is prone to trial to trial variations or subject-specific differences. Darvas et al. (2005) addressed this topic with using MEG of one subject revealing the somatotopic arrangement of the fingers. However, they found for the S1 sources, a standard deviation of the 1000 locations of the bootstrapped dipoles between 3 and 5 mm revealing an overlap for some of the fingers representation. Our results show even higher standard deviation between 2 and 28 mm that may be explained by the poorer spatial resolution of EEG in comparison to MEG (Leahy et al., 1998) and the lower SNR of EEG concerning superficial sources (Goldenholz et al., 2009; de Jongh et al., 2005). As it can be seen in Table 2.2 we failed to pinpoint a pattern of somatotopic arrangement of the fingers for all the subjects, let alone a clear pattern of which fingers could be disentangled in the human cortex. The use of realistic head models in the dipole calculation might have resulted in more accurate dipole positions (Schaefer et al., 2002). In the current study, however, we were interested in relative locations of fingers in the brain and their reproducibility and not in exact 3D locations of every finger on the cortex.

EEG being an affordable and accessible technique along with single nerve recruitment by electrical stimulation of the finger can serve as a tool in the clinic, for example for monitoring stroke rehabilitation. However, the variability of the responses and the absence of a reproducible pattern of the finger somatotopy imply that the finger representation estimated with EEG is not a recommendable subject-specific monitoring tool for a longitudinal stroke study. MEG or fMRI along with electrical finger stimulation are modalities with higher spatial resolution

(Darvas et al., 2005; Rossini et al., 2001), but patient's ease and longitudinal monitoring will be at stake for patients having to travel to the hospital. If not only refined finger representation is of interest, median nerve stimulation could be used as an alternative. Electrical stimulation of the median nerve is a popular experimental choice when stroke assessment is of interest (Forss et al., 1999; Hari and Forss, 1999; Huang et al., 2004; Rossini et al., 2001, 1998a, 1998b, Tecchio et al., 2007a, 2001, Wikström et al., 2000, 1999). It induces several peaks including an early peak around 20 ms and one around 50ms. Due to the fact that the median nerve stimulation activates both the sensory and motor areas, responses with larger amplitudes are observed when compared to the ones after electrical stimulation of the finger and with more prominent peaks. However, median nerve stimulation on stroke patients also showed limitations. For example in Tecchio et al. (2007b) median nerve stimulation responses were identifiable at the affected hemisphere only in 56 % of the patients. Yet, even when responses are identifiable we should expect an accuracy of 10 mm as indicated by Bourguignon et al. (2013) .A potential clinical use of the SEPs induced by finger stimulation could be the study of afferent pathways and brain areas recruited in S1 and S2 time locked to the appearance of early and late peaks.

2.5 Conclusions

Distinct locations of fingers representation during electrical stimulation were found for all participants. However, in a sample of five healthy young participants we failed to find non-overlapping dipole confidence limits of different fingers for all the subjects using high-density EEG. Responses appeared variable within and across recording sessions and therefore SEP induced by electrical stimulation on the fingers and recorded with EEG as a tool for subject-specific clinical assessment (for example, longitudinal post-stroke assessment) should be used with great care.

2.6 Acknowledgements

The authors would like to thank Juhani Dabek (PhD) for his help in organizing the experiment and collecting the data. The authors will also like to thank Ines de Castro Fernandes (MSc) for her contribution at the bootstrapping algorithm.

4D-EEG Consortium

In addition to the authors of the present study, the consortium consists of Gert Kwakkel, PhD, Carel G. M. Meskers, MD, PhD, Erwin E. H. van Wegen, PhD, Aukje S. Andringa, MSc, Dirk Hoevenaars, MSc, Caroline Winters, MSc and Sarah Zandvliet, MSc from the VU University Medical Center Amsterdam; Teodoro Solis-Escalante, PhD, Yuan-Yang, PhD, Martijn P. Vlaar, MSc, and Lena Filatova, PDEng, from the Delft University of Technology; Julius P. A. Dewald, PhD, and Jun Yao, MSc, from Northwestern University of Chicago.

2.7 Compliance with ethical standards

Conflict of Interest

The authors declare that they have no conflict of interest.

Ethical Approval

All procedures performed in studies involving human participants were in accordance with the ethical standards of the institutional and/or national research committee and with the 1964 Helsinki declaration and its later amendments or comparable ethical standards. This article does not contain any studies with animals performed by any of the authors.

2.8 Appendix

Definition of the electrical pulse

Prior to conducting the experiment, we tested for effects of the electrical pulse's width and intensity on the amplitude and reproducibility of the SEP responses on one participant. 15 different stimulation variants were explored, consisting of

monophasic anodic electrical pulses in combinations of 3 pulse widths and 5 intensities. Four pulse intensities were defined relatively to the sensation threshold (1.5, 2, 2.5 3 times the sensation threshold) and the 5th intensity was set just below the pain threshold. The sensation threshold was defined as the level at which the subject was able to sense half of the 10 pulses given. The width of pulses tested was 100, 400 and 500 μs. This choice was made after reviewing the literature: 100 μs was the shortest pulse width suggested by a review study (Cruccu et al., 2008), 400 μs was the pulse width used in a recent study with similar analysis (Houzé et al., 2011) and 500 μs can be considered the mean width of electrical pulses across a variety of studies. Each of the 15 experimental conditions consisted of 500 trials divided in 5 experimental blocks, giving 75 blocks of 100 trials. The order of the total number of blocks (75) was randomized in order to minimize habituation effects. A measure of reproducibility *r* was obtained by computing the spatio-temporal correlation coefficient between two averages of distinct random subsets of SEP responses (see Section 2.6).

Fig. A2.1 shows the correlation coefficient, computed between two averaged non-overlapping datasets created with the bootstrapping method for the time window 25 to 65 ms after stimulus onset. Mean and standard deviation of the bootstrapped based coefficients are depicted for the different combinations of pulses and intensities. The correlation coefficient of the pulse width 400 μs turned out more stable over intensities than for the other pulse widths. Moreover, the amplitude of the peaks (see Table A2.1) for the pulse width of 400 μs and at a threshold of two times the sensation threshold was larger than for the other two pulses' widths. We selected 400 μs as the pulse width for our experiment and as a stimulation threshold we selected the two times sensation threshold as it was not yet uncomfortable for the subject.

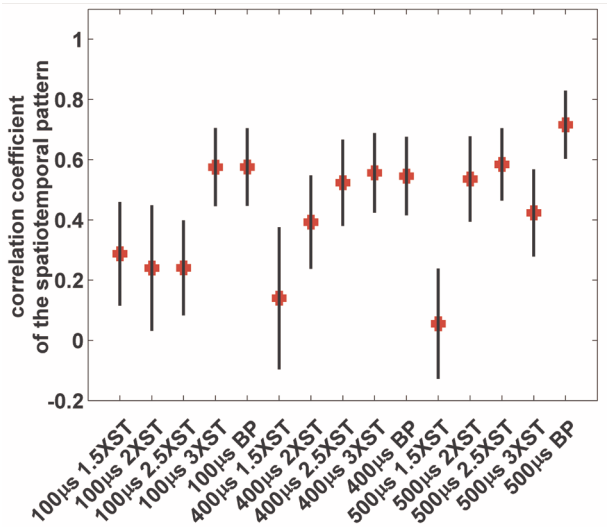

Fig. A2.1 Correlation coefficient of the spatiotemporal patterns for the time window 25 to 65 ms post stimulus and for different stimulation protocols. Mean and standard deviation over the bootstrapped based correlations are shown.

Table A2.1 The latency and amplitude of all the experimental conditions (15 pulse width-amplitude combinations) for the main peak in the global field power are presented and expressed in µV. The symbol * indicates a case in which we failed to identified the peak.

Pulse width	Times X threshold	Intensity	Latency 30-60 ms	Amplitude 30ms in µV
100 µs	1.5 sensory	3 mA	46	0.17
100 µs	2 sensory	3.5 mA	38	0.11
100 µs	2.5 sensory	4 mA	40	0.63
100 µs	3 sensory	5.5 mA	40	0.75
100 µs	below pain	7.5 mA	38	0.32
400 µs	1.5 sensory	1 mA	*	*
400 µs	2 sensory	1.5 mA	42	0.5
400 µs	2.5 sensory	2 mA	43	0.74
400 µs	3 sensory	2.5 mA	37	0.22
400 µs	below pain	3 mA	37	1.1
500 µs	1.5 sensory	1 mA	43	0.34
500 µs	2 sensory	1.5 mA	45	0.23
500 µs	2.5 sensory	2 mA	45	0.23
500 µs	3 sensory	2.5 mA	35	0.32
500 µs	below pain	3 mA	38	0.50

Global field power of the SEP responses

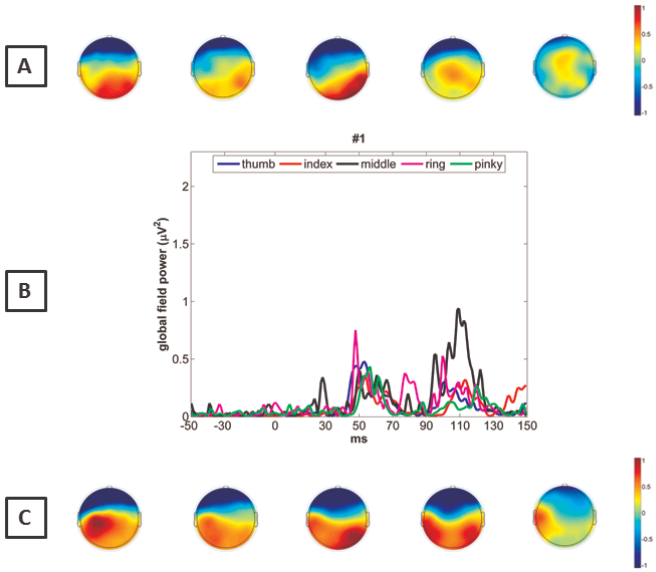

Fig. A2.2 (A) topographical distribution of the P30 peak. (B) GFPs of SEP responses after stimulation of the individual fingers of subject 1. Different colors represent different fingers. (C) topographical distribution of the P50 peak.

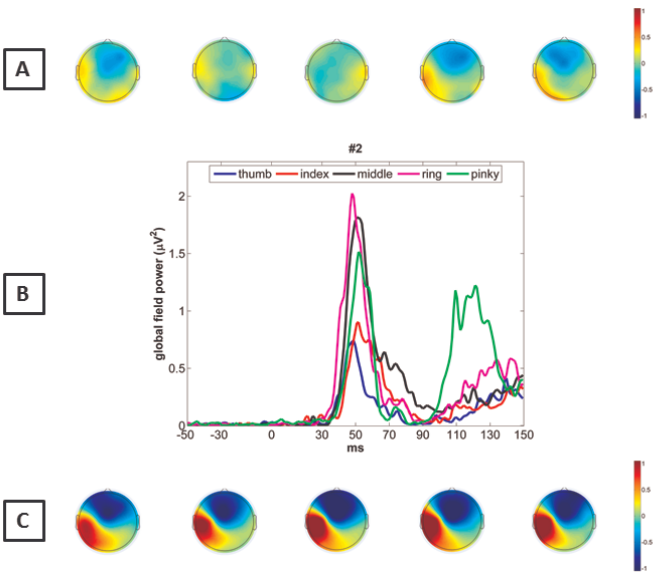

Fig. A2.3 (A) topographical distribution of the P30 peak. (B) GFPs of SEP responses after stimulation of the individual fingers of subject 2. Different colors represent different fingers. (C) topographical distribution of the P50 peak.

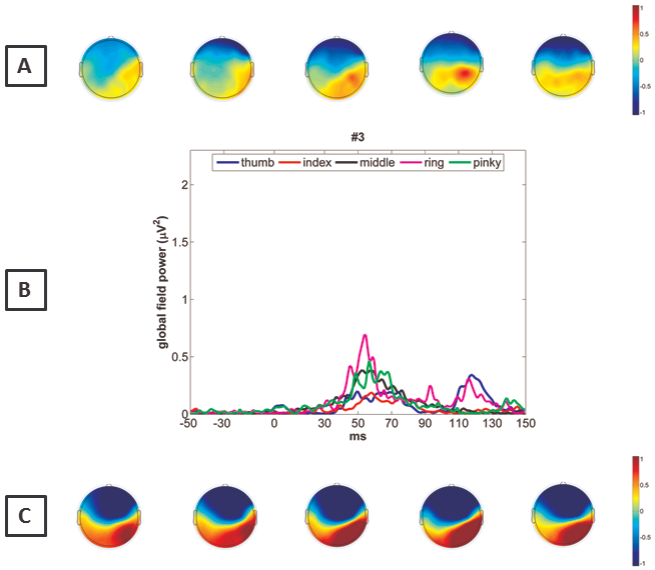

Fig. A2.4 (A) topographical distribution of the P30 peak. (B) GFPs of SEP responses after stimulation of the individual fingers of subject 3. Different colors represent different fingers. (C) topographical distribution of the P50 peak.

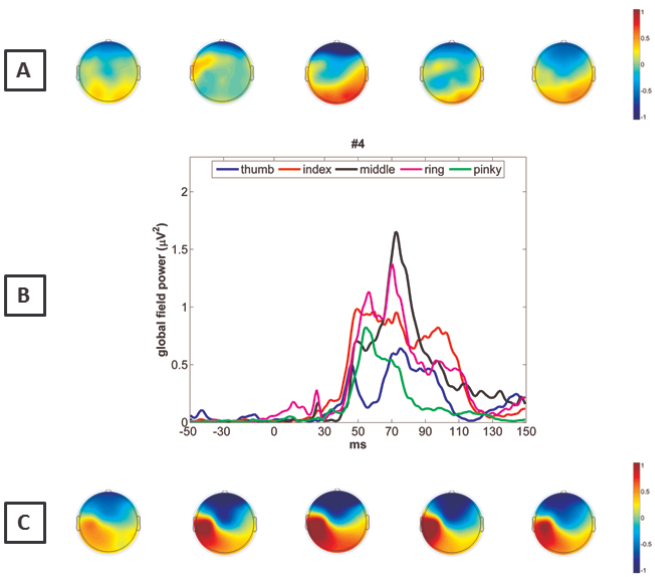

Fig. A2.5 (A) topographical distribution of the P30 peak. (B) GFPs of SEP responses after stimulation of the individual fingers of subject 4. Different colors represent different fingers. (C) topographical distribution of the P50 peak.

Chapter 3

Spatial resolution for EEG source reconstruction – a simulation study on SEPs[2]

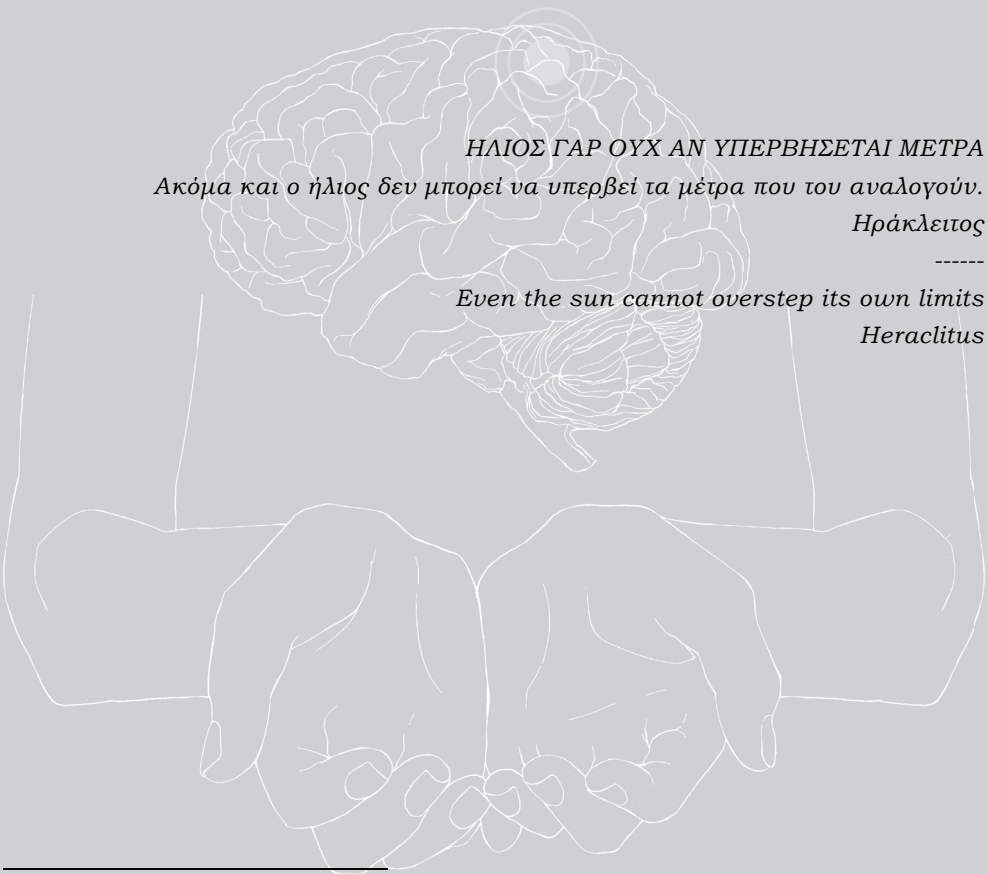

ΗΛΙΟΣ ΓΑΡ ΟΥΧ ΑΝ ΥΠΕΡΒΗΣΕΤΑΙ ΜΕΤΡΑ

Ακόμα και ο ήλιος δεν μπορεί να υπερβεί τα μέτρα που του αναλογούν.

Ηράκλειτος

Even the sun cannot overstep its own limits

Heraclitus

[2] This chapter is published in Journal of Neuroscience Methods, minor style and word changes have been made to facilitate integration in this thesis: Konstantina Kalogianni, Jan C. de Munck, Guido Nolte, Alistair N. Vardy, Frans C.T. van der Helm, Andreas Daffertshofer. *Spatial resolution for EEG source reconstruction A simulation study on SEPs. Journal of Neuroscience Methods 2018;301:9-17*

ABSTRACT

Background: The accuracy of source reconstruction depends on the spatial configuration of the neural sources underlying encephalographic signals, the temporal distance of the source activity, the level and structure of noise in the recordings, and – of course – on the employed inverse method. This plenitude of factors renders a definition of 'spatial resolution' of the electro-encephalogram (EEG) a challenge.

New method: A proper definition of spatial resolution requires a ground truth. We used data from numerical simulations of two dipoles changed with waveforms resembling somatosensory evoked potentials peaking at 20, 30, 50, 100 ms. We varied inter-dipole distances and added noise to the simulated scalp recordings with distinct signal-to-noise ratios (SNRs). Prior to inverse modeling we pre-whitened the simulated data and the leadfield. We tested a two-dipole fit, sc-MUSIC, and sc-eLORETA and assessed their accuracy via the distance between the simulated and estimated sources.

Results: To quantify the spatial resolution of EEG, we introduced the notion of separability, i.e. the separation of two dipolar sources with a certain inter-dipole distance. Our results indicate separability of two sources in the presence of realistic noise with SNR up to 3 if they are 11 mm or further apart.

Comparison with existing methods: In the presence of realistic noise, spatial pre-whitening appears mandatory preprocessing step irrespective of the inverse method employed.

Conclusions: Separability is a legitimate measure to quantify EEG's spatial resolution. An optimal resolution in source reconstruction requires spatial pre-whitening as a crucial pre-processing step.

3.1 Introduction

Electro-encephalography (EEG) is a non-invasive, affordable, and ambulant technique. Over the years, it has received substantial attention from researchers and clinicians. Apart from its excellent temporal resolution, EEG shows adequate spatial resolution and it is hence considered an imaging tool (Baillet et al., 2001; Lopes da Silva, 2004; Michel et al., 2004). While (functional) magnetic resonance imaging, (f)MRI, provides much better spatial resolution, EEG (and its magnetic counterpart, magneto-encephalography, MEG) are the modalities of choice when studying rapid responses of neural populations to a certain stimulus. When looking at evoked or induced responses, sources of interest are often located in nearby areas within the same lobe. They are activated with only a small time-shift in the order of milliseconds. A seminal example are somatosensory evoked responses induced by median nerve stimulation as a marker for tracking recovery pathways post stroke (Altamura et al., 2007; Forss et al., 1999; Huang et al., 2004; Laaksonen et al., 2012; Rossini et al., 2001; Tecchio et al., 2007a; Tzvetanov and Rousseff, 2003). Following stimulation, brief activation patterns can be found in the areas S1 and S2. To disentangle them with EEG, analyses have to rely on short signal epochs and require a comparably high spatial resolution when it comes to source reconstruction. Here, we sought to specify the term “comparably” to obtain robust estimates of the spatial resolution in EEG source reconstruction. To provide a proper definition of such a *spatial resolution*, we examined different inverse methods and evaluated their accuracy as a function of the proximity of the sources. Using EEG as an imaging tool implies addressing the inverse problem. In brief, extracting (distributed 3D) source activity within the brain from (low-dimensional 2D) scalp recordings is an ill-posed problem (von Helmholtz, 1853): infinitely many source configurations can generate identical electric potentials on the scalp. A priori assumptions or constraints can reduce this diversity. They are typically based on electro-physiological and anatomical features of the brain. In fact, over the last three or so decades, several methods have been developed to implement them. Methods fall in three categories: dipole fitting, scanning, and imaging (Darvas et al., 2004). Which method is most precise and which method explains best the

recorded data? As of yet, the literature does not provide commonly accepted answers to these questions. Several studies tried to define a gold standard in source localization. Yao and Dewald (2005) claimed that the well-known imaging approach coined low-resolution electromagnetic tomography (LORETA, Pascual-Marqui et al., 1994) has the lowest localization error after simulating two dipoles. However, Grech et al. (2008) forwarded the so-called standardized LORETA (Pascual-Marqui, 2002) when simulating a single dipole, which found recent support by Bradley et al. (2016). When interested in pre-surgical mapping, Grova et al. (2006) advised to consult the (statistical) output of different source localization algorithms. Interestingly, other studies (Becker et al., 2014; de Gooijer-van de Groep et al., 2013; Mideksa et al., 2012) suggested that subspace-based scanning methods, like multiple signal classification (MUSIC, Mosher et al., 1992), may lead to accurate solutions when compared with (LORETA-like) distributed methods. It appears that recommendations are as plentiful and diverse as methods. One reason for this might be that a direct comparison between localization methods requires defining the spatial resolution of EEG.

The presence of noise jeopardizes source localization. EEG signals are always contaminated by spatially and temporally correlated noise by means of background activity. As indicated for MEG, the spatial resolution will be enhanced by improving the SNR and by accounting for spatial characteristics of the noise (Brookes et al., 2008; Vrba, 2002; Vrba and Robinson, 2002). Spatial correlations in the noise potentially reduce the capacity of every inverse method to disentangle the sources underlying EEG. One may estimate these correlations by determining spatiotemporal covariance matrices from non-time-locked signal (ongoing activity) and remove them prior to source reconstruction. One way to do that is spatial pre-whitening, based on real data covariance matrix, which is considered a standard – albeit not well justified – pre-processing step for M/EEG (Engemann and Gramfort, 2015; Gramfort et al., 2012; Lin et al., 2006; Marzetti et al., 2008; Ou et al., 2009; Ramírez et al., 2011). Spatiotemporal pre-whitening seems to improve source estimates (Bijma et al., 2003; de Munck et al., 2002; Roś et al., 2015) but to our knowledge this has not been thoroughly tested when simulating realistic signals resembling actual measurements.

3.2 Materials and methods

In brief, we employed numerical simulations to test under which circumstances it is possible to disentangle sources in close proximity. We used two dipolar sources and a conventional realistic forward model to generate 62-channel EEG data. We studied the effects of distance between the generating sources and their temporal correlations as well as the impact of (white or realistic) noise with different signal-to-noise ratios (SNRs). For this we operationalized the notion of spatial resolution of EEG in terms of *separability*, i.e. how far apart two generating sources should be in order to distinguish them from the resulting EEG.

3.2.1 Data model

EEG measures changes in the scalp's electric potential. Current setups typically involve a large number of sensors covering the head with a specific arrangement (10-5, 10-20, 10-10, equidistant, etc.). The electric potential is believed to stem from the summation of post-synaptic potentials of (spatially aligned pyramidal) neurons. This source activity can be modeled by current dipoles. Let $j_m(t)$ represent the activity of a dipole at location $\vec{r}_m = (x_m, y_m, z_m)^T$ with orientation $\chi_m = (\varphi_m, \theta_m)^T$ and amplitude a_m. In recording number (trial) k this activity causes a time-dependent potential $b_{n,k}(t)$ at EEG electrode n. This can be formalized by

$$b_{n,k}(t) = L_{nm} j_m(t) + \varepsilon_{n,k}(t) \tag{3.1}$$

The gain L_{nm} is referred to as the leadfield and $\varepsilon_{n,k}(t)$ denotes background noise summarizing activity. The latter stems from background activity that, importantly, can be correlated in space and time. In this description one assumes the brain response $j_m(t)$ to be deterministic and independent of $\varepsilon_{n,k}(t)$ (de Munck et al., 2002). In the presence of more than one source, Eq. (1) has to be replaced by $b_{n,k}(t) = \sum_m L_{nm} j_m(t) + \varepsilon_{n,k}(t)$ or in vector notation

$$\vec{b}_k(t) = \underline{L}\vec{j}(t) + \vec{\varepsilon}_k(t) \tag{3.2}$$

where $\vec{j} = (j_1, j_2, \dots, j_M)^T$ summarizes all M dipole sources and $\underline{L}$ is the leadfield matrix mapping all the source activity to the N EEG channels $\vec{b}_k(t) = \left(b_{1,k}, b_{2,k}, \dots, b_{N,k}\right)^T$ in trial k.

Our characterization of background noise readily allows for introducing a definition of the recording's signal-to-noise ratio (SNR) in terms of

$$SNR = \frac{\langle \left| \underline{L} \cdot \vec{j}(t) \right|^2 \rangle}{\mathbb{E}\{\langle |\vec{\varepsilon}(t)|^2 \rangle\}} \tag{3.3}$$

where $\langle \cdots \rangle$ denotes the average over time t and $\mathbb{E}\{\cdots\}$ the expectation value over the realizations $k = 1, \dots, K$ (we estimated this by the mean over realizations). This definition appeared particularly useful for our simulation studies outlined below, since we had full control over the brain response $\vec{j}(t)$ and background noise $\vec{\varepsilon}_k(t)$.

Inverse methods

We selected three source localization algorithms: a stationary two dipole-fit (de Munck et al., 2002), the self-consistent (sc-)MUSIC (Shahbazi et al., 2015) and self-consistent exact (e)LORETA. We expected all the three methods to perform well in reconstructing cortical sources in close proximity.

The sc-MUSIC and sc-eLORETA algorithms are modified versions of the seminal MUSIC (Mosher et al., 1992) and eLORETA (Pascual-Marqui, 2007) methods, respectively. Both modifications account for the synchrony of generating sources and, hence, improve localization performance (Shahbazi et al., 2015) . The here newly formulated sc-eLORETA incorporates dipole fit and sc-MUSIC principles into the eLORETA spatial filter: The topography of the maximum of the eLORETA distribution is projected out of the data prior to iterating through subsequent eLORETA inverse solutions. Details of sc-eLORETA are provided in the *Appendix*.

3.2.2 Forward simulations

Head model and solution space

We incorporated a conventional three-shell boundary element method (BEM) volume conduction model as described by Oostenveld et al. (2003), expressed in MNI coordinates in mm. The geometry of BEM model was based on the “colin27” template. The forward model was also expressed in MNI coordinates and determined on a 3-mm grid using the fieldtrip open-source Matlab toolbox (Oostenveld et al., 2011). With the same toolbox, we determined the leadfield as a matrix that describes how the current flows from 11740 grid points to the 62 scalp electrodes.

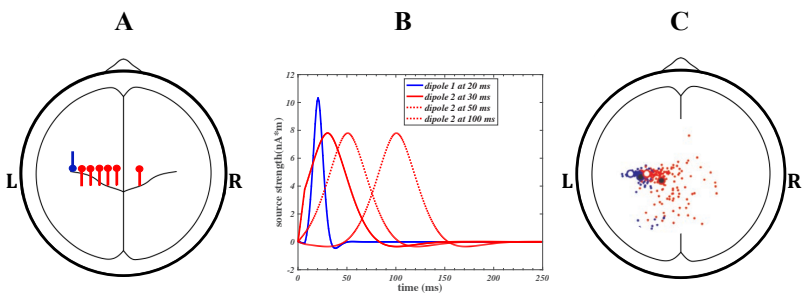

Fig. 3.1 Panel A: Positions of the simulated dipoles. Dipole 1 is plotted in blue, dipole 2 in red; the latter is shown at all spatial simulated distances. Panel B: Dipole waveforms used in the simulations (dipole 1 in blue, dipole 2 in red). For the temporal distances Δ=10, 30, and 80 ms the two dipoles were correlated by ρ=0.59, 0.2, and -0.02, respectively. Panel C: Dipole positions (dipole 1 in blue, dipole 2 in red) after 200 realizations of one condition: spatial distance d=18 mm, temporal distance Δ=80 ms and SNR=1, with additive spatially pre-whitened realistic noise. The dots filed in with white represent the true dipoles and the dots filled in with black represent the mean of the estimated dipoles.

Source position and waveforms

Focusing on somatosensory evoked potentials (SEPs) we placed sources at distinct positions in the cortex: two dipoles were placed in somatosensory areas with varying distance but fixed orientation, opposite to one another. The first one was always placed at the MNI location $\vec{r}_1 = (-40, -10, 50)$ and the second dipole

was placed more medial to the first one with an inter-dipole distance of $d = |\vec{r}_1 - \vec{r}_2| = 4,\ 10,\ 16,\ 22,\ 28,$ and 50 mm as depicted in Fig. 3.1 (panel A), both dipoles were placed in between the grid points (which were located at multiples of 3 mm, see also the Supplementary Material). The distance between the two dipoles will here be referred to as *spatial distance* d (in mm).

For all simulations, we chose the sources' time series to have SEP-like waveforms with a single main peak per dipole. The time series of dipole 1, the more lateral dipole, had an early peak around 20 ms, dipole 2 had a peak at either $10,\ 30,$ or 80 ms after dipole 1's peak (Fig. 3.1, panel B). We will refer to the distance between peaks as *temporal distance* Δ (in ms). Since both source signals overlapped in time, we finally estimated their temporal correlation via

$$\rho = \frac{\langle j_1(t) j_2(t) \rangle}{\sqrt{\langle j_1^2(t) \rangle \langle j_2^2(t) \rangle}} \tag{3.4}$$

Simulated EEG data

Scalp potentials were determined using the afore-described leadfield matrix and dipole location. The simulated EEG signals contained 62 channels (10-10 system, Oostenveld et al., 2011) referenced to average. We generated $K = 200$ trials of 250 ms each.

Noise

We added two distinct noise types to the scalp potentials and examined their effect on the source localization: (i) Gaussian *white noise* (uncorrelated in both space and time) and (ii) *realistic noise* that was spatially and temporally correlated. To construct this realistic noise, we used five minutes recorded 62-channel EEG during resting state (one healthy subject, female, age: 75 years, eyes open; Refa 64 EEG amplifier, TMSi Enschede, average referenced and sampled at 1024 Hz). These signals were segmented in epochs of 250 ms and mean centered. Segments with too high variance were rejected leaving 200 artifact-free noise segments. We scaled both white and realistic noise to obtain SNRs of $0.5,\ 1,\ 2,\ 3,\ 10,$ and 50 – see Eq. (3) for the SNR definition. We considered $SNR = 3$ a realistic

value for simulating somatosensory evoked potentials as indicated by an MEG study (Darvas et al., 2005). SNR of SEP responses might show inter-subject variations due to anatomical differences, as has recently been demonstrated in 5 healthy controls (Kalogianni et al., 2018): SNR estimates of 3.22±0.23 were found after averaging 750 trials after electrical stimulation of the fingers, which corresponds to an experimentation time of 5 min.

Pre-whitening: spatial and temporal covariance

In Eqs. (1&2), the noise terms $\varepsilon_{n,k}(t)$ or $\vec{\varepsilon}_k(t)$, respectively, may generally contain spatial and/or temporal correlations. Correlations in the noise manifest themselves as 'deterministic' components in the EEG signal. Estimating them can be used to improve source reconstruction by pre-whitening. Put differently, when reconstructing sources in the presence of background noise, one should try to account for the noise's covariance.

The spatiotemporal covariance C can be modeled as the Kronecker product of a spatial and temporal covariance matrices, $\underline{X}$ and $\underline{T}$, respectively, i.e. as

$$C = \underline{X} \otimes \underline{T} \tag{3.5}$$

These matrices, in turn, can be estimated from the multi-trial EEG data using a so-called flip-flop algorithm, as outlined by de Munck et al. (2002) and independently discovered in (Dutilleul, 1999; Leiva and Roy, 2014; Lu and Zimmerman, 2005). We would like to note that these covariances reflect the trial to trial variations of the true brain responses which are assumed to be constant. Therefore, these covariances reflect the brain state of the subject during stimulation and they do not require additional recordings during a baseline resting state.

The spatial and temporal covariance estimates resulting from the flip-flop algorithm, and $\hat{\underline{T}}$ are non-negative definite and can therefore decomposed as

$\hat{\underline{X}} = \underline{U_X}\underline{\Lambda_X}\underline{U_X^T}$ and $\hat{\underline{T}} = \underline{U_T}\underline{\Lambda_T}\underline{U_T^T}$, where $\underline{U_X}$ and $\underline{U_T}$ are orthonormal matrices and $\underline{\Lambda_X}$ and $\underline{\Lambda_T}$ are non-negative diagonal matrices. Substituting $\underline{W_X} \equiv \underline{U_X}\,\underline{\Lambda_X}^{-0.5}$ and $\underline{W_T} \equiv \underline{U_T}\,\underline{\Lambda_T}^{-0.5}$ one obtains the decompositions

$\underline{\hat{X}}^{-1} = \underline{W_X}\,\underline{W_X^T}$ and $\underline{\hat{T}}^{-1} = \underline{W_T}\,\underline{W_T^T}$ that can be used to pre-whiten the measurement noise: if $\vec{\varepsilon}$ is correlated noise with covariance $\underline{X} \otimes \underline{T}$ then $\underline{W_X^T}\,\vec{\varepsilon}\,\underline{W_T}$ is spatially and temporally uncorrelated.

In our simulations, we only consider spatial pre-whitening, though the spatial covariance matrix is derived from the flip-flop algorithm applied to resting state EEG. As a result, we pre-whiten the data and the leadfield as follows (see, de Munck et al., 2002, for details)

$$\vec{b}_W = \underline{W_X^T}\,\vec{b}\,\underline{W_T} \tag{3.6}$$

and the leadfield with

$$\underline{L_W} = \underline{W_X^T}\,\underline{L} \tag{3.7}$$

Extending the work by de Munck et al. (2002) and de Munck and Bijma (2009), we here concentrated on the effect of spatial pre-whitening using realistic noise for the three inverse algorithms tested, i.e. we ignored $\underline{T}$ and $\underline{W_T}$ in Eqs. (3.5) and (3.6), respectively.

Implementation of inverse methods

The stationary dipole fit algorithm modified by De Munck (1990) – see also (de Munck et al., 2002) was implemented in Matlab[3], building on the skeleton coding for dipole fitting in fieldtrip (Oostenveld et al., 2011). We included a global grid search for two dipoles that are up to 20 mm apart from the position of the simulated ones. With these initial values, we optimized by iterating Eqs. (27) and (32) in (de Munck et al., 2002). Using the resulting asymptotic solution, we finally determined the localization error per trial k as the Euclidian distance between the true (simulated) and the estimated dipoles, i.e. $\mathcal{E}_k = \left|\vec{r}_{k\,\mathrm{original}} - \vec{r}_{k\,\mathrm{estimated}}\right|$.

Our implementation of the sc-MUSIC algorithm was based on (Shahbazi et al., 2015). In brief, with M dominant singular value decomposition (SVD) components

[3] The corresponding code can be accessed freely upon request.

defining the signal (sub)space, the algorithm yields as many vectors with the length of the grid points. The maximum per vector is considered the sc-MUSIC solution and refers to M positions on the grid.

We implemented a self-consistent version of eLORETA (Pascual-Marqui et al., 2011). This sc-eLORETA algorithm is described in detail in the *Appendix*. Its output agrees in form with that of sc-MUSIC, i.e. we took the maximum of M distributions on the grid. Throughout analysis we assumed that $M = 2$, since we employed two 'true' sources.

A proof-of-concept for all the three tested algorithms is provided as *Supplementary Material*.

3.2.3 Evaluation

Comparing true and estimated sources: Localization error

After computing the inverse solutions of the stationary dipole fit, the sc-MUSIC, and the sc-eLORETA, every pair of estimated dipoles was compared with a pair of true dipoles[4]. Because the estimated dipoles might have been swapped relative to the simulated one, we computed the sum of distances for every trial k for the two possible permutations, $\mathcal{E}_{k,11/22} = \left|\vec{r}_{k,\mathrm{original},1} - \vec{r}_{\mathrm{k,estimated},1}\right| + \left|\vec{r}_{k,\mathrm{original},2} - \vec{r}_{k,\mathrm{estimated},2}\right|$ and $\mathcal{E}_{k,12/21} = \left|\vec{r}_{k,\mathrm{original},1} - \vec{r}_{k,\mathrm{estimated},2}\right| + \left|\vec{r}_{\mathrm{k,original},2} - \vec{r}_{k,\mathrm{estimated},1}\right|$, and considered the least of the two as minimum error denoted as $\mathcal{E}_k$. We note that in all Fig.s the estimated dipole 1 refers always to the most lateral and dipole 2 is always the most medial.

The Euclidean distance $\mathcal{E}$ between the true dipoles and the estimated dipoles was determined for each of the $K = 200$ noise realizations. The resulting mean distances from the true locations and the corresponding standard error of the mean were determined for every SNR, for every spatial and temporal distance, and for the three algorithms.

[4] The dipole fit's solutions were not necessarily located on a grid point, while sc-MUSIC and sc-eLORETA were always estimated on the grid; no interpolation was applied for any of the algorithms' output.

Separability index

Next to the comparison with the known locations, we defined a separability index $\mathcal{S}$ as the Euclidean distance[5] $\mathcal{C}_{12} = \left|\mathbb{E}\{\vec{r}_{k,\text{estimated},1}\} - \mathbb{E}\{\vec{r}_{k,\text{estimated},2}\}\right|$ of the two centers of distribution of location estimates divided by the sum of the corresponding standard deviations σ_1 and σ_2 around these centers

$$\mathcal{S} = \frac{\mathcal{C}_{12}}{\sigma_1 + \sigma_2} \tag{3.8}$$

$\mathcal{S} \geq 1$ implies that, on average, the representations of two dipoles can be separated. Through interpolation we subsequently determined how far apart the underlying sources should be in order to reach $\mathcal{S} = 1$, i.e. a *separability index* of one or proper separation of sources. We propose this distance as an operational definition for spatial resolution of EEG.

3.3 Results

Fig. 3.2 shows that spatial pre-whitening improved all methods' accuracy significantly in the realistic noise case even if signal-to-noise ratio is as low a $SNR = 0.5$. When accounting for the spatial correlations in the noise, the localization error reduced and matched that of the Gaussian white noise case. The dipole fit was more accurate in localizing the true sources both with white and realistic noise than the other inverse methods.

[5] We accounted for a possible swap between estimated dipoles $1 \leftrightarrow 2$ as outlined in 2.4.1.

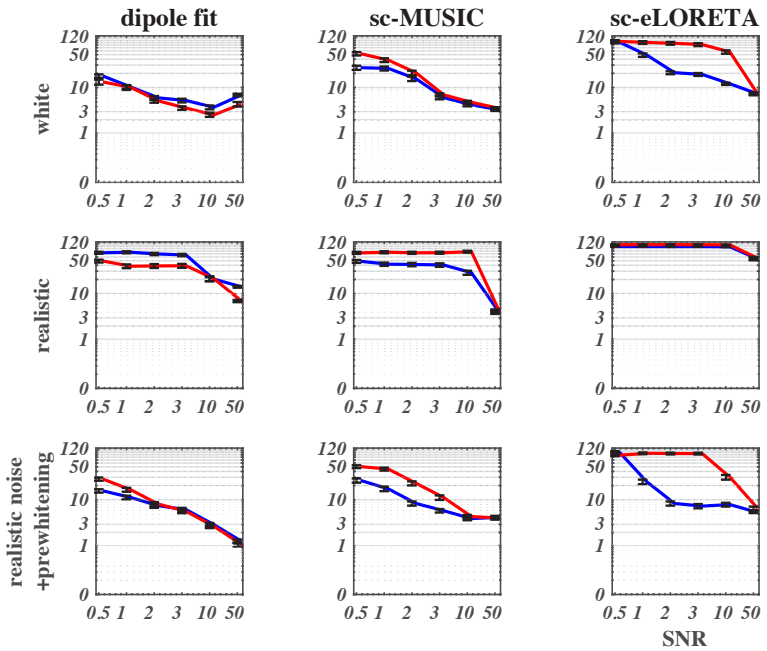

Fig. 3.2 Mean and standard error of the mean of found solutions (in mm). Here, the spatial distance d=16 mm and the temporal distance Δ=30 ms is shown. The blue symbols represent the most lateral dipole and with red the most medial dipole. The columns show the results for the three tested algorithms: stationary dipole fit, sc-MUSIC, sc-eLORETA. We found that realistic noise affects the source localization accuracy of all the algorithms (cf. 1st and 2nd row). However, spatial pre-whitening (3rd row) clearly improved accuracy of all the algorithms and produced results similar to the white noise case. Dipole fit has the best accuracy of all the algorithms; a low localization error could be observed for dipoles that were placed 16 mm part and further for a realistic data situation of $SNR = 3$. For an example of the corresponding dipole orientation see Fig. S3.6 in the Supplementary Material.

This was expected as we simulated two dipoles and used this knowledge about the number of sources by designing the fitting procedure, which might be an uncertain assumption in most practical applications. Sc-MUSIC had overall the second-best accuracy followed by sc-eLORETA. However, also for sc-eLORETA our spatial pre-whitening improved accuracy. When spatial pre-whitening was applied, the true sources were separated by 22 mm and, when dipole fitting was employed, the localization error was 3 mm at $SNR = 3$ and dropped to 1.5 mm when the sources were 50 mm apart.

A complete separation ($\mathcal{S} \geq 1$) of the two dipoles was possible when the two simulated dipoles were 50 mm apart, even at low SNRs and for all the inverse methods; see Fig. 3.3. The dipole fit had better ability in disentangling two dipoles in close proximity. Simulated dipoles that were 28 mm apart were almost separable at $SNR = 0.5$ even when realistic noise was added to the signals. For a spatial distance of 16 mm, the dipoles were just separable at $SNR = 3$. As expected, the separability increased with increasing distance of the true sources throughout inverse methods.

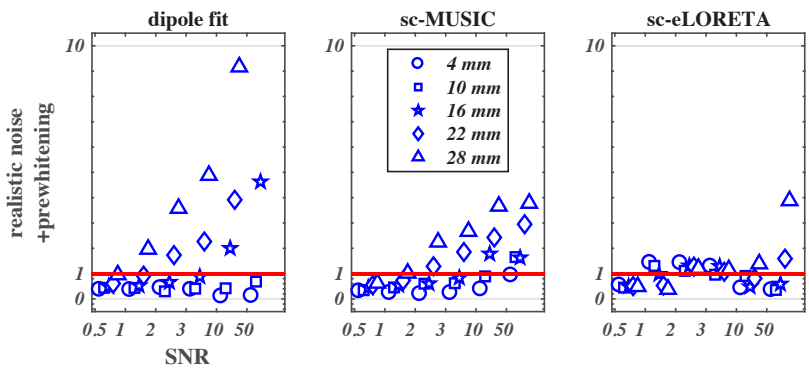

Fig. 3.3. Separability as a function of SNR. Values lower than one imply that the dipoles were not separable due to the large standard deviation. The different symbols represent the different spatial distances between the simulated dipoles. The rows show the results for the tested algorithms: stationary dipole fit, sc-MUSIC, sc-eLORETA when spatial pre-whitening is applied on the realistic noise case. The temporal distance of Δ=30 ms is shown.

For every SNR, every inverse method, and every temporal distance between the peaks of the sources' time series, there was a spatial distance that separability $\mathcal{S}$ dropped below 1 dependent of the spatial distance of the simulated dipoles. As said, we used $\mathcal{S} = 1$ to define a spatial resolution, i.e. the least distance of simulated source that could still be separated. For example, when the temporal distance was 10 ms, $SNR = 3$, the realistic noise is spatially pre-whitened and dipole fitting was used for source estimates, the separability was lower than one if the true sources were 10 mm apart but larger than one for dipoles that were 16 mm apart. After interpolation between the here-used discrete spatial distance

steps, the separability results could be summarized in Fig. 3.4. Taken together, for the two-dipole fit and for sc-MUSIC we found full separability in the realistic case of $SNR = 3$ when the underlying sources where at least 11 mm apart.

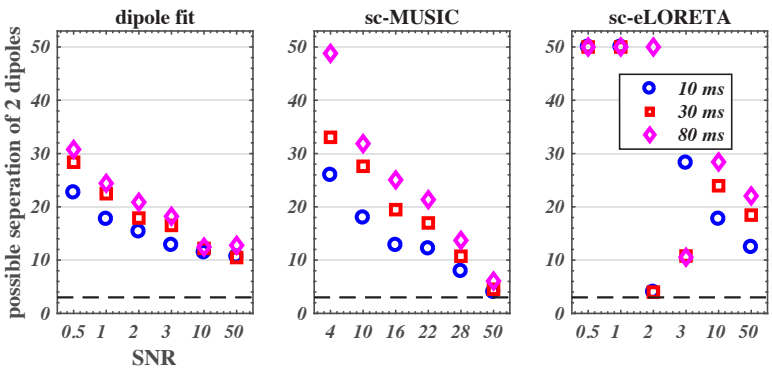

Fig. 3.4. Possible separation of the two dipoles in mm at a function of SNR. Through interpolation we estimated how far apart the original dipoles should be in order to obtain a separability of one or large, i.e. to be able to completely separate them. Blue circles represent a temporal distance of 10 ms, red squares of 30 ms and purple diamonds 80 ms. The dotted line represents the grid resolution ($= 3\,mm$). We present a possible separation up 50 mm because this was the largest simulated inter-dipole distance.

3.4 Discussion

Despite advanced pre-processing, the presence of realistic noise reduced accuracy, precision (as given by the standard error of the mean), and separability across algorithms. Still they appear somewhat disappointing as advanced source reconstruction methods, like sc-eLORETA, are often believed to provide way better accuracy and separability, which we cannot confirm with our simulations. We must admit that we here conducted source reconstruction in conditions in which sources are very close to each other while the number of included EEG electrodes was fairly small. We used the latter to highlight limitations and, by the same token, to resemble yet common clinical practice. We expect that high-density EEG with 128 or 256 electrodes will improve separability and, hence, the spatial resolution but leave it to future studies to address this in more detail. We would like to note that the theoretical limits of the here-employed inverse models are presumably way

below the suggested spatial resolution that results from our simulation, as the resolution will continue to increase in the case of perfect models.

The good news is that spatial pre-whitening of the recorded signal (and the leadfield) can in general improve accuracy irrespective of the algorithm employed. We showed that this pre-processing provides results comparable to the ones observed in the white, uncorrelated noise. The positive effect of spatial pre-whitening has already been demonstrated in the literature (Bijma et al., 2005; Engemann and Gramfort, 2015; de Munck et al., 2002; de Munck and Bijma, 2009). However, with our study we went a step further in that even sources in close proximity could be disentangled when spatial pre-whitening was applied. As said, we consider spatial pre-whitening a mandatory pre-processing step when it comes to source estimates for either linear or non-linear inverse models, as also stated for a time-frequency approach (Ramírez et al., 2011).

We found a positive association between the spatial distance of the underlying sources and the accuracy of all inverse methods. When the simulated sources were 4 mm apart, it was virtually impossible to retrieve them with any of the inverse methods applied. If the simulated dipoles were 16 mm apart and dipole fit was used as an inverse method, the localization error dropped to 10 mm and lower dependent on the SNR. Given a grid size of 3 mm and $SNR = 3$, the maximum resolution was 11 mm in the presence of realistic noise (after spatially pre-whitening). Dipole fitting and sc-MUSIC revealed about the same capacity to separate sources. If the SNR exceeded values of 10 (a rather unrealistic case) sc-MUSIC remained able to disentangle sources that were up to 4 mm apart, which is a clearly higher spatial resolution than reported by Yao and Dewald 2005. Here we can conclude that whenever the assumption of a small number of sources can be made, then least squares or scanning methods appear the best inverse modeling choices as opposed to distributed methods like (sc-)eLORETA.

In our setting, the dipole fit outperformed the alternative source reconstructions in terms of accuracy and separability. This was expected since the constraints of the algorithm (two dipolar sources) simply resembled what we designed in our simulations. We used a stationary dipole fit as a – what we consider legitimate – test for our simulations where the number of sources is already known. However,

sc-MUSIC and all the algorithms based on singular value decomposition offer the possibility of a priori estimating the number of underlying sources through identifying the number of prominent singular components. As summarized in Fig. 3.5, we found the relationship between separability and the existence of one or two prominent components after singular value decomposition of the pre-whitened simulated data with added realistic noise and $SNR = 3$.

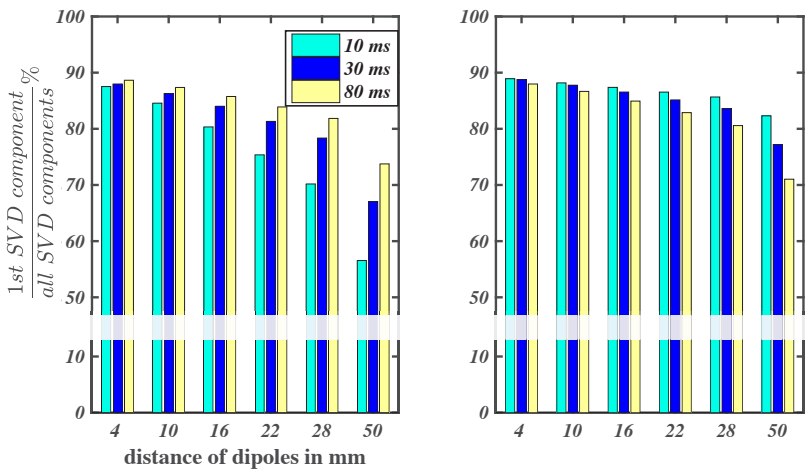

Fig.3.5 SVD of the simulated data with added pre-whitened noise (SNR=3). The ratio of the square of the 1st SVD component to the sum of squares of all the components for all the temporal and the spatial distances of the underlying sources is presented. The left panel shows the here-simulated case is, i.e. dipoles with opposite orientations with higher temporal distance the ratio of the 1st to the rest of the components increases. This suggests a less prominent 2nd component and therefore less separability of sources. In the right panel, we show the exactly opposite behavior when the simulated dipoles have the same orientation.

We always assumed two underlying sources and therefore selected the two first higher components as the signal subspace. We can verify that when dipoles are 4 mm apart the ratio between the first and the rest of the components is fairly high, implying that only a single underlying source can be modeled. This finds support by the results in Fig. 3.4 showing that separability $\mathcal{S}$ dropped below one when the dipoles were 4 mm apart or less. It seems safe to say that sc-MUSIC is an accurate choice when an unknown number of underlying sources are present in

the time window of exploration, due to the fact that it gives a good estimate of the inverse model capabilities.

Temporal correlation of time series had a comparably small but positive effect on the accuracy of the algorithms. This is a striking but positive finding. It does suggest that sources that are active in a serial way with a small time-difference can be accurately found when there are sufficiently spatially distinct from one another. In our simulation, we constructed the underlying dipoles to have opposite orientations. Testing the case where the dipoles had the same orientations provided a positive relationship of the height of the second component of SVD and the temporal distance, meaning that when dipoles had a smaller temporal distance, the second largest component was closer to zero. Further investigation is needed to see if dipoles with the same direction need to be active with a sufficient time-delay in order to be able to adequately disentangle them.

Hu et al. (2012) and Gao et al. (2015) demonstrated that somatosensory evoked source activity in S1 and S2 were almost 50 mm apart on average when looking at activity from 70 to 200 ms post stimulus. This clearly falls within our range of separability. However, when looking within S1, our study suggests that one can successfully study the underlying sources presuming that are at least 11 mm apart. This, of course, requires spatial pre-whitening (and an SNR of at least 3). For example, as shown by an MEG study the cortical responses of the median and ulnar nerve within left hemisphere S1 (early responses) are 11 mm apart (Theuvenet et al., 2006) and therefore could be disentangled with our method and the use of EEG. Tailored forward models that take into account subject-specific conductivity parameters (Dabek et al., 2016) may improve the spatial resolution of EEG. In any case, we can conclude that including pre-whitening as pre-processing steps improves any inverse method's capacity of source separation, as indicated more than 20 years ago by (Mosher et al., 1993).

3.5 Conclusion

We found that a proper separation of two sources is possible if they are placed 11 mm or further apart and if additive, EEG-based noise keeps the signal-to-noise

ratio at 3 or higher. Separability appears a legitimate measure to quantify EEG's spatial resolution. Obtaining an optimal resolution in source reconstruction, however, required spatial pre-whitening as a crucial if not mandatory pre-processing step.

Conflict of interest

The authors declare that they have no conflict of interest.

Funding

The research leading to these results has received funding from the European Research Council under the ERC grant agreement no. 291339, project name: 4D-EEG. Guido Nolte received financial support by the German Research Foundation (DFG, SFB938/Z3 and TRR-169/B4) and from the Landesforschungsförderung Hamburg (CROSS, FV25).

3.6 Appendix

We modified the eLORETA algorithm (Pascual-Marqui, 2007) by iteratively applying its filter to obtain estimates of separate sources. This iteration is similar to the method used in the sc-MUSIC algorithm described by Shahbazi et al. (2015).

Per iteration the eLORETA filter is computed and applied to the data. The computed topography corresponding to the source at the maximum of the eLORETA scan is then projected out of the data and the leadfield matrix, and the eLORETA filter is computed and applied again to find a different source. The process continues until the algorithm converges to the M distributions best explaining the locations of the m sources. The maximum of each distribution can be considered as the solution that best matches the field distribution of n point sources.

eLORETA is a weighted minimum norm estimate solution that assumes smoothness of the source distribution, implemented by the l^2-norm in the regularization term of LORETA. The assumption here is that neighboring voxels show similar activations and that there are no maximum peaks expected at the

nearby grid points. The weight matrix is defined such that a distributed linear inverse solution has a localization error of zero when tested with point sources everywhere in the brain. In this way, deep sources are taken into account, minimizing the bias towards superficial sources.

The spatial filter of eLORETA is computed by a quickly converging algorithm (Pascual-Marqui, 2007; Pascual-Marqui et al., 2011), which starts with

$$\underline{\Omega}_m^2 = \underline{L}_m^T (\underline{L}\underline{\Omega}^{-1}\underline{L}^T + \kappa\underline{H})^+ \underline{L}_m \tag{A3.1}$$

where, $\underline{L}_m$ is the forward matrix of the m^{th} grid point, $\underline{\Omega}_m \in \mathbb{R}^{3\times3}$ denotes a block matrix around the M diagonal elements of $\underline{\Omega}$ and $\underline{\Omega}$ is the smoothness constraint. $\underline{\Omega}$ is subsequently substituted into

$$\underline{W}_{eloreta} = \underline{\Omega}^{-1}\underline{L}(\underline{L}\underline{\Omega}^{-1} + \underline{L}^T + \kappa\underline{H})^+ \tag{A3.2}$$

to form the eLORETA spatial filter. In the case of sc-eLORETA, the $\underline{W}_{\text{eLORETA}}$ is applied to the data and a projection matrix is given as

$$\underline{Q} = \underline{I} - \underline{A}(\underline{A}^T\underline{A})^{-1}\underline{A}^T \tag{A3.3}$$

where $\underline{A} = [T_1 T_2 \ldots T_{n-1}]$ is the $N\times(n-1)$ matrix containing the previously found dipole patterns as columns; N is the number of M/EEG channels; cf. Eq. 2 in (Shahbazi et al., 2015). This iterative procedure yields n separate source locations. As such, sc-eLORETA can be directly compared to the stationary dipole fit and sc-MUSIC.

3.7 Supplementary material

Fig. S3.1 presents a validity test for the three algorithms for a very weak noise situation ($SNR = 50$). In the case of dipole fit, the distance from the simulated dipole is 0, while in the case of sc-MUSIC and sc-eLORETA the localization error is 2 mm. Note that 2 mm is the distance of the simulated dipole to the closest grid point and due to the fact that sc-MUSIC and sc-eLORETA are constrained on the grid points, this is the least possible localization error.

We observe that when two dipoles are simulated (200 realizations), the accuracy of the algorithms decreases. The smallest localization error appears when the dipoles are separated 50 mm and when with the simulated dipoles are 4 mm apart the localization error varies from 3.5 (dipole fit) to 100 mm (the most medial dipole with sc-eLORETA). The correlation of sources' time series did not play an important role in the case of dipole fit or sc-ELORETA but did so in the case of sc-MUSIC (more correlated, better accuracy).

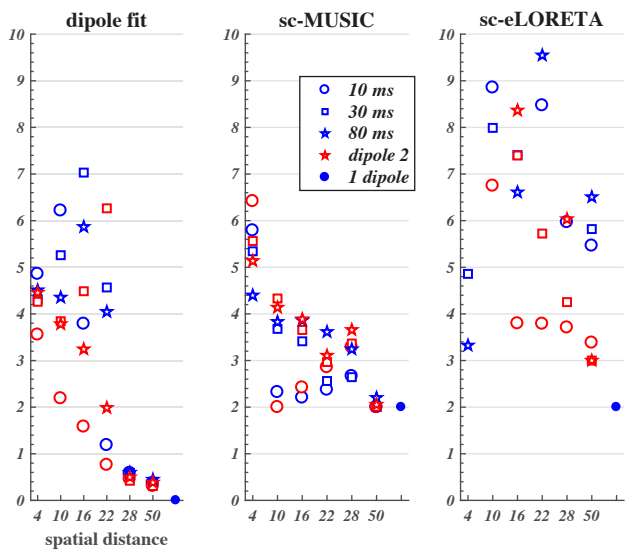

Fig. S3.1 Mean distance from simulated dipole(s). Comparison of one dipole simulation versus two dipoles simulation for the ideal case of added white noise and $SNR = 50$. The black line depicts the grid size (3 mm). The different symbols represent the different temporal distances of the sources time-series peaks.

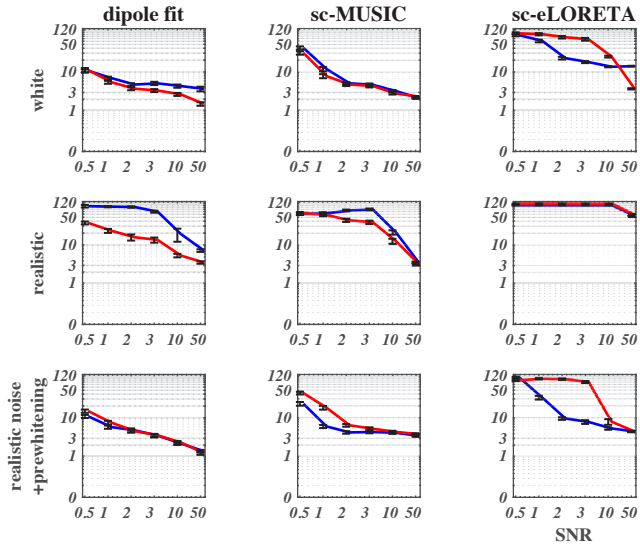

Fig. S3.2 Mean and standard error of the mean of found solutions (in mm). Here, the spatial distance d=16 mm and the temporal distance Δ=10 ms is shown. The blue symbols represent the most lateral dipole and with red the most medial dipole. The columns show the results for the three tested algorithms: stationary dipole fit, sc-MUSIC, sc-eLORETA. We found that realistic noise affects the source localization accuracy of all the algorithms (com. 1st and 2nd row). However, spatial pre-whitening (3rd row) clearly improved accuracy of all the algorithms and produced results similar to the white noise case. Dipole fit has the best accuracy of all the algorithms; a low localization error could be observed for dipoles that were placed 16 mm part and further for a realistic data situation of $SNR = 3$.

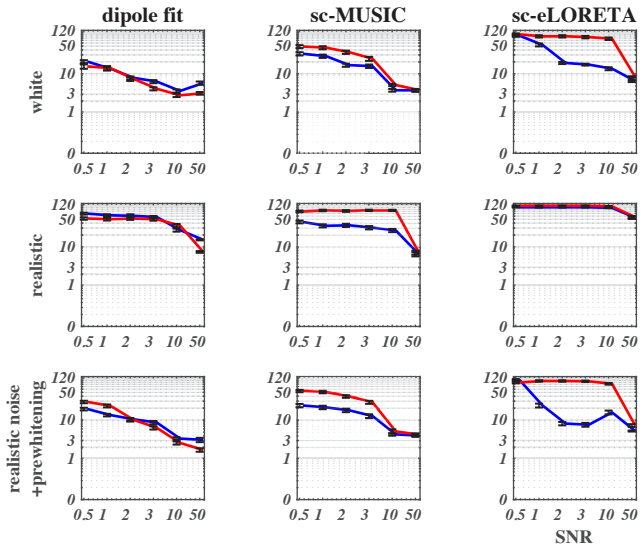

Fig. S3.3 Mean and standard error of the mean of found solutions (in mm). Here, the spatial distance d=16 mm and the temporal distance Δ=80 ms is shown. The blue symbols represent the most lateral dipole and with red the most medial dipole. The columns show the results for the three tested algorithms: stationary dipole fit, sc-MUSIC, sc-eLORETA. We found that realistic noise affects the source localization accuracy of all the algorithms (com. 1st and 2nd row). However, spatial pre-whitening (3rd row) clearly improved accuracy of all the algorithms and produced results similar to the white noise case. Dipole fit has the best accuracy of all the algorithms; a low localization error could be observed for dipoles that were placed 16 mm part and further for a realistic data situation of $SNR = 3$.

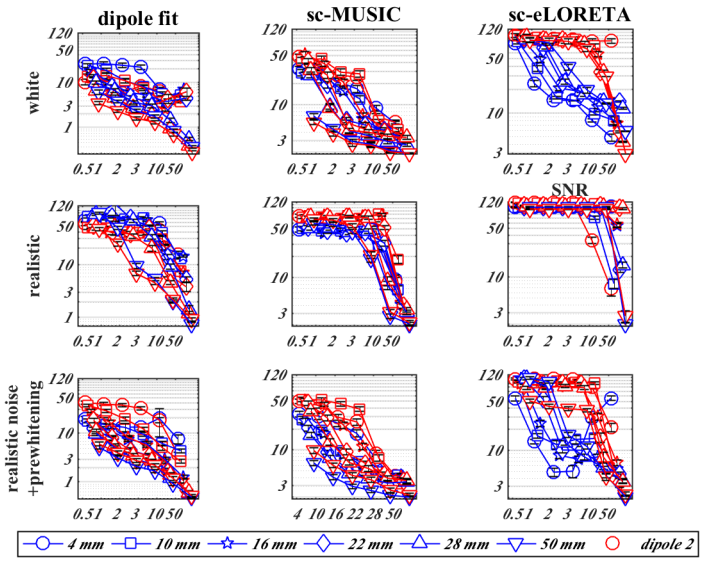

Fig. S3.4 Mean and standard error of the mean of found solutions (in mm). Here, the temporal distance Δ=30 ms is shown. The blue symbols represent the most lateral dipole and with red the most medial dipole. The different symbols represent the different spatial distances between the simulated dipoles. The columns show the results for the three tested algorithms: stationary dipole fit, sc-MUSIC, sc-eLORETA. We found that realistic noise affects the source localization accuracy of all the algorithms (com. 1st and 2nd row). However, spatial pre-whitening (3rd row) clearly improved accuracy of all the algorithms and produced results similar to the white noise case. Dipole fit has the best accuracy of all the algorithms; a low localization error could be observed for dipoles that were placed 16 mm part and further for a realistic data situation of $SNR = 3$

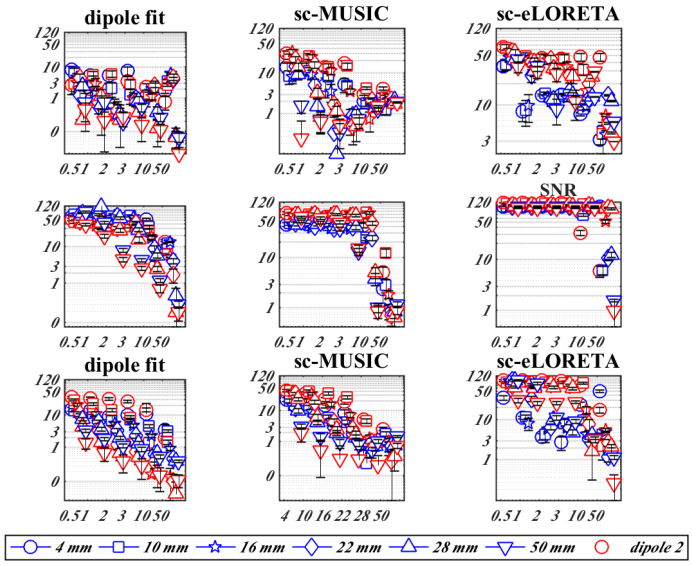

Fig. S3.5 Localization bias: distance of mean location (200 realizations) from simulated dipole and standard error of localization bias (in mm). Here, the temporal distance Δ=30 ms is shown. The blue symbols represent the most lateral dipole and with red the most medial dipole. The different symbols represent the different spatial distances between the simulated dipoles. The columns show the results for the three tested algorithms: stationary dipole fit, sc-MUSIC, sc-eLORETA.

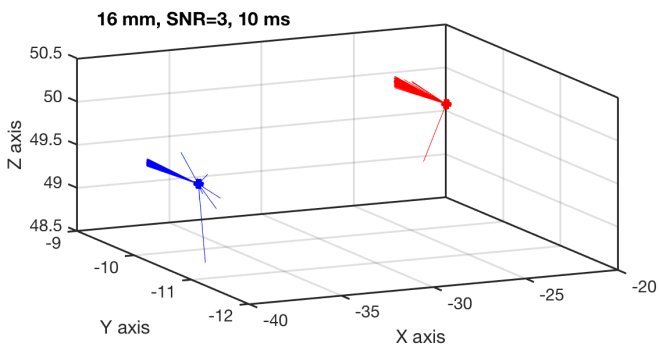

Fig. S3.6 Effect of dipole orientation: the mean location (200 realizations) is plotted as a filled dot and around it the vectors (lines) with orientation (x,y,z) of 200 realizations. The blue symbols represent the most lateral dipole and with red the most medial dipole. The spatial distance d=16 mm and the temporal distance Δ=30 ms and the SNR= 3 is shown.

Chapter 4

Are longitudinal SEP recordings a biomarker for proportional motor recovery post stroke?[6]

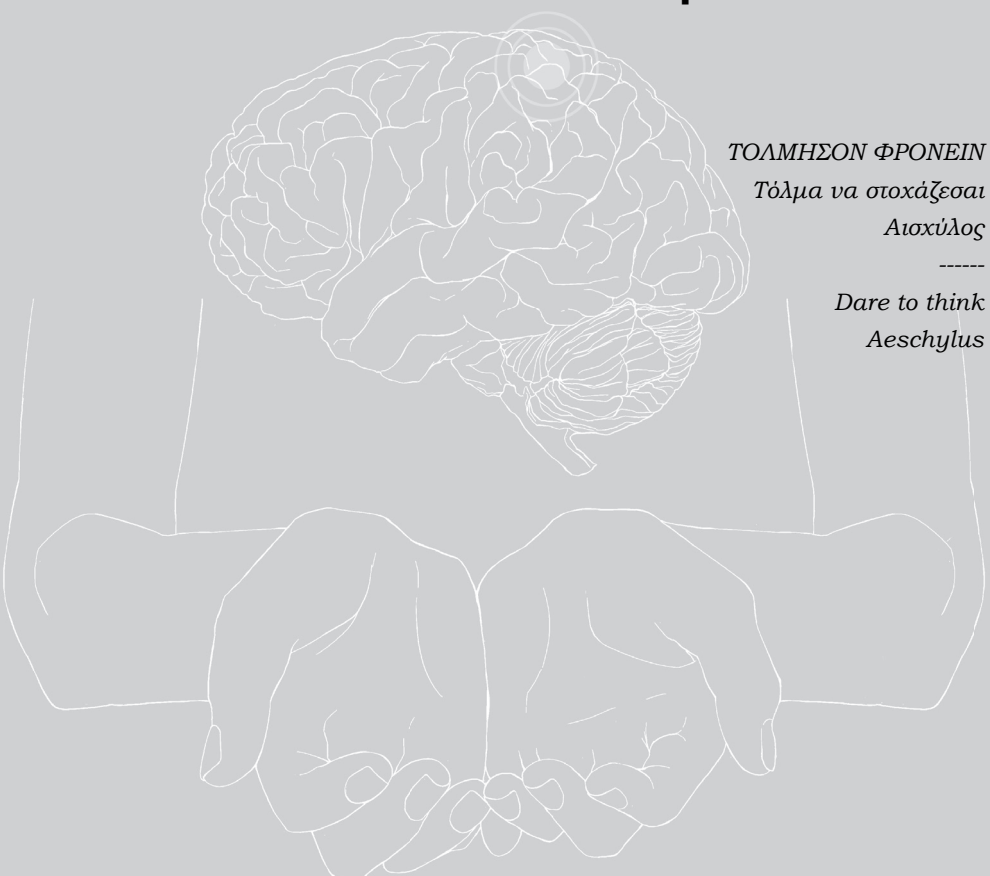

ΤΟΛΜΗΣΟΝ ΦΡΟΝΕΙΝ
Τόλμα να στοχάζεσαι
Αισχύλος

Dare to think
Aeschylus

[6] Submitted: Konstantina Kalogianni, Mique Saes, Martijn P. Vlaar, Erwin van Wegen, Gert Kwakkel, Alfred C. Schouten, Frans C.T. van der Helm, Andreas Daffertshofer, Jan C. de Munck, on behalf of the 4D-EEG consortium, Are longitudinal SEP recordings a biomarker for proportional motor recovery post stroke?

ABSTRACT

Background: At present, it is not well understood which patients will regain motor control post ischemic stroke.

Objective: This study explores the use of somatosensory evoked potentials (SEPs) as biomarkers for early prediction of proportional motor recovery post stoke.

Methods: In 16 first-ever ischemic hemispheric stroke patients (12 completed), SEPs induced by electrical stimulation of the median nerve were recorded at three time points post stroke (T0:1-4 weeks post-stroke, T1:5-6 weeks post-stroke, T2:12 weeks post stroke) using 64-channel electroencephalography (EEG). In addition, six unimpaired participants were recorded twice. Based on Fugl-Meyer scores of the Upper extremity (FM-UE), patients were divided into fitters and non-fitters following the 70% proportional recovery rule. A support vector machine algorithm (SVM) was used to predict, based on normalized SEP parameters, which patients belong to each group.

Results: In the controls, the interclass correlation coefficients of three of the four amplitude/latency SEP parameters were significant. The variability of these parameters was much higher in patients than in controls. Normalized SEP parameters at T1 were associated with fitters (n=7) and non-fitters (n=5), The resulting SVM had an accuracy of 86% tested through a leave-one-out procedure. When the SVM was fed with the SEP features of the controls, they were all classified in the same category as the fitters.

Conclusions: Our results suggest that normalized SEP parameters recorded five weeks post stroke have predictive value for stroke recovery. The predictive capacity of SEP, demonstrated in this study, needs to be confirmed in a larger sample of this ongoing cohort.

4.1 Introduction

Despite the continuously advancing care, stroke remains the second-leading cause of disease burden (Feigin et al., 2015; Miller et al., 2010). In the next years we will continue to see an increase in the global burden of stroke, mainly due to the increase in the absolute number of disability-adjusted life years in developing countries and the ageing population (Bernhardt et al., 2017; Feigin et al., 2015). The challenge set out for stroke rehabilitation research is to reduce patients' disability and handicap by optimizing early prediction and therapeutic care (Bernhardt et al., 2017; Ward, 2017).

Stroke recovery is heterogeneous in its nature, making early prediction paramount for optimizing discharge policies and selecting the most appropriate therapy early post stroke (Langhorne et al., 2011). Several cohort studies have shown that the patterns of recovery in terms of body functions such as Fugl Meyer motor scores (FM-UE) (Kwakkel et al., 2003) and activities such as Action Research Arm Test (Nijland et al., 2010a; Stinear, 2010) are highly predictive for the upper paretic limb in the first days after stroke (Nijland et al., 2010a; Stinear, 2017). The Fugl-Meyer (FM) score is a measure that captures intra-limb motor control and therewith the patient's ability to control multiple degrees of freedom during meaningful tasks such as reaching (Kordelaar et al., 2013). FM scores of the upper (UE) and lower extremity (LE) can be considered a reliable and valid measure of motor recovery post stroke (Duncan et al., 1983; Gladstone et al., 2002) genuinely reflecting true neurological repair (Bernhardt et al., 2017; Kwakkel et al., 2017).

Prabhakaran et al. (2008) have formulated the so-called proportional recovery rule, which states that patients recover approximately 70% of the maximum possible motor recovery based on the FM-UE. This has been confirmed by Winters and co-workers (2015) in 211 patients with a first-ever ischemic stroke. In that study, it was also found that about 30% of their cohort of first ever ischemic stroke patients did not follow this "70% rule" (so-called non-fitters). In particular, patients with initial poor FM-UE did not fit to the "70% rule". Stratification based on the combination of clinical and neurophysiological parameters may help to optimize therapy selection during recovery and especially for those patients with initial low FM-UE scores

(Boyd et al., 2017; Ward, 2017; Winters et al., 2016a). Hence, there is an urgent need for stroke rehabilitation recovery trials to identify the neurophysiological biomarkers that can distinguish fitters from non-fitters of spontaneous neurobiological recovery early post stroke (Bernhardt et al., 2017; Boyd et al., 2017; Corbett et al., 2017; Ward, 2017).

Brain imaging techniques can be used to unveil the mechanisms of stroke recovery by giving more insights into the physiology of the brain during the recovery process, especially for patients that do not fit in the aforementioned recovery model. Functional imaging techniques like functional magnetic resonance imaging (fMRI) can help to uncover the relationship between recovery and task-related functional properties of the motor system after stroke (Ward et al., 2003). Recent studies emphasized the need for clinically useful, easy to perform and non-invasive imaging techniques that can generate new prediction models of stroke recovery (Rollnik, 2015; Ward, 2015).

The predictive value of intactness of somatosensory integrity for identifying fitters from non-fitters of proportional recovery is still a neglected field in stroke research. However, several studies suggest that somatosensory impairment is highly associated with stroke severity (Connel et al., 2008; Meyer et al., 2016). To date, the likelihood for return of voluntary finger extension within the first 8 weeks post stroke was strongly associated with intactness of somatosensory and lower limb function as well as absence of visuospatial neglect after stroke (Winters et al., 2016b). However, studies in which the integrity of somatosensory function is investigated are almost lacking in the literature.

Somatosensory evoked potentials (SEPs) or fields (SEFs), measured with electroencephalography (EEG) or magnetoencephalography (MEG), respectively, are non-invasive techniques that may reveal the role of somatosensory integrity early post stroke. (Hari and Forss, 1999). After electrical stimulation of the median nerve, several peaks can be detected in the stimulus-related EEG/MEG response in the S1 (early responses from 20 to 60 ms) or S2 cortices (later responses from 100 to 300 ms, Forss et al., 1994a) contralateral to the stimulation. Abnormal responses measured with MEG/EEG correlate with clinically observed impairment of stroke patients and longitudinal alterations of their responses after stroke onset

can reveal recovery (Laaksonen et al., 2013). Small SEF amplitudes or absence of early SEF responses (20-30 ms) correlate with a more severe impairment (Feys et al., 2000; Huang et al., 2004; Keren et al., 1993; Oliviero et al., 2004; Tecchio et al., 2007a; Tecchio et al., 2006; Tzvetanov and Rousseff, 2003; Wikström et al., 2000, 1999). Moreover, interhemispheric latency differences of the early peaks correlate with a high level of impairment (Oliviero et al., 2004; Tecchio et al., 2001). In contrast to MEG, EEG is an easy to perform and ambulant method which can be applied not only in research settings but also in hospitals and rehabilitation centers. With that, longitudinal studies using EEG can be executed irrespective of location of admission, or even in patients own home. Longitudinal tracking of patients with SEP recordings may offer new insights into the dynamics of stroke recovery as recommended recently by the stroke recovery and rehabilitation roundtable task force (Boyd et al., 2017; Ward, 2017, 2015).

In the present study, we prospectively explored the relationship between SEP responses measured three times after stroke onset and the longitudinally recorded clinical motor and sensory scores, recorded four times post stroke. The goal of the present study was to generate a verifiable quantitative hypothesis that predicts which patients will follow the spontaneous neurobiological recovery rule and which ones will fail, on the basis of SEP biomarkers.

4.2. Methods

4.2.1 Subjects and clinical testing

The present study is part of a larger cohort study (European Research Council, 4D-EEG project), wherein EEG and clinical parameters are recorded. The cohort study protocol had been approved by the Medical Ethical Reviewing Committee of the VU University Medical Center Amsterdam (registration number 2014.140). All participants gave their written informed consent prior to the measurements.

Sixteen participants with a first-ever ischemic hemispheric stroke (75±11 years, 9 male, 9 with a lesion in the right hemisphere) were included in this study (see Table A4.3 in the Appendix for more details). Additional inclusion criteria were: 1) < three weeks post stroke onset, 2) upper limb paresis (NIHSS 5a/b >0), 3) ≥ 18

years of age, 4) Mini Mental State Examination score ≥ 20. Exclusion criteria were: 1) upper extremity orthopedic limitations before stroke onset, 2) other neurological disorders. Because from each patient also an MRI scan was made half a year post stroke, we also excluded patients with a pace maker. However, MRI data were not used in the present study. In addition, six unimpaired participants (54±5 years, five men) were included, who met the two last inclusion criteria and were recorded twice with a week in between the measurements.

Clinical testing of the patients and EEG recordings were performed from the sub-acute phase (one week post-stroke) to the chronic stage (six months post-stroke): at one-four weeks (T0), five-six weeks (T1), three months (T2) and six months (T3) after stroke. Clinical testing and EEG were recorded with one day in between. At T3 no EEG was recorded. Sensory impairment of the affected upper extremity was measured using the sensory part of the Erasmus MC modified Nottingham sensory assessment (EMNSA) (Stolk-Hornsveld et al., 2006). The maximum score of EMNSA used here (only the sensory part) is 32. Upper limb function was assessed with the FM-UE score and the Action Research Arm Test (ARAT), reflecting the amount of upper limb motor function and capacity, respectively (Fugl-Meyer et al., 1975; Lyle, 1981). The score of FM-UE can reach up to 66 in unimpaired participants or in patients if motor function is fully restored. The ARAT consists of 19 subtests covering grasp, grip, pinch and gross movements. The maximum score that can be achieved is 57.

4.2.2 High density EEG recordings

Each patient was measured three times (T0, T1, T2) with EEG, see also Fig. 4.1. Unimpaired participants were measured two times (T0, T1) with EEG with approximate 10 days (mean±std: 9±4 days) in between the measurements. During the recordings, participants were sitting comfortably with their hand and forearm positioned on their lap with the fingers on top (supine position). A pillow served to secure a stable position and provide comfort and relaxation to prevent muscle activity. The experiment was performed within a NEN1010 approved measurement 4D-EEG VAN (www.4deeg.eu), which was equipped with high-density EEG. The

van travelled to the patient's residence to enhance patient's comfort and minimize dropouts.

Data were recorded with a 64-channel EEG system (TMSi, Netherlands) with the ground electrode placed at the left mastoid and referenced to the common average during recording. Sampling rate was 2048 Hz and apart from anti-aliasing filters no online filters were applied. Electrode impedance was kept below 20 kΩ. Electrode positions and anatomical landmarks of the nasion and both pre-auricular points were digitized using a 3D infrared camera with the ANT Neuro Xensor system (ANT Neuro, Enschede, Netherlands).

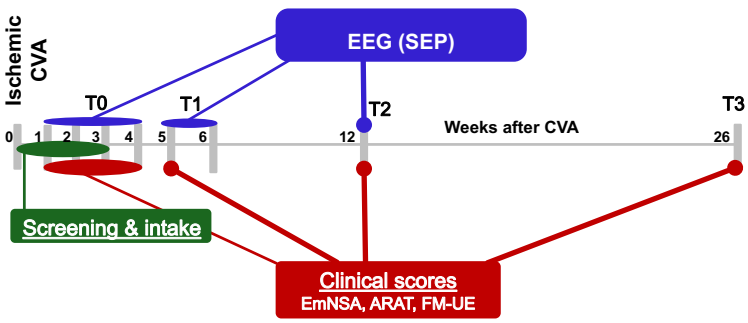

Fig. 4.1 Graphical illustration of measurements (EEG, clinical scores) after stroke onset.

Electrical stimulation at the median nerve was applied at both affected and unaffected side of patients and dominant and non-dominant side of the unimpaired participants. Electric pulses had a duration of 400 µs and an intensity just above the individual thumb twitch threshold (Cruccu et al., 2008), tested on both sides. The stimulation was repeated 500 times at a varying rate between 3 and 4 Hz. Patients with lacking or a very light thumb twitch or patients who experienced pain during the recordings were excluded from this study. Finally, EEG recordings with low signal-to-noise ratio were also excluded.

4.2.3 Data analysis

Proportional recovery of FM-UE

The difference between the initial FM-UE scores at T0 and at six months post stroke (T3) ($\delta\mathrm{FMUE}_{\mathrm{observed}} = \mathrm{FMUE}_{T3} - \mathrm{FMUE}_{T0}$) served to describe the amount of motor recovery of the upper paretic limb. According to the proportional recovery rule (Prabhakaran et al., 2008) patients are expected to reach at six months post stroke (T3) approximately 70% of the difference between the initial FM-UE score and the maximum possible score:

$$\delta\mathrm{FMUE}_{\mathrm{predicted}} = 0.7 \cdot (66 - \mathrm{FMUE}_{T0}) + \mathrm{offset} \tag{4.1}$$

We applied this proportional recovery model to our 16-patients dataset and separated them into groups of fitters ($\delta\mathrm{FMUE}_{\mathrm{observed}} \geq \delta\mathrm{FMUE}_{\mathrm{predicted}}$) and non-fitters ($\delta\mathrm{FMUE}_{\mathrm{observed}} < \delta\mathrm{FMUE}_{\mathrm{predicted}}$) using hierarchical clustering with Mahalanobis distances (Winters et al., 2015).

EEG preprocessing & analysis

The EEG data were pre-processed offline using Matlab (R2013b; The Mathworks, Natick, MA) and the toolboxes Fieldtrip (Oostenveld et al., 2011) and EEGlab (Delorme and Makeig, 2004). After elimination of the stimulation artifact by linear interpolation (lasting for approximately 6 ms after stimulus onset), data were band-pass filtered between 1 and 250 Hz using a bi-directional 4$^{\mathrm{th}}$ order Butterworth filter. Data were segmented in 250 ms stimulus-locked epochs including a 50-ms pre-stimulus interval. Noisy epochs and channels were identified visually and discarded. Artifact-free data typically consisted of about 400 trials (80% of the total number of trials) and about 50 channels (78% of the total number of channels). After re-referencing to the average of the remaining channels, the SEPs were computed by averaging the remaining trials. For each dataset, this resulted in a SEP for the affected hemisphere (AH) and one for the unaffected hemisphere (UH) or in the case of unimpaired participants a SEP for the non-dominant (ND) and one for the dominant (D) side.

The P20 and P50 SEP components were identified on the basis of their latency and using a butterfly plot of the 62 EEG signals. The P20 was identified from 19 to 25 ms and is referred to as P20. The P50 component was identified between 45 and 55 ms. For every SEP recording and every participant, we identified the channel in the contralateral to the stimulation site exhibiting the largest negative or positive value around the time indicated for P20 and P50. Peak latency was estimated at the maximal peak amplitude only when a dipolar pattern (validated through a topographical distribution) of a P20 or a P50 peak was present; whenever that was not the case, we marked the response as non-identifiable.

In order to access the test-retest variability in unimpaired participants, we computed the interclass correlation coefficient (ICC) of amplitudes and latencies of controls as described in (Mcgraw and Wong, 1996). We used a one-way random effects model as we sought to test the absolute agreement among measurements.

$$ICC = \frac{MS_R - MS_w}{MS_R + MS_w} \tag{4.2}$$

where MS_R is the mean square for all unimpaired participants' measurements of one time (T0, T1) and MS_w is the mean square within measurements, T0 and T1.

Comparing EEG with clinical evaluations

The large inter-subject variability in AH and UH amplitudes as well as in P20 and P50 amplitudes (presented in Fig. 4.3 in the results section) motivated looking at a combination of these parameters. To reduce effects of inter-subject differences in tissue conductivity and arm length, we computed the ratio of amplitudes of P20 and P50 and the difference between the latencies of P20 and P50 as features for classification:

$$F1 = \frac{ampP50_{UH}}{ampP20_{UH}} - \frac{ampP50_{AH}}{ampP20_{AH}} \tag{4.3}$$

$$F2 = (latP50_{UH} - latP20_{UH}) - (latP50_{AH} - latP20_{AH}) \tag{4.4}$$

In (4.3), $F1$ represents the difference between P50 amplitude in AH and UH, where P50 amplitude is normalized by the P20 amplitude, as the generators of those two peaks are very closely located to each other in S1. Since their amplitudes are roughly proportional to local tissue conductivity, the ratios in (4.3) largely are insensitive for conductivity effects. A higher $F1$ represents a higher asymmetry between the hemispheres as represented by the amplitudes of the underlying neuronal currents. In (4.4), $F2$ represents the difference between P50 *latency* in AH and UH. P50 latency is normalized to the P20 latency as latency may depend on arm length (van 't Ent et al., 2010). A positive $F2$ implies that information (from P20 to P50) is more slowly processed at the UH than at the AH.

We used the features $F1$ and $F2$ to distinguish the fitters and the non-fitters to the proportional recovery rule by employing a linear support vector machine (SVM) classifier. The accuracy of the SVM was determined with a leave-one out method.

4.3 Results

4.3.1 Clinical scores and proportional motor recovery

Fig. 4.2 depicts the normalized scores by their maximum value of the longitudinal FM-UE, ARAT, and EMNSA tests for all 16 patients included in this study. The FM-UE scores separated the data into two groups, one consisting of nine patients with high FM-UE at T3 values and one consisting of seven patients with low values at T3. The group of high FM-UE consisted of two subgroups of patients: One that showed recovery from T0 to T3 (three patients) and another one with already a high initial score at T0 that did not show further recovery (six patients). ARAT scores largely followed the FM-UE scores and EMNSA displayed always high scores except for two patients with low scores during all sessions and one patient who did show sensory recovery.

Fig. 4.2 D illustrates how of the dataset agreed with the 70% proportional recovery rule (4.1) observed in larger datasets. There was a small percentage of patients that did not fit to the proportional recovery rule (*N*=6) or 37.5% of the included patients (N=16). As for the fitters, there was a linear relationship between

$\delta\mathrm{FMUE}_{\mathrm{predicted}}$ and $\delta\mathrm{FMUE}_{\mathrm{observed}}$ described by a least-squares regression line in the form of $\delta\mathrm{FMUE}_{\mathrm{predicted}} = 0.74 \cdot \delta\mathrm{FMUE}_{\mathrm{observed}} + 2.4$.

4.3.2 SEP measurements at T0, T1, T2

Fig. 4.3 displays the amplitude of AH and UH of P20 and P50 peak for all participants. Peak amplitudes in the unimpaired participants for both P20 and P50 were mostly stable across the two sessions. The ICCs of P20, P50 amplitude, and P50 latency were significant (*p*=.01, *p*=.0003, *p*=.02, respectively) but not the ICC of P20 latency (*p*=.1). We did observe inter-subject variability in amplitudes of unimpaired participants of around 1 μV (mean±std, D side: P20 amplitude, T0: 2±1, T1: 1.8±1.7, P50 amplitude, T0: 2.6±0.6, T1: 2.3±0.8; ND side: P20 amplitude, T0: 1.8±1.3, T1: 2±1.6, P50 amplitude, T0: 2.1±0.6, T1: 2.3±0.6).

Patients showed larger differences between the amplitudes of P20 and P50 at both AH (mean±std, AH: P20 amplitude, T0: 1.7±1.3, T1: 1.7±1.3, T2: 1.5±1.1. P50 amplitude, T0: 4±4.4 T1: 4±3. T2: 3.8±3.1) and UH (UH: P20 amplitude, T0: 2.3±1.6, T1: 2.3±1.8, T2: 2.2±1.8. P50 amplitude, T0: 4.78±1.3 T1: 4.2±2.9. T2: 3.9±2.4). P20 amplitudes at UH were generally larger than amplitudes at AH, with the exception of five measurement points in three patients. Moreover, the variability in amplitude among patients was much larger than the variability of amplitudes across measurement times and within patients. More details on the patients' P20 and P50 amplitudes and latencies can be found in the Appendix.

The P20 peak at the AH hemisphere could not be identified in four patients (# 4,5,11,16) in all three EEG measurements post stroke. Those patients are depicted in Fig. 4.3 with zero amplitudes. The P50 peak was not identifiable in three (# 4, 11,16) out of the 16 patients. At UH, peaks were more easily identified with a few exceptions shown in the Appendix. EEG data of these patients were excluded from further analysis leaving 12 patients (seven fitters and five non-fitters), as illustrated in Fig. 4.4.

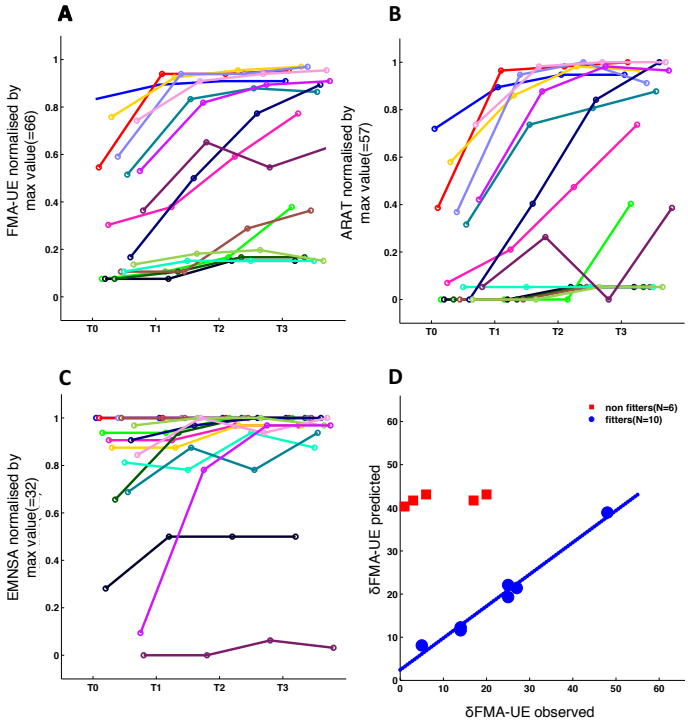

Fig. 4.2 Normalized clinimetrics (by their maximum value) at T0 T1, T2, T3. Different colors represent different patients and are consistent across A) FM-UE, B) ARAT, C) EMNSA, and D) Proportional motor recovery measured by FM-UE: predicted versus observed $\delta\mathrm{FM-UE}$. The blue circles represent the fitters (*N*=10) and the red squares represent the non-fitters (N=6). The blue line represents the least squares regression line of the fitters: $\delta\mathrm{FMUE}_{\mathrm{predicted}} = 0.74 \cdot \delta\mathrm{FMUE}_{\mathrm{observed}} + 2.4$.

Table 4.1. Clinical scores at T0, T1, T2, T3 and fitting to the proportional recovery rule of patients with non-identifiable peaks

	ARAT				EmNSA				Fugl-Meyer				
	T0	**T1**	**T2**	**T3**	**T0**	**T1**	**T2**	**T3**	**T0**	**T1**	**T2**	**T3**	Prop. recovery
#4	0	0	5	5	10	10	3	3	9	16	16	16	Non-fitter
#5	4	12	20	25	39	51	27	42	29	29	31	31	Fitter
#11	18	42	34	55	58	57	46	50	22	28	25	30	Fitter
#16	3	15	24	43	36	42	0	22	0	0	2	1	Fitter

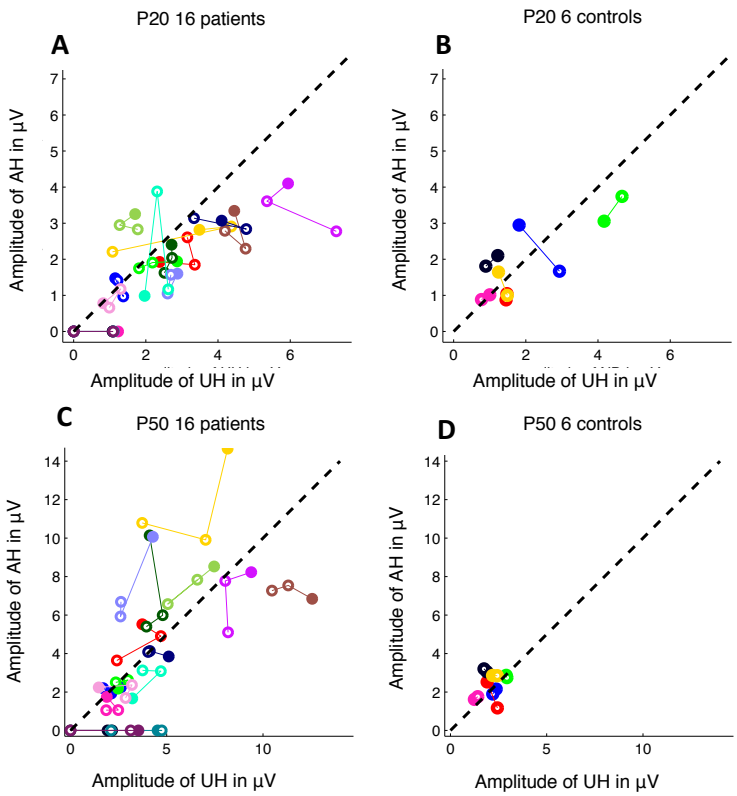

Fig. 4.3 Amplitudes of A) P20 of 16 patients ,B) six controls, C) P50 of 16 patients and D) six controls. Along the abcissa the amplitudes of the unaffected (UH) or non dominant (ND) hemisphere are plotted, along the ordinate the affected (AH) or dominant (D) hemisphere..The filled dot represents the T0 (patients and controls) measurement and the non-filled dot represents the T1 (patients and controls) and T2 (patients).

4.3.3 Predicting recovery with EEG

Not identified SEP peaks and clinical scores

Clinical scores of patients with non-identifiable SEP peaks (4, 11, 15 and 16) are shown in table 4.1. We observed that patients 4 and 16 show low clinical scores longitudinally (except for ARAT score at T3 for patient 16). However, that is not the case for patient 5 and 11 who show rather average values on both motor and sensory scores. Patient 4 does not fit to the 70% proportional recovery rule and

patients 5,11 and 16 belong to the fitters group. We found no association between missing SEP values and clinical scores.

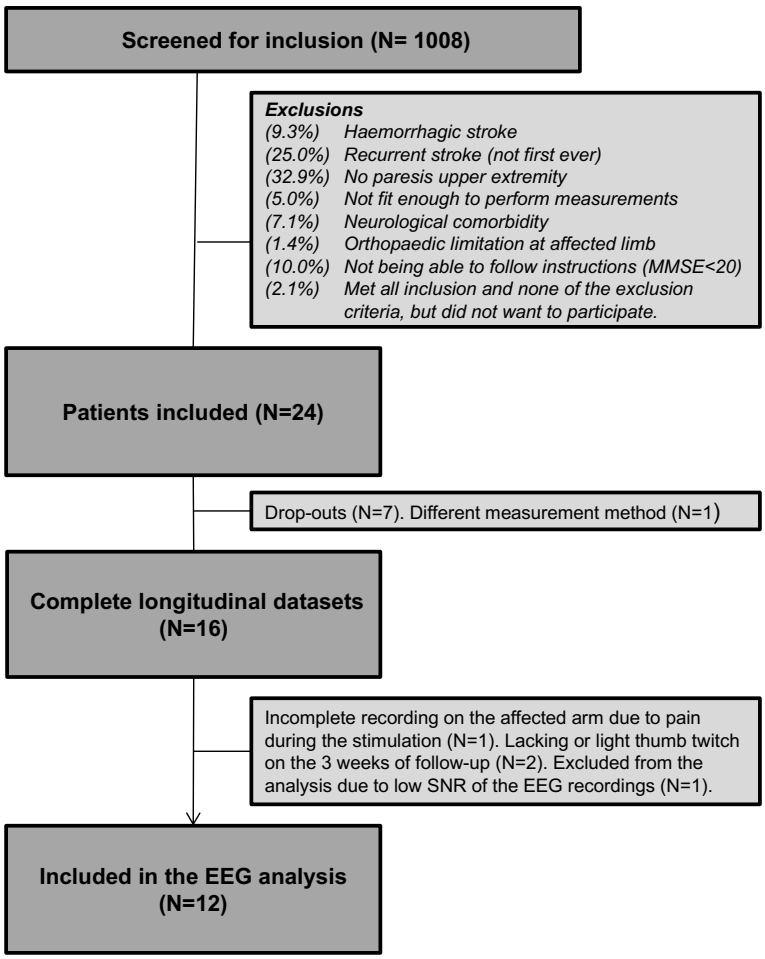

Fig. 4.4 Patient exclusion flowchart. The first two boxes are estimated after screening of patients in one hospital (Reinier de Graaf, Delft, Netherlands).

Prediction of non-fitters with SEP parameters

In Fig. 4.5 we summarize the results of the clustering analysis of the clinical scores of the 12 patients that did not meet the additional exclusion criteria. Two groups of patients emerged from the hierarchical clustering analysis. The two groups matched those of the clustering analysis of the T3 values of the normalized clinical scores as well as the fitters and non-fitters of the proportional recovery model.

Hence, we divided our dataset in two groups, one of fitters consisting of seven patients and one of non-fitters consisting of five patients.

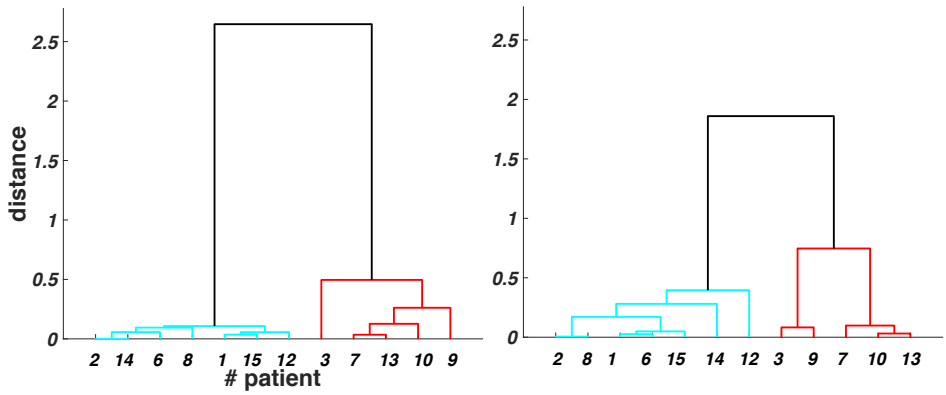

Fig. 4.5 Dendrograms for hierarchical clustering using Mahalanobis distances. Twelve patients were clustered based on normalized clinical scores at the left and proportional recovery at the right.

Finally, Fig. 4.6 shows that $F1$ and $F2$ at T1 identified the fitters and the non-fitters with an accuracy of 83%. We added the $F1$ and $F2$ parameters of the unimpaired participants in the same graph by corresponding the non-affected hemisphere to the dominant side and vice versa. One observes in Fig. 4.6 that these SEP data fell in the same category as the well-predicted patients (fitters). When the features $F1$ and $F2$ were taken at T0 instead of T1, an accuracy of 50% could be obtained Features $F1$ and $F2$ at T2 led to a 58% accuracy of correct prediction.

4.4 Discussion

In the present preliminary study, we monitored the longitudinal change of clinical scores and SEP data in a group of 16 patients suffering from stroke. We confirmed that the 70% proportional recovery rule of FM-UE (T0 versus T3) applied to our data (with 37.5 % of the patients not fitting to the rule). More importantly, by using differences between P20 and P50 peak responses of the SEP we could distinguish

fitters from non-fitters of the 70% proportional recovery rule with an accuracy of about 83%.

The proportional recovery rule holds true for 62.5 % of the patients, consistent with previous studies with larger datasets (Buch et al., 2016; Byblow et al., 2015; Prabhakaran et al., 2008; Winters et al., 2016c, 2015). An important difference between our dataset and studies with a larger group of patients (Winters et al., 2015; Zarahn et al., 2011) is that the first measurement of clinical scores (and the associated EEG) in the present study was performed between one and four weeks post-stroke, whereas in the other cohort studies the initial measurement was assessed within 72 hours post-stroke. Although non-fitters to the proportional recovery rule represent a small percentage of patients, it is of high interest to identify the phenotype of those patients. In accordance to other studies (Krakauer and Marshall, 2015; Winters et al., 2015), our patients with low FM-UE scores at both T0 (FM-UE 0-17) and T3 (FM-UE < 20) were the non-fitters to the proportional recovery model. However, clinical biomarkers such as initial FM-UE scores were unable to distinguish prospective 'recovers' from 'non-recovers' of spontaneous neurobiological recovery (Winters et al., 2015). As a consequence, with the use of only the proportional recovery rule we could not predict which patients would improve at T3 (FM-UE ≥ 20) and which patients would not (FM-UE < 20).

The electrophysiological biomarkers were designed to reflect interhemispheric differences, thereby reducing the effects of natural anatomic variation over subjects, such as skull thickness and arm length. For instance, the definition of $F1$ is based on the amplitude ratio of P20 and P50 in order to obtain a measure of interhemispheric difference of neural activity. Because the underlying sources of P20 and P50 are closely located in the cortex these amplitudes will be similarly affected by the local skull conductivity and therefore the effect of inter-subject variation in skull conductivity is reduced. A more fundamental approach would have been to use calibrated head models as proposed by e.g. Dabek et al. (2016), combined with dipole source amplitude estimation. Our proposed $F2$ refers to the conduction velocity difference between the hemispheres. We took the difference between P20 and P50 peak latency in the definition of $F2$ to obtain a parameter that is insensitive to the patient's anthropometry (van 't Ent et al., 2010). In this

way, both $F1$ and $F2$ represent interhemispheric differences and we suggest that interhemispheric differences represented by $F1$ and $F2$ could be used as indicators of neuronal processes during stroke recovery. This suggestion is further endorsed by our result that 83% prediction accuracy of fitters and non-fitters is achieved with these features and the result that all unimpaired participants fell in the same category as the fitters. These results may be related to another finding, by (van Putten and Tavy, 2004; Tzvetanov et al., 2005; Winters et al., 2016b), that the intactness of proprioceptive input to the primary motor cortex is highly predictive for functional recovery post stroke. Furthermore, there might be a relation to recent diffusion tensor imaging (DTI) study by (Buch et al., 2016), who revealed that non-fitters exhibit a high corticospinal tract asymmetry two weeks post-stroke indicating that interhemispheric imbalances in early post stroke could have a predictive value (Ward, 2017).

However, we are well aware that our results based on SEP parameters are quite specific and cannot be directly compared to studies that used mechanical stimulation of the fingers such as (Forss et al., 1994b), because those stimuli give different responses. Of the widely used electrical median nerve stimulation it is known that peaks both around 20 ms 50 ms and both P20 and P50 are both believed to be generated in Brodmann area 3b. It has been proposed that P20, is more likely to reflect excitatory postsynaptic potentials, while P50 may stem from inhibitory postsynaptic potentials (Wikström et al., 1996). P50 is often considered to contain additional predictive value when monitoring stroke patients (Macdonell, 1991; Wikström et al., 2000). ICCs were more significant for both P50 latency and P50 amplitude of unimpaired individuals when compared to P20 latency and amplitude (section 4.3.2). Contrary to (Feys et al., 2000; Huang et al., 2004; Keren et al., 1993; Oliviero et al., 2004; Tecchio et al., 2007a, 2006; Tzvetanov and Rousseff, 2003; Wikström et al., 2000, 1999) we did not find an one-to-one relationship between not identifiable P20 and P50 SEP peaks and clinical scores (patients 4, 5, 11, and 16).

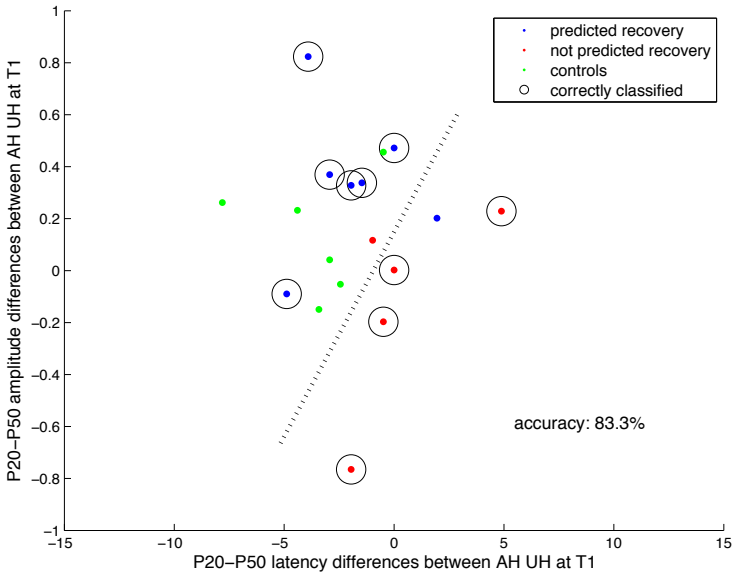

Fig. 4.6 Prediction of fitters vs non-fitters to the "70% proportional recovery rule" with the use of two EEG features at T1 (see formula's 4.2 and 4.3). The blue dots represent the patients with well-predicted recovery according to the proportional recovery and the red dots represent the non-fitters to the model. Green dots represent the unimpaired participants. The clustering according to the classifier is represented with larger black circles. After training a linear classifier with the leave-one-out method we found two incorrectly classified patients (one fitter and one non-fitter) and an accuracy of 83.3%.

We developed a prognostic model to predict stroke recovery six months post stroke based on SEP features extracted five weeks post stroke. If the prognostic model defined in this study can be replicated in a larger cohort, then SEP-EEG measurements at five weeks post-stroke may become an important tool to predict future recovery and to develop patient specific therapy for those patients for whom prognosis (according to the current prognostic models) is not possible. Once the entire dataset is complete, we will cross validate the current proposed model.

4.5. Conclusions

Our results confirm that circa 70% of the patients follow proportional recovery rule as assessed with the FM-UE recovery score. Compared to unimpaired participants SEP responses of stroke patients show a much larger inter-subject variability

indicating that SEP responses possibly contain valuable prognostic information. Data analysis suggest that SEP parameters reflecting hemispheric differences in functional brain activity during sensory processing is able to predict which patients fit the proportional recovery model. When confirmed in a larger independent data set, our study shows that biomarkers derived from SEP responses can potentially be used as complimentary parameters to the existing recovery models.

4.6 Acknowledgements

4D-EEG Consortium

In addition to the authors of the present study, the consortium consists of Carel G. M. Meskers, MD, PhD, Aukje S. Andringa, MSc, Dirk Hoevenaars MSc and Caroline Winters, MSc, from the VU University Medical Center Amsterdam; Teodoro Solis-Escalante, PhD, Yuan-Yang, PhD and Lena Filatova, PDEng, from the Delft University of Technology; Julius P. A. Dewald, PhD, and Jun Yao, MSc, from Northwestern University of Chicago.

4.7 Compliance with ethical standards

Conflict of interest

The authors declare that they have no conflict of interest.

Ethical approval

All procedures performed in studies involving human participants were in accordance with the ethical standards of the institutional and/or national research committee and with the 1964 Helsinki declaration and its later amendments or comparable ethical standards. This article does not contain any studies with animals performed by any of the authors.

4.8 Appendix

Tables A4.1 and A4.2 show the latencies and the amplitudes of the SEP peaks at T0, T1, T2 for AH and UH, respectively. All 16 patients included in this study are presented. The cases with not identifiable peaks are marked as NaN.

Table A4.1 Amplitudes and latencies for the P20 and P50 peaks at T0, T1, T2 at the affected hemisphere (non-identified values are marked as NaN).

Affected hemisphere												
	T0				T1				T2			
PAT	P20 lat.	P20 amp.	P50 lat.	P50 amp.	P20 lat.	P20 amp.	P50 lat.	P50 amp.	P20 lat.	P20 amp.	P50 lat.	P50 amp.
#1	24.90	1.47	45.41	1.93	24.90	0.97	49.32	2.20	24.90	1.41	48.34	2.24
#2	22.95	1.93	45.41	5.52	23.44	1.85	54.69	4.90	24.90	2.61	54.69	3.64
#3	24.90	1.94	45.41	2.17	24.90	1.91	45.41	2.62	24.90	1.75	45.41	2.50
#4	NaN	NaN	NaN	NaN	NaN	NaN	NaN	NaN	NaN	NaN	NaN	NaN
#5	NaN	NaN	54.69	1.75	NaN	NaN	54.69	1.06	NaN	NaN	53.22	1.06
#6	24.90	2.82	51.76	14.65	24.90	2.91	48.83	9.91	24.90	2.21	49.80	10.79
#7	20.51	2.40	54.69	10.14	24.90	2.04	54.69	5.99	24.90	1.62	54.69	5.40
#8	24.90	1.60	54.20	10.07	22.95	1.05	50.78	5.93	23.44	1.57	46.88	6.69
#9	24.90	3.34	45.41	6.85	24.90	2.30	54.69	7.54	24.90	2.79	54.69	7.27
#10	24.90	0.98	54.69	1.67	23.44	3.88	54.69	3.09	24.90	1.17	51.27	3.13
#11	NaN	NaN	NaN	NaN	NaN	NaN	NaN	NaN	NaN	NaN	NaN	NaN
#12	24.90	3.07	45.41	3.85	24.90	2.84	45.41	4.13	24.90	3.14	45.41	4.08
#13	21.97	3.25	47.85	8.52	22.46	2.95	46.39	6.57	22.46	2.83	45.41	7.83
#14	24.90	0.78	45.41	2.24	20.51	1.18	45.90	2.37	20.02	0.66	50.78	1.69
#15	22.95	4.10	49.32	8.23	22.46	3.61	46.39	7.78	23.44	2.78	45.41	5.10
#16	NaN	NaN	NaN	NaN	NaN	NaN	NaN	NaN	NaN	NaN	NaN	NaN

Table A4.2 Amplitudes and latencies for the P20 and P50 peaks at T0, T1, T2 at the unaffected hemisphere (non-identified values are marked at NaN).

Unaffected hemisphere												
	T0				T1				T2			
PAT	P20 lat.	P20 amp.	P50 lat.	P50 amp.	P20 lat.	P20 amp.	P50 lat.	P50 amp.	P20 lat.	P20 amp.	P50 lat.	P50 amp.
#1	21.48	1.15	45.41	2.13	23.93	1.37	45.41	1.70	23.93	1.22	48.34	2.62
#2	24.41	2.38	54.69	3.73	24.90	3.35	54.69	4.69	24.90	3.15	54.69	2.41
#3	24.90	2.87	45.41	2.47	24.90	2.18	45.41	2.99	24.90	1.81	45.41	2.36
#4	24.90	1.08	45.41	2.16	NaN	NaN	NaN	NaN	22.95	1.08	45.41	1.93
#5	23.44	1.23	52.25	1.89	NaN	NaN	45.41	2.48	NaN	NaN	49.80	1.85
#6	23.44	3.48	47.36	8.16	23.44	4.37	45.41	7.02	21.48	1.08	47.36	3.72
#7	20.02	2.72	45.41	4.11	20.02	2.73	54.69	4.79	20.02	2.52	54.69	3.94
#8	23.44	2.87	45.41	4.28	21.48	2.60	45.41	2.60	24.90	2.69	45.41	2.62
#9	23.44	4.45	54.20	12.56	24.90	4.77	53.71	11.31	24.90	4.19	54.69	10.46
#10	23.44	1.97	45.41	3.21	24.41	2.31	53.71	4.70	22.46	2.62	50.78	3.74
#11	NaN	NaN	51.27	4.53	24.90	1.11	50.29	4.74	NaN	NaN	45.90	2.11
#12	24.90	4.10	54.69	5.10	24.90	4.78	45.41	4.13	24.90	3.33	50.29	4.04
#13	23.44	1.70	46.88	7.46	22.46	1.27	45.90	5.05	23.44	1.78	45.90	6.59
#14	20.02	0.82	45.41	1.47	24.90	1.30	45.41	3.19	24.90	0.99	45.41	2.86
#15	21.97	5.94	49.32	9.39	22.46	5.36	48.34	8.04	21.97	7.28	48.34	8.18
#16	NaN	NaN	47.36	3.53	NaN	NaN	NaN	NaN	21.97	1.09	48.83	3.12

Table A4.3 shows the 16 patient characteristics as assessed 72 hours post stroke. Table A4.4 shows the clinical scores of the 16 patients at T0, T1, T2, with blue are presented the fitters to proportional recovery model and with red the non fitters

Table A4.3 Patient characteristics, and Bamford classification as assessed 72 hours post stroke. LACI: lacunar anterior cerebral infraction; PACI: partial anterior cerebral infraction; TACI: total anterior cerebral infraction. F2R means forced to write with the right hand

#ID	age	gender	handedness	affected body side	Bamford classification
1	73	m	R	L	LACI
2	86	f	R	R	LACI
3	52	f	R	R	LACI
4	64	m	R	R	TACI
5	58	m	R	R	PACI
6	75	f	R	L	PACI
7	75	f	R	L	PACI
8	63	m	L	R	LACI
9	77	m	R	L	PACI
10	93	f	R	R	PACI
11	79	m	F2R	L	PACI
12	76	f	R	R	PACI
13	94	f	R	L	PACI
14	77	m	R	L	LACI
15	72	m	R	L	PACI
16	78	m	R	L	TACI

Table A4.4 Clinical scores (ARAT, FM-UE, EMNSA) of 16 patients at T0, T1, T2, T3. With blue are depicted the patients that fitted to the proportional recovery rule and with red the patients that did not fit to the proportional recovery rule as in Fig. 4.2 D,

	ARAT				FM-UE				EMNSA			
ID/T	**T0**	**T1**	**T2**	**T3**	**T0**	**T1**	**T2**	**T3**	**T0**	**T1**	**T2**	**T3**
1	41	51	54	54	55	59	60	60	32	32	32	32
2	22	55	56	57	36	62	62	63	32	32	32	32
3	0	0	0	23	5	7	11	25	30	30	32	32
4	0	0	3	3	5	5	10	10	9	16	16	16
5	4	12	27	42	20	25	39	51	29	29	31	31
6	33	49	56	55	50	61	63	64	28	28	31	31
7	0	0	3	3	5	7	11	11	21	30	32	32
8	21	54	57	52	39	62	62	64	32	32	32	32
9	0	0	3	3	7	7	19	24	32	32	32	32
10	3	3	3	3	7	10	10	10	26	25	30	28
11	18	42	46	50	34	55	58	57	22	28	25	30
12	0	23	48	57	11	33	51	59	29	31	32	32
13	0	0	3	3	9	12	13	10	31	32	32	31
14	42	56	57	57	49	60	62	63	27	32	30	32
15	24	50	56	55	35	54	59	60	3	25	31	31
16	3	15	8	22	24	43	36	42	0	0	2	1

Chapter 5

EEG biomarkers in chronic stroke – correlating event-related responses and resting state activity with motor and sensory scales

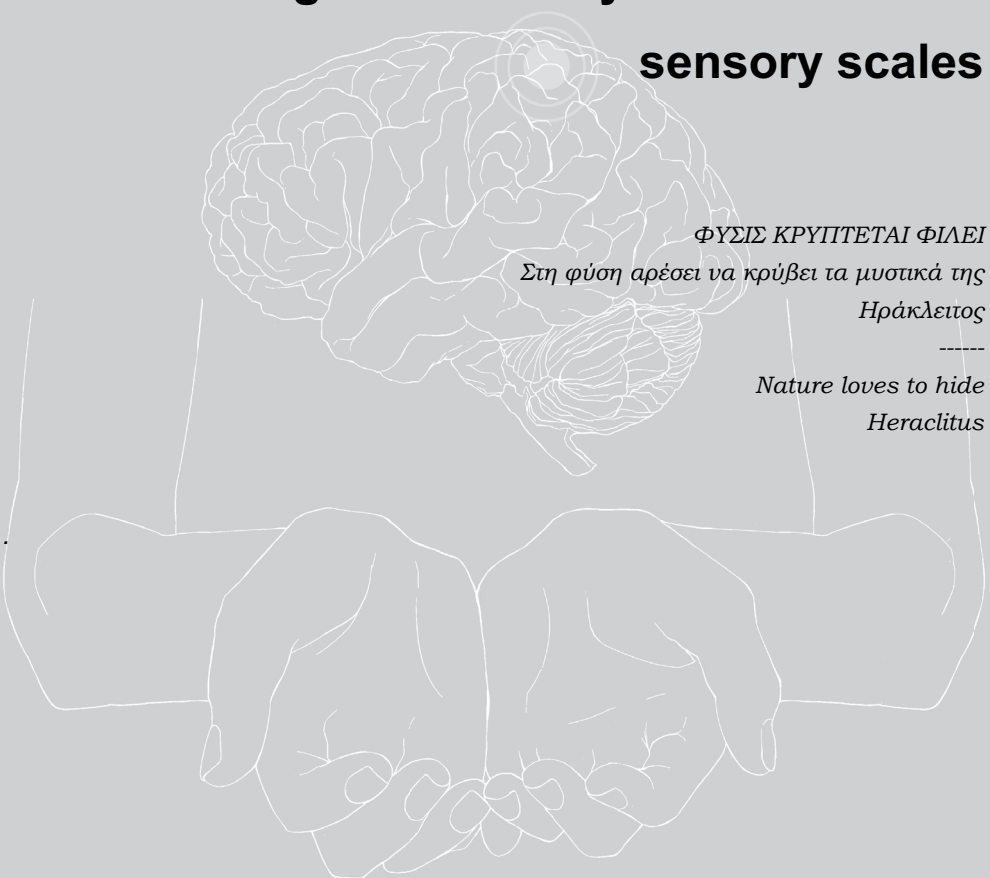

ΦΥΣΙΣ ΚΡΥΠΤΕΤΑΙ ΦΙΛΕΙ
Στη φύση αρέσει να κρύβει τα μυστικά της
Ηράκλειτος

Nature loves to hide
Heraclitus

ABSTRACT

Evaluating sensory and motor impairment and recovery after stroke may benefit from affordable and ambulant imaging modalities like electroencephalography (EEG). However, there is currently neither a standard protocol nor a standard outcome measure for clinical practice to evaluate impairment after stroke with EEG. The goal of this study is to test if electrical stimulation of the index finger eliciting somatosensory activity is associated with clinical stroke measures. Accordingly, we supplemented the data by resting state activity as a baseline. The electrical stimulation at the finger failed to generate clear-cut evoked potentials, which called for non-time locked frequency analysis. Based on earlier studies, we determined asymmetries via EEG power ratios between left and right hemispheres in different frequency bands. Both after stimulation and during resting state, we found differences between chronic stroke patients (N=21) and healthy age-matched unimpaired participants (N=9). Interhemispheric asymmetries were correlated with clinical motor and sensory scales. We confirm asymmetries in the delta band (1.5-4 Hz) during resting state but also after electrical stimulation of the fingers in chronic stroke patients. We concluded that these asymmetries are almost significantly correlated (p=0.06) with clinical motor scales supporting the potential for characterizing chronic stroke. We did not find any significant correlation of beta nor alpha asymmetry with clinical scores

5.1 Introduction

Stroke is a leading cause of physical disability worldwide. According to Parker et al. (1986), approximately 87% of all stroke survivors suffer from paresis of the upper extremity immediately after stroke onset. Stroke recovery typically contains a fast, initial recovery pattern followed by a slower recovery pattern and saturates within three months post stroke. Yet, recovery can continue for years during the so-called chronic stage defined as >6 months post stroke (Cramer, 2008). Focal injuries in motor areas after ischemic stroke can cause changes in intra- and inter-hemispheric interactions across the motor and/or sensory networks, including primary motor cortex, dorsal and ventral premotor cortex, supplementary motor area, parietal cortex, and secondary somatosensory cortex but also prefrontal cortex (Grefkes and Fink, 2011). It seems that the brain 'tries' to remap the sensorimotor interactions to reconnect motor areas with somatosensory input (Bolognini et al., 2016; Ward and Cohen, 2004). Common clinical practice does not involve detailed imaging, like for example magnetic resonance imaging (MRI), to assess such changes but rather follows the patient from the acute to the chronic stage with clinical motor and sensory scales; e.g., the Fugl-Meyer scale, or the Erasmus Nottingham Sensory Assessment score. This is due to MRI practical limitations (Singer et al., 2004), but is also due to the financial burden of neural imaging. Here we advocate electroencephalography (EEG) as a safe, easy-to-apply, affordable, and ambulant imaging method that can be used to access sensory impairment, even post stroke (Rollnik, 2015; Ward, 2017, 2015).

Monitoring sensory areas during ischemic stroke recovery with the use of EEG has been suggested for evaluating rehabilitation strategies and eventually adjusting them in a patient-specific manner (Bolognini et al., 2016). A proper understanding of changes in the sensory areas may help improving the functional outcome (Winward et al., 1999). Somatosensory evoked potentials or fields (SEPs or SEFs, respectively) are conventional measures for studying the somatosensory areas (Hari and Forss, 1999). They are estimated as an event-related average based on the assumption that to every stimulation (event) a neural population responds in the same way. Seminal for this approach is the stimulation of the median nerve at

the wrist. While providing robust SEPs, median nerve stimulation involves both efferent and afferent pathways. Median nerve stimulation includes Ia, Ib, II afferents and efferent fibers, where the latter can induce muscles twitches (Dawson, 1956; Kuiken et al., 2007; Mauguiere, 1999). However, in particular changes in the afferent pathways are currently believed to have predictive capacity for stroke recovery (Laaksonen et al., 2012). An alternative is electric stimulation of the finger because it primarily involves Aβ afferents (Dowman, 1997). Electrical finger stimulation in stroke has been applied before. For instance, MEG studies associated the absence or lack of early SEF finger-stimulated responses in the chronic stage of stroke with worse clinical scores (Rossini et al. 1998a, 1998b, 2001).

Stimulus-evoked response fall into two categories: so-called evoked responses that are almost instantaneous and appear largely additive to ongoing activity, and induced ones that are delayed and are, hence, indicative of (high-level) processing. Stimulation, however, may also alter ongoing activity. Here important is the possible modulation of spontaneous brain rhythms (Bullock, 1992), which can be explained by mere changes in spectral power (David et al., 2006) but also by changes in phase (Nikulin et al., 2007). In fact, various rhythms have been reported to change post stroke even in the absence of external stimulation. Stroke is typically lateralized because of which altered brain activity comes with significant left/right asymmetry in spectral distributions (Finnigan and van Putten, 2013; van Putten, 2007, 2006; Sheorajpanday et al., 2011), which have been suggested as a tool for monitoring recovery (Anastasi et al., 2017; Sheorajpanday et al., 2009; Stojanović and Djurasić, 2013), even in the acute stage (van Putten and Tavy, 2004).

Poor function of the somatosensory cortex is associated with stroke severity (Connel et al., 2008; Meyer et al., 2016). The goal of the study was to determine if SEP-related parameters after finger stimulation may help characterizing chronic stroke. In view of the literature we also evaluated spectral asymmetries during resting state and SEP. In our experiments, we included N=21 chronic ischemic stroke patients and N=9 age-matched unimpaired participants. All outcomes were correlated with clinical scores for motor and sensory function.

5.2 Methods

5.2.1 Subjects

Twenty-one patients with chronic hemiparesis after stroke participated in this study (61±9 years, six female, all at least six months post stroke, with initial hemiparesis, eight with a lesion in the left hemisphere).

Inclusion criteria were: 1) first-ever ischemic stroke in an area supplied by the anterior, medial, and/or posterior cerebral arteries, 2) ≥ 18 years of age, 3) Mini Mental State Examination score ≥ 20, 4) able to sit in a wheel chair for at least two hours. Exclusion criteria were: 1) a pacemaker or other metallic implants which are not allowed in the MRI scanner (due to an MRI recorded in another trial of the study), 2) upper extremity orthopedic limitations before stroke onset, 3) other neurological disorders, and 4) botuline-toxine injections or medication that may influence upper limb function in past three months.

Nine unimpaired age-matched participants (60±11 years, three women) served as a control group, who met the two last inclusion criteria.

The present study is part of a larger EEG cohort study on stroke (European Research Council, 4D-EEG project), wherein EEG and clinical parameters are determined.

This EEG cohort study protocol has been approved by the Medical Ethical Reviewing Committee of the VU University Medical Center Amsterdam (registration number 2014.140). All participants gave their written informed consent prior to the measurements. This study was conducted in accordance with The Declaration of Helsinki.

5.2.2 Clinical testing

Clinical testing of the patients was performed the day before or after the EEG measurements. Sensory impairment (SI) of the affected upper limb was measured using the Erasmus MC modified Nottingham sensory assessment (EmNSA) (Stolk-Hornsveld et al., 2006): The maximum score of the EmNSA is 40. The EmNSA consists of five subtests with 8 as the maximum score of every subtest. SI was summarized as described in (Stolk-Hornsveld et al., 2006): Patients who achieved a full score on each subtest of the EmNSA were classified to be without sensory

impairment. Patients with a reduced score in one or two subtests were marked as mildly impaired, whereas participants with a reduced score on more than two subtests of the EmNSA were considered severely impaired.

Upper limb function was assessed with the upper limb subtest of the Brunnstrom Fugl-Meyer Assessment (FMA-UE), reflecting the amount of motor function, as a measure of functional recovery (Fugl-Meyer et al., 1975). The FMA-UE is a stroke specific impairment scale, which determines the ability to execute dissociated movement, and is believed to reflect true neurological recovery (Levin et al., 2009). The maximum score of FMA is 66 for healthy individuals or patients with fully restored motor function. More details about patient characteristics and their corresponding FMA and SI can be found in the Appendix.

5.2.3 EEG recordings

During the EEG recordings, participants were sitting comfortably with their hand and forearm positioned on their lap with the fingers on top (supine position). Between forearm and lap a pillow was placed to secure a stable position and provide comfort. The experiment was performed within a NEN1010 approved measurement van, which was equipped with high-density EEG, and travelled to participant's residence to enhance patient's comfort and minimize dropout.

Signals were recorded with a 64-channel EEG system (TMSi, Netherlands) with the ground electrode placed at the left mastoid and referenced to the common average during recording. Sampling rate was 2048 Hz and apart from anti-aliasing, no filters were applied online. The electrodes' impedance was kept below 20kΩ. The electrodes' positions and the anatomical landmarks of the nasion and both pre-auricular points were digitized using a 3D infrared camera with the ANT Neuro Xensor system (ANT Neuro, Enschede, Netherlands).

EEG was recorded during rest (resting state) and during electrical stimulation of the index finger. Resting state was recorded with the eyes open and patients fixating at a cross, displayed at a screen in front of them. Five segments of one minute were recorded in order to reduce fatigue. Participants were asked to relax and were allowed to blink normally.

Electrical stimulation at the index finger was applied after the resting state. Stimulation was applied at both affected and unaffected side of the patients and dominant and non-dominant side of the unimpaired participants. Electric pulses had a duration of 400 µs and an intensity of two times the sensory threshold. The sensory threshold was assessed by asking the participants to count the received pulses at their unaffected side. The individual sensory threshold was set at the intensity where subjects were able to count five out of ten applied pulses. The stimulation was repeated 500 times (without a pause) at a varying rate between 3 and 4 Hz (inter-stimulus interval: 250-330 ms). During the stimulation, participants were asked to fixate at a cross, displayed at a screen in front of them.

5.2.4 Data Analysis

The EEG data were pre-processed offline using Matlab (R2013b; The Mathworks, (Natick, MA) with the Fieldtrip (Oostenveld et al., 2011) and EEGlab toolboxes (Delorme and Makeig, 2004).

SEP preprocessing & analysis

After replacing the stimulus artifact in the EEG by linear interpolation (lasting for approximately 6 ms after stimulus onset, therefore the time segment from 0 to 6 ms after the stimulation onset was interpolated), data were band-pass filtered between 1.5 and 250 Hz using a 4^{th}-order bi-directional Butterworth filter. Data were segmented in 250 ms stimulus-locked epochs including a 50-ms pre-stimulus interval. Noisy epochs and channels were identified visually and discarded using the BIAP software (http://www.demunck.info/software/index.html). Artifact-free data typically consisted of about 400 trials (80% of the total number of trials) and about 50 channels (78% of the total number of channels). After re-referencing to the common average of the remaining channels, SEPs were computed resulting in SEPs of the affected hemisphere (AH), the unaffected hemisphere (UH) for patients and dominant (D) and non-dominant side (ND) for unimpaired participants. Peaks were identified visually. We especially focused at two early peaks recorded above the primary somatosensory cortex (Kaas, 1983): a peak around 20 ms (P20) and a peak around 50 ms (P50) after stimulus onset.

Resting state preprocessing

Resting state data were band-pass filtered between 1.5 and 250 Hz, similar to the SEP preprocessing. The same channels as during electrical stimulation of the fingers were excluded. Resting state data were also re-referenced to the common average of the remaining channels. Data were segmented in two seconds intervals and were visually inspected for artifacts. The resting state segments with too high variance were excluded.

Spectral analysis

Since the time interval between stimuli was too short to determine the spectrograms of the stimulus-locked responses, non-time locked SEPs were determined by concatenating eight time-locked segments resulting in two-second segments (corresponding to a frequency resolution of 0.5 Hz). The power spectral densities (PSD) of both resting state and non-time locked SEP recordings were determined by averaging the spectral power of all two-second segments (i.e. Welch's periodogram method). Next, we computed the mean power over the frequency ranges of interest: delta (1.5-4 Hz), alpha (8-12.5 Hz), and beta (11.5-30 Hz). This yielded in power values per EEG channel per frequency band.

Two ROIs were defined around somatosensory and motor areas, including occipital and parietal electrodes. The left ROI included the electrodes (labeling according to the 10-20 system): F1, F3, F5, FC1, FC3, FC5, C1, C3, C5, CP1, CP3, CP5, P1, P3, P5; the right ROI: F2, F4, F6, FC2, FC4, FC6, C2, C4, C6, CP2, CP4, CP6, P2, P4, P6. The frequency band power per ROI were defined as the average of the frequency band power of all electrodes within a ROI. The averaged power P over all electrodes within a ROI and over the f frequency bins of the specific frequency band will from hereon be referred as delta power, alpha power, and beta power. The resting state power will be from hereon referred as baseline power and the power after electrical stimulation of the finger will be referred as modulated power.

Asymmetry

To estimate the difference between modulated power and baseline we determined an asymmetry ratio of two homologous ROIs. The asymmetry A was calculated separately for all the frequency bands power as follows:

$$A = \frac{\overline{P_{UH}(f, ROI_{UH})}}{\overline{P_{AH}(f, ROI_{AH})}} \quad (1)$$

where the subscripts of AH and UH refer to the affected and unaffected hemisphere, respectively. A was computed for each site of stimulation condition (AH and UH) and for the no-stimulation condition (resting state). For unimpaired participants, UH in (1) corresponded to the dominant side (D) and AH to the non-dominant side (ND). A larger than 1 implies the power in the respective frequency band to be higher in UH (or D), whereas for A smaller than 1 the power is higher in AH (or ND). We would like to note that discontinuities in the SEP signal due to concatenating eight 250 ms epochs into two-second segments may have resulted in noisy power spectral densities. However, this artifact is expected to be significantly reduced when computing the asymmetry ratio, as the asymmetry ratio was calculated using segments from the same time window.

Statistics

Spectral power. The frequency band power of D and ND obtained from healthy participants were compared with stroke subjects. UH was compared with the D and AH to the ND using a Mann-Whitney U test.

Asymmetry per frequency band. Asymmetry index A of the modulated power was compared with the resting state A using Pearson correlation, computed for both the affected (or non-dominant) side stimulation and the unaffected (or dominant) side stimulation.

The A-values of the stroke patients were finally correlated with the corresponding FMA and SI scores (Pearson correlation).

5.3 Results

5.3.1 SEP responses

Fig. 5.1 shows the superposition of all channels after the calculation of SEPs for three patients.

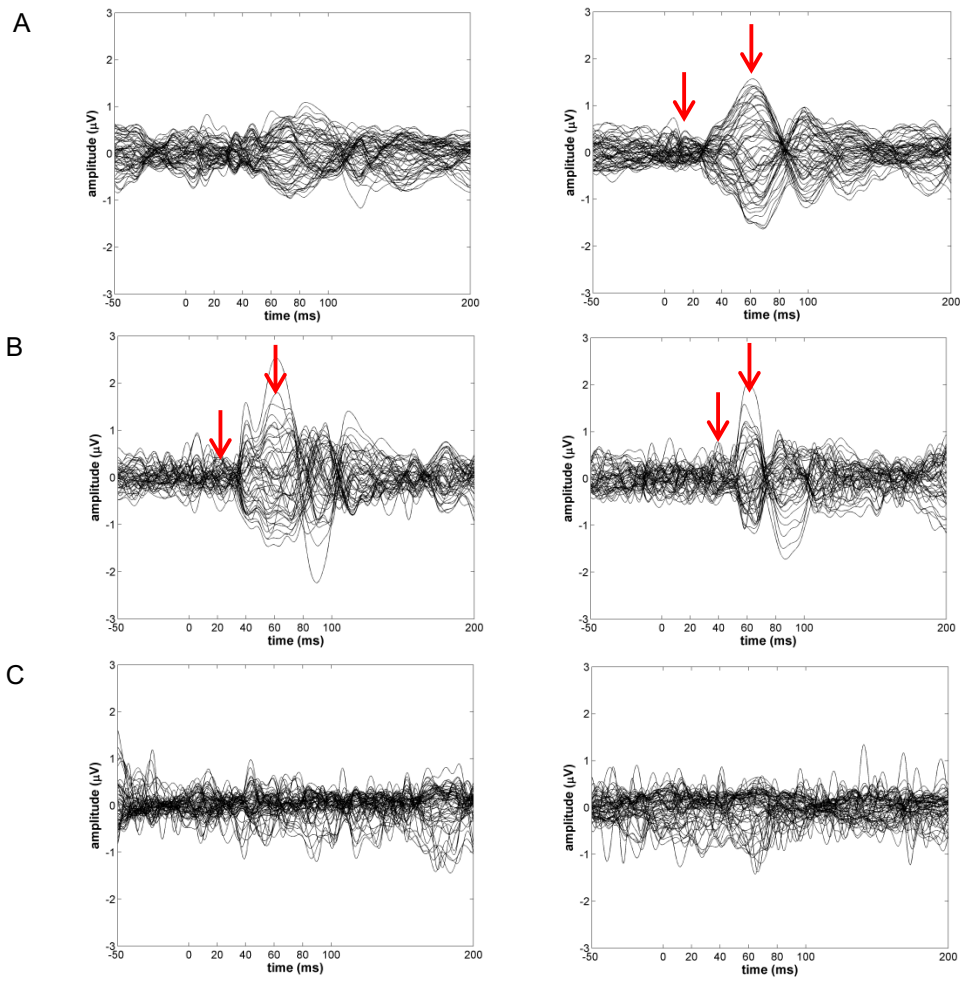

Fig. 5.1 Butterfly plot of EEG signals (left column affected side, right column unaffected side) of all channels in the [-50, 200] ms stimulus interval indicating SEP responses in three typical patients. A) SEP peaks could only be identified at UH, B) SEP peaks were identified in both hemispheres, C) no peaks could be identified. The peaks are indicated with red arrows.

Example A corresponds to identifiable SEP peaks only at the unaffected hemisphere and is representative for seven patients in our dataset. Example B corresponds to identifiable SEP peaks at both hemispheres and is representative for two patients. All healthy participants in this study were represented by example B. Example C corresponds to non-identifiable peaks at both the affected and unaffected hemisphere and corresponds to twelve patients. Fig. 5.2 summarizes FMA scores and SI levels of categories A, B, C. Except for one patient, identifiable SEP responses in at least one hemisphere (group A&B) were associated with FMA scores higher than 50. We could not observe any pattern in the FMA of patients with no identifiable SEP peaks (group C).

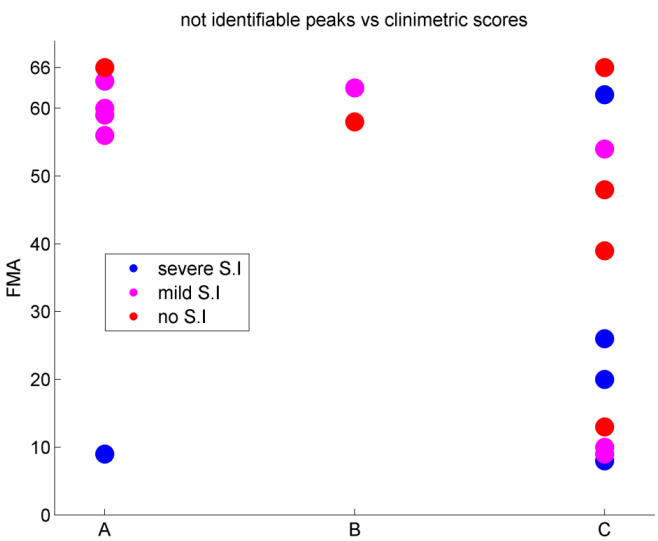

Fig. 5.2 FMA and SI grouping of all patients: peaks only at UH (group A), peaks in both hemispheres (group B), no peaks could be identified (group C).

5.3.2 Spectral power

Fig. 5.3 depicts the delta power values of all patients and all healthy participants after afferent stimulation at AH and UH and during rest.

Delta power was significantly larger in patients compared to unimpaired participants for all three conditions: resting state, stimulation at UH versus stimulation at D, and stimulation at AH versus stimulation at ND (RS: p=.003, UH:

p=.04, AH: *p*=.01). Differences in beta and alpha power between patients and unimpaired participants were not significant (beta: RS: *p*=.3 UH: *p*=.4, AH: *p*=.3; alpha: RS: *p*=.1, UH: *p*=.4, AH: *p*=.4).

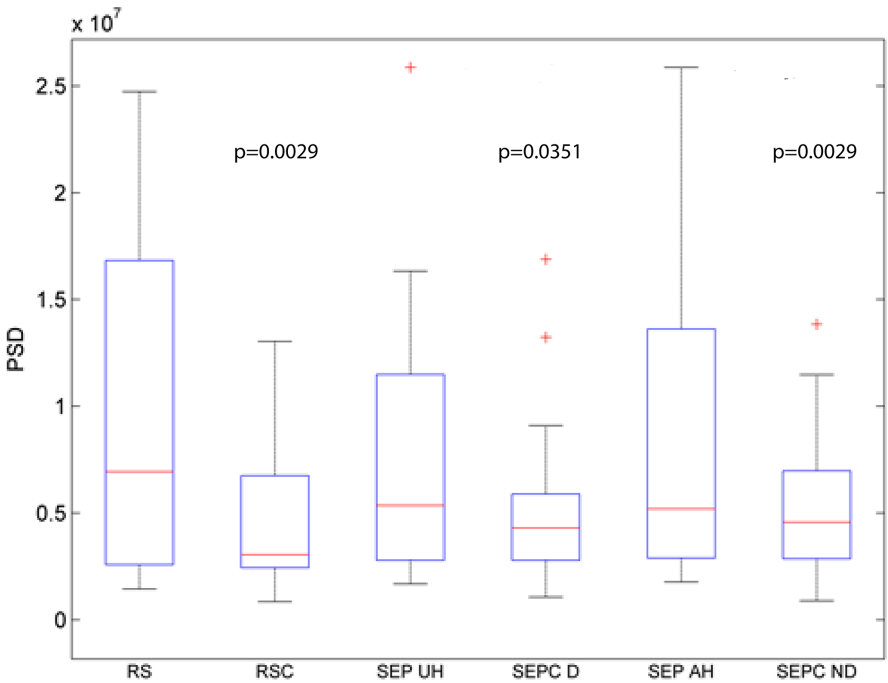

Fig. 5.3 Delta power in all patients (*N*=21) and healthy unimpaired participants (*N*=9). The *p* values were computed for the comparison of the groups of healthy unimpaired participants and patients for the three conditions: resting state (patients: RS; unimpaired participants: RSC), electrical stimulation of the unaffected site (SEP UH) versus electrical stimulation of the dominant site in unimpaired participants (SEPC D) and electrical stimulation of the affected site (SEP AH) versus electrical stimulation of the dominant site in unimpaired participants (SEPC ND)

5.3.3 Asymmetry

Fig. 5.4 shows the asymmetry ratio A for the delta band after SEP stimulation of all patients and unimpaired participants against the corresponding resting state asymmetry ratio. In unimpaired participants, SEP and resting state delta asymmetry largely agreed both when stimulating dominant or non-dominant

hemisphere (corr. of delta asymmetry D: r=0.93, p<.05, ND: r=0.95, p<.05). The asymmetry ratio was in the immediate vicinity of $A = 1$ (mean±std:1±0.06), i.e. the delta power was symmetrically distributed. In the patients, we also found $A \approx 1$ but encountered a larger standard deviation (0.4, in the case of stimulation of the affected side). We further observed that stimulation-related delta asymmetry in patients was very similar to the resting state delta asymmetry both when affected (r=0.9, p<.05) or unaffected hemisphere were stimulated (r=0.9, p<.05). Similarities between SEP and resting state were also observed in alpha and beta frequency bands (alpha: AH: r=0.84, p<.05, UH: r=0.62, p<.05; beta: AH: r=0.77, p<.05, UH: r=0.62, p<.05).

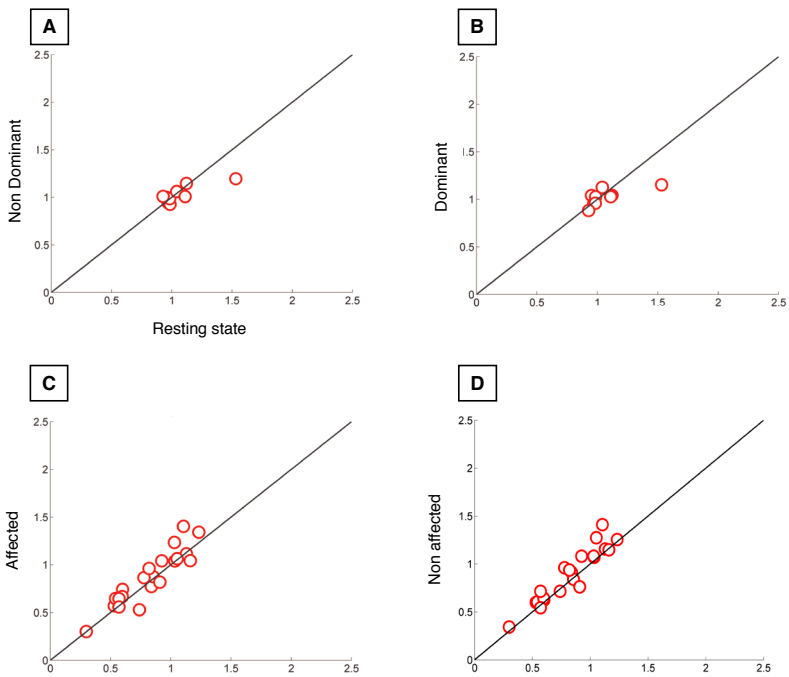

Fig. 5.4 Asymmetry ratio of delta power after SEP stimulation (vertical axis) versus asymmetry ratio delta power during resting state (horizontal axes); stimulation of the dominant side in unimpaired participants (A), the non-dominant side of unimpaired participants (B), the not affected side of patients (C), the affected side of patients (D).

5.3.4 Correlation asymmetry with FMA and SI scores

Fig. 5.5 depicts the relationship of FMA and sensory impairment to the delta band asymmetry. Since asymmetries during resting state and afferent stimulation were highly correlated, we here only show the asymmetry during resting state. We found a significant correlation (r=0.6, p=.006) of the resting state asymmetry of the delta band and the FMA scores. SI scores did not correlate significantly with delta band asymmetry (r=0.1, p=.5); cf. Fig. 5.5, panel B. Similarly, delta asymmetry after stimulation of the AH (or UH) correlated with FMA and not with SI (FMA AH: r=0.5, p=.01, FMA UH: r=0.5, p=.01, SI AH: r=0.5, p>.05, SI UH: r=0.08, p>.05). We did not find any significant correlation of beta nor alpha asymmetry with FMA or SI scores (for both p>.05).

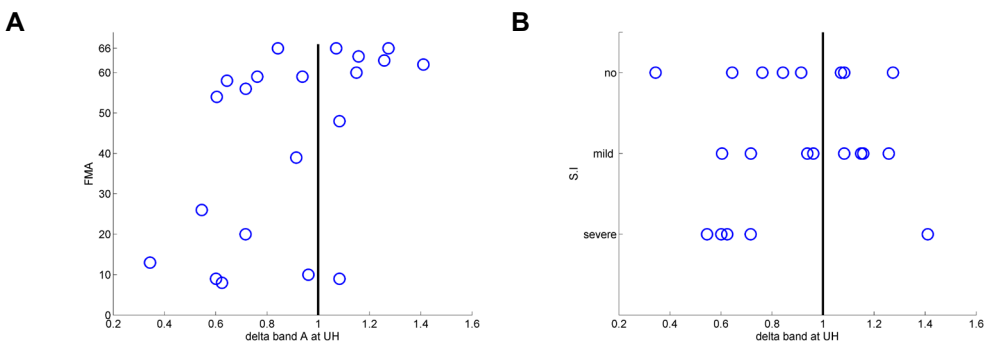

Fig. 5.5 Asymmetry ratio of delta power during resting state plotted versus FMA (panel A) and SI (panel B) The black line represents symmetry (A=1).

5.4 Discussion

We investigated the use of SEPs after electrical stimulation of the index fingers and the assessment of resting state activity for monitoring chronic stroke patients. Analyzing stimulus-related responses yielded poor results that let us to conclude that using electrical stimulation of the fingers may not be optimal for stroke recovery assessment. For 55% of the patients included in this study, identification of the 'expected' peaks at the SEP response was not possible. The analysis of stimulus-induced modulations of ongoing beta and alpha activity did not provide

additional information about stroke recovery. However, we found further support that delta asymmetry during both resting state (Finnigan and van Putten, 2013) and afferent electrical stimulation of the index finger correlated with FMA scores, i.e. with motor function in chronic stroke patients.

Our search for biomarkers of chronic stroke patients explored responses recorded with EEG after electrical stimulation of the fingers. We employed a stimulation protocol from which we found reproducible responses with a high signal-to-noise-ratio in healthy volunteers (see Appendix Kalogianni et al., 2018) and expected similar finding for stroke patients. However, it was not always possible to identify SEP responses in patients, although all chronic stroke subjects in our study indicated that they clearly felt the stimulation delivered at their index fingers. Previous studies also indicated that it is not always possible to identify SEP or SEF peaks in chronic stroke patients (Castillo et al., 2008; Rossini et al., 2001;). Tecchio et al., 2007 indicated that patients with unidentifiable responses at the AH presented subcortical involvement. Since all our healthy unimpaired participants had responses with identifiable peaks, one may assume that a lack of responses in the AH of stroke patients might be related to the exact location and volume of the lesion of each patient. Missing structural information about the lesions made this comparison impossible. Further studies are needed if one wants to investigate this relationship in detail. The large amount of absent SEPs at the UH in our study could be due to the relatively low stimulation intensity at two times the sensation threshold. Although, our stimulation threshold agreed with those suggested in the literature (Cruccu et al., 2008). Previous studies suggest that stimulation close to pain threshold is more likely to elicit SEP responses with larger amplitude and more prominent peaks (e.g., Wang et al., 2004). However, to assure patients' comfort we stimulated at twice the sensation threshold.

Electrical stimulation of the median nerve is a popular experimental choice in research studies when stroke assessment is of interest (Forss et al., 1999; Hari and Forss, 1999; Huang et al., 2004; Rossini et al., 2001, 1998a, 1998b, Tecchio et al., 2007b, 2001; Tzvetanov et al., 2005; Wikström et al., 1999, 2000). It induces several peaks including an early peak around 20 ms and one around 50ms. Due to the fact that the median nerve stimulation activates both the sensory and motor

areas (through stimulation of Ia, Ib and II afferents), responses with larger amplitudes are observed when compared to the ones after electrical stimulation of the finger and with more prominent peaks. Although median nerve stimulation led to identifiable responses (Kalogianni et al., submitted), one should expect a less specific area of activation in the cortex in comparison to the activation after finger stimulation.

Increased delta power in resting state has been observed in perilesional areas of acute stroke patients (Cillessen et al., 1994; Jackel and Harner, 1989; Murri et al., 1998; Zappasodi et al., 2007). Abnormal low-frequency magnetic activity in a longitudinal follow-up has been found to correlate with larger lesions (Laaksonen et al., 2013). As summarized by Finnigan and Putten (2013) increased delta power at acute or subacute stage correlates with poor functional outcome and has a substantial prognostic value. Our results confirm that also, in chronic stroke, enhanced delta power at the affected hemisphere in comparison with lower delta power at the unaffected hemisphere correlates with poor motor scores at six months post stroke.

Resting state spectral power asymmetry was highly correlated with spectral power asymmetry during electric stimulation, at all frequency bands and both hemisphere, but stimulus-induced power was not always higher than resting state power when comparing power at ROI during rest and power after stimulus at the same ROI. This indicates that power modulations are not purely additive to the ongoing neural activity. However, a longer inter-stimulus interval (than used in this study, 250 ms) is necessary to investigate the induced or delayed oscillations after the transient stimulation and whether these oscillations correlate with stroke severity.

5.5 Conclusion

SEPs based on electrical stimulation of the fingers at a comfortable stimulation threshold cannot be used as a tool for characterizing chronic stroke because response peaks are difficult to identify. We can confirm previous findings that asymmetry of delta power correlates with Fugl-Meyer scores, demonstrating that EEG does provide a potential biomarker for stroke severity. The delta asymmetry

can already be estimated from recordings during resting state. Apparently, the activity evoked by finger stimulation is so weak that with regard to delta asymmetry the earlier reported correlation between sensory scores and delta asymmetry at rest remains valid. Hence, resting state alone may suffice as experimental paradigm to assess cortical correlates of motor function in chronic stroke.

5.6 Appendix

5.6.1 Detailed patients' characteristics

ID	FMA(0-66)	sensory impairment	months post stroke	gender	age	affected side	handedness
1	**13**	**none**	**83**	**M**	**64**	**L**	**R**
2	39	none	50	M	62	R	R
3	62	severe	7	M	77	L	R
4	9	severe	212	F	66	R	R
5	63	mild	36	F	76	L	R
6	8	severe	22	M	54	L	R
7	54	mild	27	M	67	R	R
8	58	none	76	M	55	L	L
9	9	mild	72	M	59	L	R
10	66	none	68	F	68	R	R
11	59	none	41	F	49	L	R
12	66	none	11	M	57	L	R
13	10	mild	82	M	48	L	R
14	64	mild	23	M	65	L	R
15	59	mild	54	F	50	R	R
16	48	none	35	M	50	L	R
17	56	mild	11	M	56	R	R
18	66	none	89	M	48	L	R
19	60	mild	11	F	61	R	R
20	26	severe	15	M	72	L	R
21	20	severe	144	M	68	L	L

Chapter 6

Discussion & Conclusions

ΟΥΔΕΝ ΕΙΔΑ ΟΥΤΕ ΔΙΔΑΣΚΩ ΤΙ ΑΛΛΑ ΔΙΑΠΟΡΩ ΜΟΝΟΝ
Δεν γνωρίζω ούτε διδάσκω κάτι αλλά μόνο έχω απορίες (προβληματισμούς)
Σωκράτης

Neither do I know nor I teach anything, I only have questions
Socrates

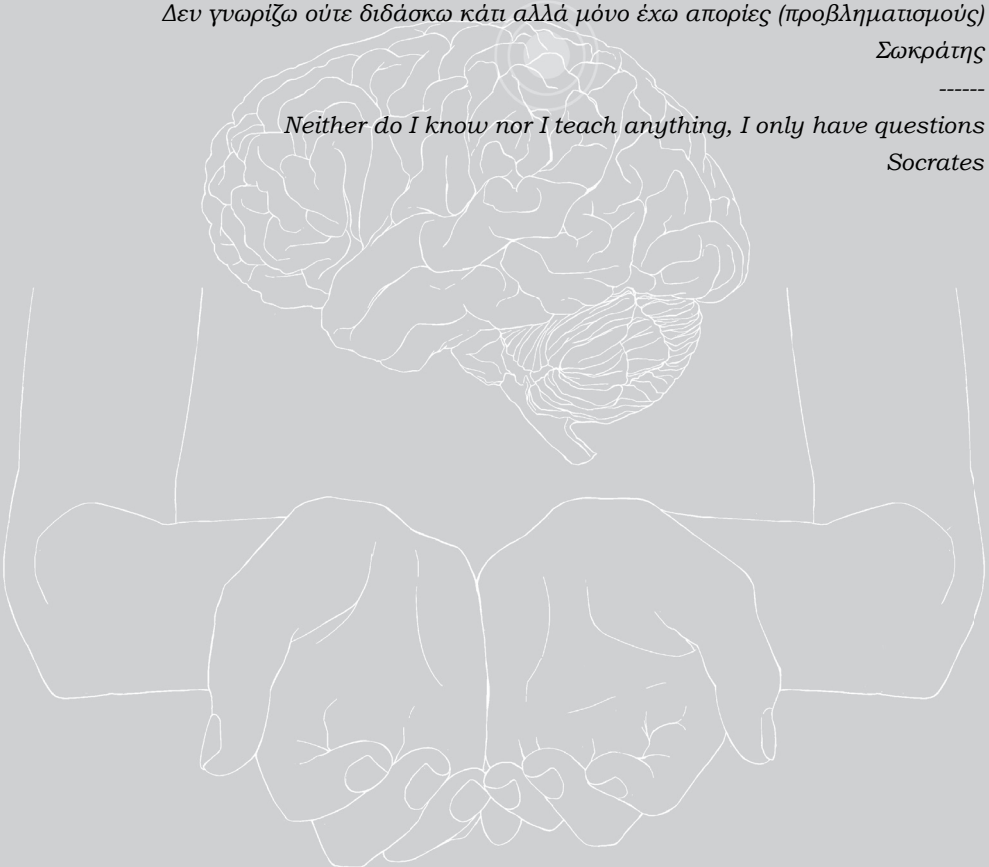

The goal of this thesis was to develop a methodology for tracking longitudinal changes after ischemic stroke within the somatosensory cortex using somatosensory evoked potentials (SEPs), with the ultimate aim to test for the validity of SEP as a biomarker in the clinical assessment of stroke. Tracking such expectedly subtle changes in a refined area in somatosensory cortices (S1/2) requires reproducible measurements with high spatial resolution. I started by studying the reproducibility of SEPs in healthy individuals after electric stimulation of the fingers in **Chapter 2.** What was meant as preparation to optimize protocols in patients revealed limited reproducibility of S1 responses to finger stimulation possibly due to a poor spatial separability of source-reconstructed EEG. This motivated my study in **Chapter 3** on the spatial resolution of EEG. There, I used synthetic data from numerical forward simulations and investigated the separability of proximate sources based on surface EEG. After these more principled chapters, I went into application by studying the capacity of SEP as a biomarker for predicting stroke recovery in **Chapters 4 & 5**.

The major conclusions of my thesis are as follows:

a) The complete separation of the cortical representations of different fingers as determined by EEG and electrical finger stimulation appears impossible due to the large overlap of the dipole representations for different fingers and the relatively low reproducibility of the test-retest design.

b) The EEG's 'spatial resolution' can be defined as the separability of sources. In typical clinical settings, it is about 1 cm, under the proviso of a sufficiently large signal-to-noise ratio (around 3). To achieve this resolution, a spatial pre-whitening is a mandatory pre-processing step when source-reconstructing surface EEG.

c) When assessing S1 responses in stroke, the amplitude and latency parameters of SEPs evoked by stimulation of the median nerve shows the capacity of improving the prognostic model for stroke recovery. This is particularly true for the interhemispheric differences of these parameters.

d) Lateralization of spectral power in lower frequency bands (here delta power asymmetries), recorded either at rest, or during electrical simulation, can be confirmed as a monitoring indicator tool for chronic stroke patients. In contrast

to the aforementioned responses after stimulation of the median nerve, stimulus-locked responses after electrical stimulation of the index finger are not associated with the severity of sensory and motor impairments after stroke.

Before answering the research questions listed in the introduction (**Chapter 1**), I will discuss the relationship between the results obtained in the separate chapters of this thesis.

6.1 General topics

6.1.1 Finger vs median nerve SEPs

Stimulation of the afferent sensory pathway by transient stimuli, i.e. SEPs, is a common approach when studying the somatosensory system. There are various different stimulation protocols that potentially provide distinct insight in the function of, e.g., the somatosensory cortices, S1/2. As of yet, however, there are no standardized ways of inducing SEPs and, hence, retrieving these insights. This might be due to several challenges when interpreting the cortical responses to stimulation. For instance, the latency and the amplitude of the responses are largely dependent on stimulus interval, stimulus duration and stimulation site.

In the present thesis, electrical stimulation of the fingers (Chapters 2 and 5) and the median nerve (Chapter 4) were employed to investigate SEPs. Electrical stimulation of the finger is an attractive experimental choice as it primarily recruits a single type of nerves (Aβ fibers) and likely activates a refined cortical area. However, the results of Chapters 2 and 5 discouraged the use of SEP induced by finger stimulation as a biomarker for stroke recovery. In healthy controls, responses appeared variable within and across recording sessions and finger representations largely overlapped. As shown in Chapter 5, in 55% of the included patients (N=21) event-related responses could neither be identified when fingers of the affected or unaffected side were stimulated.

To quantify the evoked responses, the interclass correlations (ICCs) of the test-rest reproducibility of SEP responses after electrical stimulation of the finger (intensity: 2× sensation threshold) and the median nerve (intensity: just above the thumb

twitch) were assessed in Chapter 4. In Tables 6.1 and 6.2 the results of six healthy controls have been summarized. Median nerve responses of the first test were significantly correlated with the re-test responses (except for the latency of P/N20 at the dominant hemisphere) of the re-test session. The responses after electrical stimulation of the index finger were not significantly reproducible, as shown in Tables 6.1 and 6.2 (except for the dominant P/N20 amplitude response). The SNR determined as in Chapter 2 (Equation 2.1) was also lower after electrical stimulation of the finger than after electrical stimulation of the median nerve (mean±std SNR dominant side=3.9±1.0, non-dominant side 3.4±0.6 versus dominant side=1.7±0.4, non-dominant side 1.7±0.2) – note that the SNR generally depends on the number of repetitions. The insufficient reproducibility for most of the extracted parameters provides additional evidence (rather than that given at Chapters 2 and 5) that event-related responses after electrical stimulation of the index finger are a less appropriate method to study the somatosensory cortex and the longitudinal changes of stroke recovery.

The electrical stimulation of the finger was performed with fairly comfortable stimulation amplitudes to prevent patient dropouts (Chapter 5). In the unaffected side we chose for a stimulation intensity of twice the individual sensation threshold as also reported in other studies (e.g. Baumgartner et al., 1993; Buchner et al., 1994) and used the same intensity at the affected side. Even if the stimulation amplitude was determined at the unaffected hemisphere, we always asked if the patient clearly felt the stimulation pulses at their affected site. Stimulation intensity close to pain threshold (≥ 3× sensation threshold) will induce responses with higher SNR and higher reproducibility (Wang et al., 2004). However, these responses were not suitable for our purpose because they can be expected to be associated with additional areas activated due to attention to the painful stimuli (Chien et al., 2014).

Table 6.1 P-values of ICCs of SEP peaks after stimulation of the index finger (IF) and the median nerve (MN) of the dominant hemisphere in controls; significant values are in bold.

	Lat P/N20	Amp P/N20	Lat P50	Amp P50
IF SEPs	0.81	**0.03**	0.94	0.88
MN SEPs	0.11	**0.01**	**0.0004**	**0.02**

Table 6.2 P-values of ICCs of SEP peaks after stimulation of the index finger (IF) and the median nerve (MN) of the non-dominant hemisphere in controls; significant values are in bold.

	Lat P/N20	Amp P/N20	Lat P50	Amp P50
IF SEPs	0.36	0.13	0.66	0.35
MN SEPs	0.79	**0.01**	**0.003**	**0.02**

6.1.2 Variable SEP amplitudes in healthy controls: what does it mean?

As discussed above, SEP responses after stimulation of the median nerve are highly reproducible within subjects. However, SEP amplitudes and latencies did vary considerably between subjects (Chapter 4). Are SEP responses mainly determined by confounding factors like the length of the arm, skull conductivity and thickness, age and gender? Or, do they depend more on electrophysiological characteristics, like the number of activated neurons and conductivity speeds?

To answer part of this question, I correlated the median nerve SEP responses of the six healthy controls of Section 6.1.1 with age and gender but could not find any significant correlation with response amplitudes and latencies both in dominant and non-dominant side. Unfortunately, the length of the arm and individual skull conductivity had not been recorded in the healthy controls, which did not allow for determined correlations between these parameters and SEP responses. The data presented in Chapter 4 showed that SEP responses after median nerve stimulation were variable across healthy controls. Since they did not depend on age and gender, it appears reasonable to hypothesize that subject specificity may stem from individual skull conductivity, the length of the arm, and genetic anatomical characteristics. Note that this has already been indicated by a study on monozygotic and dizygotic pairs by Van't Ent et al. (2010). Looking at latency differences and amplitude ratios, as proposed in Chapter 4, may eliminate subject

specific differences (length of the arm, scalp conductivity) and may help to achieve sensitivity of these parameters to stroke recovery-related changes.

6.1.3 Interhemispheric asymmetries after stroke.

In clinical neurophysiology, it is a common practice to test for differences between the two hemispheres. Interhemispheric differences of resting state spectral characteristics have an important value in monitoring recovery of stroke patients (van Putten, 2007; Sheorajpanday et al., 2009). Interhemispheric differences of SEP source locations in the early weeks post-stroke are associated with cerebral plasticity (Altamura et al., 2007; Rossini et al., 2001; Tecchio et al., 2006). Here, I used sc-MUSIC after data pre-whitening (Chapter 3) to test for interhemispheric asymmetries post stroke. In what follows, I present preliminary results at source level of participants that were recorded longitudinally (cf. Chapter 4) and who had a structural MRI available at the time of completing this thesis (4 healthy controls and 9 patients). These MRIs served to construct subject-specific, realistic head models. As explained in Chapter 3, prior to sc-MUSIC, a principal component analysis (PCA) was applied to disentangle the signal and the noise subspaces. In stroke patients, PCA always resulted in a single component as the signal subspace, which corresponded to the P50 peak (validated by correlating the PCAs topography to the P50 peak topography). This implies that there is a single, dominant source at the affected and one at the unaffected hemisphere. Interhemispheric differences were estimated by projecting the source location of the unaffected (or non-dominant side for healthy controls) hemisphere to the affected hemisphere (or the dominant side for healthy controls) and, subsequently, computing the Euclidean distance between the two sources. Let me denote this distance as ‘interhemispheric source asymmetry’ (ISA). ISAs of the patients were correlated with the Fugl-Meyer score and the sensory impairment as accessed by the Erasmus MC modified Nottingham sensory assessment (EMNsa).

ISAs in healthy controls were around 3 cm (mean±std: 26±6 mm) in agreement with an MEG study by Tecchio et al. (2007). Patients showed larger levels of ISA than healthy controls (mean±std over patients 1-4 weeks post stroke: 26±17 mm, 5 weeks post stroke:30±15 mm, 12 weeks post stroke:29±20 mm). In this arguably

small population (N=9), the ISAs did not correlate with motor or sensory impairment at the same measurement time (p>.05).

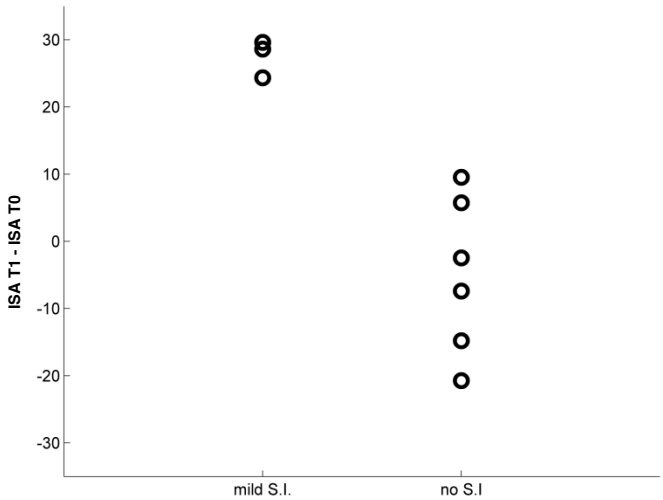

Fig. 6.1 Difference of interhemispheric source asymmetries at T0 (1-4 weeks after stroke) and T1 (five weeks post stroke), plotted against sensory impairment (S.I) at T3 (six months post stroke). Nine patients (# 1,2,3,5,6,8,9,13,14) were analyzed, more details of patients' characteristics can be found in Chapter 4.

Further, I investigated the difference between ISA in T0 (1-4 weeks post stroke) and ISA in T1 (5 weeks post stroke) and correlated it with the sensory impairment six months post stroke. A higher interhemispheric difference at T1 post stroke than at T0 (T1 ISA-T0 ISA>10 mm) correlated with mild sensory impairment six months post stroke (Fig. 6.1). Although this finding requires further validation in a larger sample, it does indicate that large interhemispheric differences of SEP source locations at early weeks post stroke (T0) in comparison to lower or almost the same interhemispheric differences at five weeks post stroke (T1) may predict good sensory function at six months post stroke.

6.2 Research questions

6.2.1 Is finger stimulation a valid approach for investigating S1?

In Chapter 2, I explored the use of SEPs induced by finger stimulation as a possible EEG biomarker for stroke recovery. Disentangling fingers' cortical representation would mean that changes occurring after stroke can be studied in great detail with the use of EEG. Moreover, a proper EEG biomarker should be highly reproducible, at least in healthy controls. However, the low reproducibility of SEPs after electrical stimulation of the fingers and the limitations in discriminating between representations of the fingers led us conclude that SEPs induced by electrical stimulation of the fingers should be used with great care when monitoring stroke recovery.

6.2.2 How can we define EEG's spatial resolution and what is the resolution?

The overlapping representation of the fingers, as found in Chapter 2, indicated that the EEG's spatial resolution using SEP may be worse than 3-5 mm, which is the distance of representation of the fingers in Brodmann area 3b as revealed by an fMRI study (Martuzzi et al., 2014). This called for a study to define the spatial resolution of EEG. A high spatial resolution of EEG is important when studying small anatomical changes. For example, early after stroke neural populations in the somatosensory area re-organize in order to remap the motor projections (Ward and Cohen, 2004).

Defining the spatial resolution of a brain imaging method is not trivial. EEG's spatial resolution depends on several parameters, including the number and location of underlying sources., In Chapter 3, we defined the spatial resolution of EEG as the distance between two cortical sources where the confidence limits of the source reconstruction that do not overlap. We used synthetic data generated through numerical forward simulation which guaranteed all knowledge of source activity (ground truth). When mimicking conventional clinical settings, the spatial resolution of source-localized EEG was about 1 cm presuming a sufficiently large signal-to-noise ratio (SNR ≥ 3). Achieving this resolution required to account for spatial correlations of the noise and to minimize them via spatial pre-whitening).

With the use of EEG, one can study stroke-related changes within that area with a resolution of about 1 cm given that two sources are active during the same time window of exploration. Simultaneous activations within areas that are closer than this threshold are not separable with EEG.

Although the resolution relies on choices of our simulation study (e.g., 64 EEG electrodes, small time delay between sources), it does provide a quantifiable and verifiable measure of the EEG's spatial resolution. It can be expected that a more dense electrode array and a finer grid will improve EEG's spatial resolution only marginally (Akalin Acar and Makeig, 2013; Lantz et al., 2003).

If a single source is present (like shown in Section 6.1.3), then our notion of 'resolution' is not appropriate as it is based on the separability of sources. In that case one should test for the accuracy of the inverse method employed. Longitudinal changes related to stroke as studied in Section 6.1.3 may be assessed with the accuracy provided by the inverse method of choice.

6.2.3 Can SEP parameters, early or a few weeks after stroke, be used to improve the prediction of the rehabilitation curve of stroke patients?
Can SEPs induced by finger stimulation provide useful insights about chronic stroke patients?

Biomarkers for longitudinal stroke monitoring should be reproducible between recordings (test-retest design). Parameters extracted from SEP recordings after median nerve stimulation were found reproducible as shown in healthy participants in a test-retest setup in Section 6.1.1. SEP induced by electrical stimulation at the median nerve (Chapter 4) rather than electrical stimulation on the finger (Chapter 5) can serve as a prognostic model for stroke recovery. After normalizing the recorded latency and amplitude parameters to reduce the influence of length of the arm and thickness of the skull, I managed to extract parameters relevant for stroke recovery. In Chapter 4, it was demonstrated that SEP features five weeks post stroke can provide prognostic information about stroke severity at six months post-stroke. A potentially important contribution of this study is a possible biomarker to predict stroke recovery can be identified already five weeks after stroke.

6.3 Future direction of the research: recommendations

The size and area of brain lesions after stroke vary and so does the electrical conductivity in the brain due to changes of oxygenation in the lesioned area. When altered tissue conductivity is present, source modeling must be adjusted. Improper values of conductivity induce a large error in source localization accuracy (Akalin Acar and Makeig, 2013). Although modeling of the lesion is feasible (Pustina et al., 2016), the altered conductivity is typically not incorporated in present volume conduction models for stroke patients. Future research is needed to validate to what extent subject-specific tissue conductivity values can improve source modeling in stroke patients (Dabek et al., 2016).

As stressed at several instances in my thesis, I advocate spatial pre-whitening as a mandatory pre-processing step in inverse modelling. When also taking into account the temporal correlations of the noise, one can expect further improvements of the accuracy of pretty much every inverse method (Bijma et al., 2003; Engemann and Gramfort, 2015; de Munck et al., 2002). However, its effect on spatial resolution of EEG should be further tested and quantified starting with simulation studies since they provide the ground truth of the generating sources. An extension of the simulation study, presented in Chapter 3, may serve as a starting point to quantify the effect of temporal pre-whitening.

6.4 The 4D-EEG project

The present thesis is part of the ERC advanced project 4D-EEG (n. 291339). 4D-EEG aims to understand how stroke patients regain control of their arm. It is a collaborative project of four universities: Delft University of Technology, VU University Medical Center, Amsterdam, Vrije Universiteit Amsterdam, and Northwestern University, Chicago. For the purposes of the 4D-EEG project a large dataset of acute and chronic stroke patients was and is still being recorded. In brief, patients undergo a complete assessment protocol including EEG recordings with sensory and motor tasks, MRI scans, fMRI recordings and clinical assessments.

Here I would like to note that most of the experimental choices made in Chapters 4 and 5 reflect a trade-off between protocol variety and measurement time. The duration of the SEP recordings had to be limited to a maximum of 15 minutes (1000 repetitions with an inter-stimulus interval of 250 to 330 ms) for both affected and unaffected hemisphere, to leave sufficient time for the rest of the EEG protocol that was limited to 90 minutes (along with preparation of the measurement that was 25 minutes). More research is necessary to determine if more repetitions or larger inter-stimulus intervals are necessary to obtain a better signal to noise ratio. As mentioned in Chapter 4, a more detailed test of the methodology developed in this thesis, will be conducted at a later stage when the 4D-EEG dataset is complete.

Bibliography

van ’t Ent D, van Soelen ILC, Stam KJ, de Geus EJC, Boomsma DI. Genetic influence demonstrated for MEG-recorded somatosensory evoked responses. Psychophysiology 2010;47:1040–6.

Akalin Acar Z, Makeig S. Effects of forward model errors on EEG source localization. Brain Topogr 2013;26:378–96.

Al-Rawi MAW, Hamdan FB, Abdul-Muttalib AK. Somatosensory evoked potentials as a predictor for functional recovery of the upper limb in patients with stroke. J Stroke Cerebrovasc Dis 2009;18:262–8.

Altamura C, Torquati K, Zappasodi F, Ferretti A, Pizzella V, Tibuzzi F, et al. fMRI-vs-MEG evaluation of post-stroke interhemispheric asymmetries in primary sensorimotor hand areas. Exp Neurol 2007;204:631–9.

Anastasi AA, Falzon O, Camilleri K, Vella M, Muscat R. Brain Symmetry Index in Healthy and Stroke Patients for Assessment and Prognosis. Stroke Res Treat 2017.

Baillet S, Mosher JC, Leahy RM. Electromagnetic brain imaging. IEEE Signal Process Mag 2001;18:14–30.

Barbati G, Sigismondi R, Zappasodi F, Porcaro C, Graziadio S, Valente G, et al. Functional Source Separation from Magnetoencephalographic Signals. Hum Brain Mapp 2006;27:925–34.

Baumgartner C, Doppelbauer A, Sutherling WW, Lindinger G, Levesque MF, Aull S, et al. Somatotopy of human hand somatosensory cortex as studied in scalp EEG. Electroencephalogr Clin Neurophysiol 1993;88:271–9.

Becker H, Albera L, Comon P, Gribonval R, Wendling F, Merlet I. A performance study of various brain source imaging approaches. Proc. 2014 IEEE Int. Conf. Acoust. Speech Signal Process. Proceeding(ICASSP), 2014, p. 5869–73.

Berger H. Über das Elektroenzephalogramm des Menschen. Arch Für Psychiatr Und Nervenkrankheiten 1929;87:527–70.

Bernhardt J, Hayward KS, Kwakkel G, Ward NS, Wolf SL, Borschmann K, et al. Agreed definitions and a shared vision for new standards in stroke recovery research : The Stroke Recovery and Rehabilitation Roundtable taskforce. Int J Stroke 2017;12:444–50.

Bijma F, de Munck JC, Heethaar RM. The spatiotemporal MEG covariance matrix modeled as a sum of Kronecker products. Neuroimage 2005;27:402–15.

Bijma F, de Munck JC, Huizenga HM, Heethaar RM. A mathematical approach to the temporal stationarity of background noise in MEG/EEG measurements. Neuroimage 2003;20:233–43.

Bolognini N, Russo C, Edwards DJ. The sensory side of post-stroke motor rehabilitation. Restor Neurol Neurosci 2016;34:571–86.

Bourguignon M, Jousmäki V, Marty B, Wens V, Op de Beeck M, van Bogaert P, et al. Comprehensive functional mapping scheme for non-invasive primary sensorimotor cortex mapping. Brain Topogr 2013;26:511–23.

Boyd LA, Hayward KS, Ward NS, Stinear CM, Rosso C, Fisher RJ, et al. Biomarkers of Stroke Recovery: Consensus-Based Core Recommendations from the Stroke Recovery and Rehabilitation Roundtable*. Neurorehabil Neural Repair 2017;31:864–76.

Bradley A, Yao J, Dewald J, Richter C. Evaluation of Electroencephalography Source Localization Algorithms with Multiple Cortical Sources. PLoS One 2016;11:e0147266.

Brookes MJ, Vrba J, Robinson SE, Stevenson CM, Peters AM, Barnes GR, et al. Optimising experimental design for MEG beamformer imaging 2008;39:1788–802.

Brunet D, Murray MM, Michel CM. Spatiotemporal Analysis of Multichannel EEG: CARTOOL. Comput Intell Neurosci 2011;2011:1–15.

Buch ER, Rizk S, Nicolo P, Cohen LG, Schnider A, Guggisberg AG. Predicting motor improvement after stroke with clinical assessment and diffusion tensor imaging. Neurology 2016;86:1924–5.

Buchner H, Fuchs M, Wischmann H-A, Dössel O, Ludwig I, Knepper A, et al. Source analysis of median nerve and finger stimulated somatosensory evoked potentials: multichannel simultaneous recording of electric and magnetic fields combined with 3D-MR tomography. Brain Topogr 1994;6:299–310.

Bullock TH. Introduction to Induced Rhythms: A Widespread, Heterogeneous Class of Oscillations. Induc. Rhythm. Brain, 1992, p. 1–26.

Byblow WD, Stinear CM, Barber PA, Petoe MA, Ackerley SJ. Proportional recovery after stroke depends on corticomotor integrity. Ann Neurol 2015;78:848–59.

Castillo EM, Boake C, Breier JI, Men D, Garza HM., Passaro A, et al. Aberrant Cortical Functionality and Somatosensory Deficits After Stroke. J Clin Neurophysiol 2008;25:132–8.

Chien JH, Liu CC, Kim JH, Markman TM, Lenz F a. Painful cutaneous laser stimuli induce event-related oscillatory EEG activities that are different from those induced by nonpainful electrical stimuli. J Neurophysiol 2014;112:824–33.

Cillessen JPM, van Huffelen AC, Kappelle LJ, Algra A, van Gijn J. Electroencephalography Improves the Prediction of Functional Outcome in the Acute Stage of Cerebral Ischemia. Am Hear Assoc 1994:1968–73.

Connel L., Lincoln N, Radford K. Somatosensory impairment after stroke : frequency of different deficits and their recovery. Clin Rehabil 2008;22:758–67.

Corbett D, Carmichael ST, Murphy TH, Jones TA, Schwab ME, Jolkkonen J, et al. Enhancing the alignment of the preclinical and clinical stroke recovery research pipeline : Consensus-based core recommendations from the Stroke Recovery and Rehabilitation Roundtable translational working group. Int J Stroke 2017;12:462–71.

Cramer SC. Repairing the human brain after stroke: I. Mechanisms of spontaneous recovery. Ann Neurol 2008;63:272–87.

Cruccu G, Aminoff MJ, Curio G, Guerit JM, Kakigi R, Mauguiere F, et al. Recommendations for the clinical use of somatosensory-evoked potentials. Clin Neurophysiol 2008;119:1705–19.

Dabek J, Kalogianni K, Rotgans E, van der Helm FCT, Kwakkel G, van Wegen EEH, et al. Determination of head conductivity frequency response in vivo with optimized EIT-EEG. Neuroimage 2016;127:484–95.

Darvas F, Pantazis D, Kucukaltun-Yildirim E, Leahy RM. Mapping human brain function with MEG and EEG: methods and validation. Neuroimage 2004;23 Suppl 1:S289-99.

Darvas F, Rautiainen M, Pantazis D, Baillet S, Benali H, Mosher JC, et al. Investigations of dipole localization accuracy in MEG using the bootstrap. Neuroimage 2005;25:355–68.

David O, Kilner JM, Friston KJ. Mechanisms of evoked and induced responses in MEG / EEG. Neuroimage 2006;31:1580–91.

Dawson G. D. The relative excitability and conduxtion velocity of sesnory and motor nerve fibres in man. JPhysiol 1956;131:436–51.

Dawson G. D. A summation technique for the detection of small evoked potentials. Electroencephalogr Clin Neurophysiol 1954;6:65–84.

Delorme A, Makeig S. EEGLAB : an open source toolbox for analysis of single-trial EEG dynamics including independent component analysis. J Neurosci Methods 2004;134:9–21.

Dowman R. Interstimulus interval has no effect on a mid-latency scalp potential generated by innocuous-related activity in the primary somatosensory cortex. Brain Topogr 1997;10:145–54.

Druschky K, Kaltenhäuser M, Hummel C, Druschky A, Pauli E, Huk WJ, et al. Somatotopic organization of the ventral and dorsal finger surface representations in human primary sensory cortex evaluated by magnetoencephalography. Neuroimage 2002;15:182–9.

Duncan PW, Propst M, Nelson SG. Reliability of the Fugl-Meyer Assessment of Sensorimotor Recovery Following Cerebrovascular Accident. Phys Ther 1983;63:1606–10.

Dutilleul P. The mle algorithm for the matrix normal distribution. J Stat Comput Simul 1999;64:105–23.

Engemann DA, Gramfort A. Automated model selection in covariance estimation and spatial whitening of MEG and EEG signals. Neuroimage 2015;108:328–42.

Feigin VL, Mensah GA, Norrving B, Murray CJL, Roth GA, Bahit MC, et al. Atlas of the global burden of stroke (1990-2013): The GBD 2013 study. Neuroepidemiology 2015;45:230–6.

Feys H, Van Hees J, Bruyninckx F, Mercelis R, De Weerdt W. Value of somatosensory and motor evoked potentials in predicting arm recovery after a stroke. J Neurol Neurosurg Psychiatry 2000;68:323–31.

Finnigan S, van Putten MJAM. EEG in ischaemic stroke: Quantitative EEG can uniquely inform (sub-) acute prognoses and clinical management. Clin Neurophysiol 2013;124:10–9.

Forss N, Hari R, Salmelin R, Ahonen A, Hämäläinen M, Kajola M, et al. Activation of the human posterior parietal cortex by median nerve stimulation. Exp Brain Res 1994a;99:309–15.

Forss N, Hietanen M, Salonen O, Hari R. Modified activation of somatosensory cortical network in patients with right-hemisphere stroke. Brain 1999;122:1889–99.

Forss N, Salmelin R, Hari R. Comparison of somatosensory evoked fields to airpuff and electric stimuli. Electroencephalogr Clin Neurophysiol 1994b;92:510–7.

Fugl-Meyer A, Jääskö L, Leyman I, Olsson S, Steglind S. The post-stroke hemiplegic patient. 1. a method for evaluation of physical performance. Scand J Rehabil Med 1975;7:13–31.

Gao L, Sommerlade L, Coffman B, Zhang T, Stephen JM, Li D, et al. Granger causal time-dependent source connectivity in the somatosensory network. Sci Rep 2015;5:10399.

Gladstone DJ, Danells CJ, Black SE. The Fugl-Meyer Assessment of Motor Recovery after Stroke: A Critical Review of Its Measurement Properties. Neurorehabil Neural Repair 2002;16.

Goldenholz DM, Ahlfors SP, Hämäläinen MS, Sharon D, Ishitobi M, Vaina LM, et al. NIH Public Access. Hum Brain Mapp 2009;30:1077–86.

de Gooijer-van de Groep KL, Leijten FSS, Ferrier CH, Huiskamp GJM. Inverse modeling in magnetic source imaging: Comparison of MUSIC, SAM(g2), and sLORETA to interictal intracranial EEG. Hum Brain Mapp 2013;34:2032–44.

Goszczynska H, Kowalczyk L, Kuraszkiewicz B. Correlation Matrices as a Tool to Analyze the Variability of EEG Maps. In: Pietka E, Kawa J, Wieclawek W, editors. Inf. Technol. Biomed., vol. 284, Switzerland: Springer International Publishing; 2014, p. 311–20.

Gramfort A, Kowalski M, Hämäläinen M. Mixed-norm estimates for the M/EEG inverse problem using accelerated gradient methods. Phys Med Biol 2012;57:1937–61.

Grech R, Cassar T, Muscat J, Camilleri KP, Fabri SG, Zervakis M, et al. Review on solving the inverse problem in EEG source analysis. J Neuroeng Rehabil 2008;5:25.

Grefkes C, Fink GR. Reorganization of cerebral networks after stroke: new insights from neuroimaging with connectivity approaches. Brain 2011;134:1264–76.

Grova C, Daunizeau J, Lina J-M, Bénar CG, Benali H, Gotman J. Evaluation of EEG localization methods using realistic simulations of interictal spikes. Neuroimage 2006;29:734–53.

Hallez H, Vanrumste B, Grech R, Muscat J, de Clercq W, Vergult A, et al. Review on solving the forward problem in EEG source analysis. J Neuroeng Rehabil 2007;4:46.

Hämäläinen H, Kekoni J, Sams M, Reinikainen K, Näätänen R. Human somatosensory evoked potentials to mechanical pulses and vibration : contributions of SI and SII somatosensory cortices to PS0 and P100 components. Electroencephalogr Clin Neurophysiol 1990;75:13–21.

Hämäläinen MS, Hari R, Ilmoniemi RJ, Knuutila J, Lounasmaa O V. Magnetoencephalography - theory, instrumentation, and applications to noninvasivee studies of the working human brain. Rev Mod Phys 1993;65:413–505.

Hari R, Forss N. Magnetoencephalography in the study of human somatosensory cortical processing. Philos Trans R Soc Lond B Biol Sci 1999;354:1145–54.

von Helmholtz H. Ueber einige gesetze der vertheilung elektrischer stroeme in koerperlichen leitern, mit anwenung auf die thierisch- elektrischen versuche. Ann Phys Chem 1853;89:211–233, 353–377.

Houzé B, Perchet C, Magnin M, Garcia-Larrea L. Cortical representation of the human hand assessed by two levels of high-resolution EEG recordings. Hum Brain Mapp 2011;32:1894–904.

Hu L, Zhang ZG, Hu Y. A time-varying source connectivity approach to reveal human somatosensory information processing. Neuroimage 2012;62:217–28.

Huang M, Davis LE, Aine C, Weisend M, Harrington D, Christner R, et al. MEG response to median nerve stimulation correlates with recovery of sensory and motor function after stroke. Clin Neurophysiol 2004;115:820–33.

Jackel RA, Harner RN. Computed EEG topography in acute stroke. Neurophysiol Clin Neurophysiol 1989;19:185–97.

de Jongh A, de Munck J, Gonçalves S, Ossenblok P. Differences in MEG/EEG epileptic spike yields explained by regional differences in signal to noise ratios. J Clin Neurophysiol 2005;22:153–8.

Jordan KG. Emergency EEG and continuous EEG monitoring in acute ischemic stroke. J Clin Neurophysiol 2004;21:341–52.

Kaas JH. What, if Anything, is SI ? Organization of First Somatosensory Area of Cortex. Physiol Rev 1983;63:206–31.

Kalogianni K, Daffertshofer A, van der Helm FCT, Schouten AC, de Munck JC. Disentangling somatosensory evoked potentials of the fingers: limitations and clinical potential. Brain Topogr 2018;31(3):498-512.

Kalogianni K, Saes M, Vlaar MP, van Wegen E, Kwakkel G, Schouten AC, et al. Are longitudinal SSEP recordings a biomarker for proportional motor recovery post stroke? n.d.

Kandel ER, H.Schwartz J, Jessel TM. Principals of Neural science. 4th ed. New York: McGraw-Hill; 2000.

Keren O, Ring H, Solzi P, Pratt H, Groswasser Z. Upper Limb Somatosensory Evoked Potentials as a Predictor of Rehabilitation Progress in Dominant Hemisphere Stroke Patients. Stroke 1993;24:1789–93.

Kirschstein T, Kohling R. What is the source of EEG? Clin EEG Neurosci 2009;40:146–9.

Kordelaar J Van, Wegen EEH Van, Nijland RHM, Daffertshofer A, Kwakkel G. Understanding Adaptive Motor Control of the Paretic Upper Limb Early Poststroke : The EXPLICIT-stroke Program. Neurorehabil Neural Repair 2013;27:854–63.

Krakauer JW, Marshall RS. The proportional recovery rule for stroke revisited. Ann Neurol 2015;78:845–7.

Krishnamurthi R V, Feigin VL, Forouzanfar MH, Mensah GA, Connor M, Bennett DA, et al. Global and regional burden of first-ever ischaemic and haemorrhagic stroke during 1990-2010: Findings from the Global Burden of Disease Study 2010. Lancet Glob Heal 2013;1:e259–81.

Kristeva-Feige R, Rossi S, Pizzella V, Tecchio F, Romani GL, Erne S, et al. Neuromagnetic fields of the brain evoked by voluntary movement and electrical stimulation of the index finger. Brain Res 1995;682:22–8.

Kuiken T, Marasco PD, Lock B, Harden RN, Dewald JP. Redirection of cutaneous sensation from the hand to the chest skin of human amputees with targeted reinnervation. Proc Natl Acad Sci U S A 2007;104:20061–6.

Kwakkel G, Kollen B, Twisk J. Impact of time on improvement of outcome after stroke. Stroke 2006;37:2348–53.

Kwakkel G, Kollen BJ, Grond J Van Der, Prevo AJH. Probability of Regaining Dexterity in the Flaccid Upper Limb. Stroke 2003;34.

Kwakkel G, Lannin NA, Borschmann K, English C, Ali M, Churilov L, et al. Standardized measurement of sensorimotor recovery in stroke trials : Consensus-based core recommendations from the Stroke Recovery and Rehabilitation Roundtable. Int J Stroke 2017;12:451–61.

Laaksonen K, Helle L, Parkkonen L, Kirveskari E, Mäkelä JP, Mustanoja S, et al. Alterations in Spontaneous Brain Oscillations during Stroke Recovery. PLoS One 2013;8.

Laaksonen K, Kirveskari E, Mäkelä JP, Kaste M, Mustanoja S, Nummenmaa L, et al. Effect of afferent input on motor cortex excitability during stroke recovery. Clin Neurophysiol 2012;123:2429–36.

Langhorne P, Bernhardt J, Kwakkel G. Stroke rehabilitation. Lancet 2011;377:1693–702.

Lantz G, Grave de Peralta R, Spinelli L, Seeck M, Michel CM. Epileptic source localization with high density EEG: how many electrodes are needed? Clin Neurophysiol 2003;114:63–9.

Leahy RM, Mosher JC, Spencer ME, Huang MX, Lewine JD. A study of dipole localization accuracy for MEG and EEG using a human skull phantom. Electroencephalogr Clin Neurophysiol 1998;107:159–73.

Lehmann D, Skrandies W. Reference-free identification of components of checkerboard-evoked multichannel potential fields. Electroencephalogr Clin Neurophysiol 1980;48.

Leiva R, Roy A. Classification of higher-order data with separable covariance and structured multiplicative or additive mean models. Commun Stat - Theory Methods 2014;43:989–1012.

Lin F-H, Witzel T, Ahlfors SP, Stufflebeam SM, Belliveau JW, Hämäläinen MS. Assessing and improving the spatial accuracy in MEG source localization by depth-weighted minimum-norm estimates. Neuroimage 2006;31:160–71.

Lopes da Silva F. Functional localization of brain sources using EEG and/or MEG data: volume conductor and source models. Magn Reson Imaging 2004;22:1533–8.

Lu N, Zimmerman DL. The likelihood ratio test for a separable covariance matrix. Stat Probab Lett 2005;73:449–57.

Luck SJ. An Introduction to Event-Related Potentials and Their Neural Origins. In: MIT Press, editor. An Introd. to Event-Related Potential Tech., Cambridge: 2005.

Lyle RC. A performance test for assessment of upper limb function in physical rehabilitation treatment and research. Int J Rehabil Res 1981;4:483–492.

Macdonell RAL. Serial changes in somatosensory evoked potentials following cerebral infarction. Electroencephalogr Clin Neurophysiol 1991;80:276–83.

Martuzzi R, van der Zwaag W, Farthouat J, Gruetter R, Blanke O. Human finger somatotopy in areas 3b, 1, and 2: a 7T fMRI study using a natural stimulus. Hum Brain Mapp 2014;35:213–26.

Marzetti L, Del Gratta C, Nolte G. Understanding brain connectivity from EEG data by identifying systems composed of interacting sources. Neuroimage 2008;42:87–98.

Mauguiere F. Somatosensory evoked potentials: normal responses, abnormal waveforms and clinical applications in neurological diseases. In: Niedermeyer E, editor. Electroencephalogr. Basic Princ. Clin. Appl. Relat. Fields, Baltimore: Williams and Wilkins; 1999.

McAllister RMR, Urban LA, Dray A, Smith PJ. Comparison of the sensory threshold in healthy human volunteers with the sensory nerve response of the rat in vitro hindlimb skin and saphenous nerve preparation on cutaneous electrical stimulation. J Hand Surg Am 1995;20B:437–43.

Mcgraw KO, Wong S. Forming Inferences About Some Intraclass Correlation Coefficients Forming Inferences About Some Intraclass Correlation Coefficients. Psychol Methods 1996;1:30–46.

Meyer S, Bruyn N De, Lafosse C, Dijk M Van, Michielsen M, Thijs L, et al. Somatosensory Impairments in the Upper Limb Poststroke : Distribution and Association With Motor Function and Visuospatial Neglect 2016.

Michel CM, Murray MM. Towards the utilization of EEG as a brain imaging tool. Neuroimage 2012;61:371–85.

Michel CM, Murray MM, Lantz G, Gonzalez S, Spinelli L, Grave de Peralta R. EEG source imaging. Clin Neurophysiol 2004;115:2195–222.

Mideksa KG, Hellriegel H, Hoogenboom N, Krause H, Schnitzler A, Deuschl G, et al. Source analysis of median nerve stimulated somatosensory evoked potentials and fields using simultaneously measured EEG and MEG signals. 34th Annu. Int. Conf. IEEE EMBS San Diego, California, USA, 2012, p. 4903–6.

Miller EL, Murray L, Richards L, Zorowitz RD, Bakas T, Clark P, et al. Comprehensive overview of nursing and interdisciplinary rehabilitation care of the stroke patient: A scientific statement from the American heart association. Stroke 2010;41:2402–48.

Mosher JC, Lewis PS, Leahy RM. Multiple Dipole Modeling and Localization from Spatio-Temporal MEG Data. IEEE Trans Biomed Eng 1992;39:541–57.

Mosher JC, Spencer ME, Leahy RM, Lewis PS. Error bounds for EEG and MEG dipole source localization. Electroencephalogr Clin Neurophysiol 1993;86:303–21.

de Munck JC. The estimation of time varying dipoles on the basis of evoked potentials. Electroencephalogr Clin Neurophysiol Evoked Potentials 1990;77:156–60.

de Munck JC, Bijma F. Three-way matrix analysis, the MUSIC algorithm and the coupled dipole model. J Neurosci Methods 2009;183:63–71.

de Munck JC, van Dijk BW, Spekreijse H. Mathematical dipoles are adequate to describe realistic generators of human brain activity. IEEE Trans Biomed Eng 1988;35:960–6.

de Munck JC, Huizenga HM, Waldorp LJ, Heethaar RM. Estimating stationary dipoles from MEG/EEG data contaminated with spatially and temporally correlated background noise. IEEE Trans Signal Process 2002;50:1565–72.

de Munck JC, de Jongh A, van Dijk BW. The Localization of Spontaneous Brain Activity : An Efficient Way to Analyze Large Data Sets. IEEE Trans Biomed Eng 2001;48:1221–8.

de Munck JC, Vijn PCM, Lopes da Silva FH. A Random Dipole Model for Spontaneous Brain Activity. IEEE Trans Biomed Eng 1992;39:791–804.

Murri L, Gori S, Massetani R, Bonanni E, Marcella F, Milani S. Evaluation of acute ischemic stroke using quantitative EEG: a comparison with conventional EEG and CT scan. Neurophysiol Clin Neurophysiol 1998:249–57.

Niedermeyer E, da Silva F. Electroencephalography: Basic Principles, Clinical Applications, and Related Fields. 5th Editio. Lippincott; 2004.

Nierula B, Hohlefeld FU, Curio G, Nikulin V V. No somatotopy of sensorimotor alpha-oscillation responses to differential finger stimulation. Neuroimage 2013;76:294–303.

Nijland R, Van Wegen E, Verbunt J, Van Wijk R, Van Kordelaar J, Kwakkel G. A comparison of two validated tests for upper limb function after stroke: The wolf motor function test and the action research arm test. J Rehabil Med 2010a;42:694–6.

Nijland R, van Wegen EEH, Harmeling-van der Wel BC, Kwakkel G. Presence of finger extension and shoulder abduction within 72 hours after stroke predicts functional recovery: early prediction of functional outcome after stroke: the EPOS cohort study. Stroke 2010b;41:745–50.

Nikulin V V, Linkenkaer-Hansen K, Nolte G, Lemm S, Müller KR, Ilmoniemi RJ, et al. A novel mechanism for evoked responses in the human brain. Eur J Neurosci 2007;25:3146–54.

Oliviero A, Tecchio F, Zappasodi F, Pasqualetti P, Salustri C, Lupoi D, et al. Brain sensorimotor hand area functionality in acute stroke: insights from magnetoencephalography. Neuroimage 2004;23:542–50.

Oostenveld R, Fries P, Maris E, Schoffelen J-M. FieldTrip: Open Source Software for Advanced Analysis of MEG, EEG, and Invasive Electrophysiological Data. Comput Intell Neurosci 2011:1–9.

Oostenveld R, Stegeman DF, Praamstra P, Oosterom A Van. Brain symmetry and topographic analysis of lateralized event-related potentials. Clin Neurophysiol 2003;114:1194–202.

Ou W, Hämäläinen MS, Golland P. A distributed spatio-temporal EEG/MEG inverse solver. Neuroimage 2009;44:932–46.

Parker V, Wade D, Hewer- Langton R. Loss of arm function after stroke: measurement, frequency, and recovery. Int Rehabil Med 1986:69–73.

Pascual-Marqui RD. Discrete, 3D distributed, linear imaging methods of electric neuronal activity. Part 1: exact, zero error localization 2007:74–6.

Pascual-Marqui RD. Standardized low resolution brain electromagnetic tomography (sLORETA): technical details. Methods Find Exp Clin Pharmacol 2002;24 Suppl D:5–12.

Pascual-Marqui RD, Lehmann D, Koukkou M, Kochi K, Anderer P, Saletu B, et al. Assessing interactions in the brain with exact low-resolution electromagnetic tomography. Philos Trans R Soc A 2011;369:3768–84.

Pascual-Marqui RD, Michel CM, Lehmann D. Low Resolution Electromagentic Tomography: A New Method for Localizing Electrical Activity in the Brain. Int J Psychophysiol 1994;18:49–65.

Penfield W, Boldrey E. Somatic motor and sensory represenation in the cerebral cortex of man as studied by electrical stimulation. Brain 1937;60:389–443.

Penfield W, Rasmussen T. The Cerebral Cortex of Man: A Clinical Study of Localization of Function. New York: Macmillan; 1950.

Péréon Y, Aubertin P, Guihéneuc P. Prognostic significance of electrophysiological investigations in stroke patients: somatosensory and motor evoked potentials and sympathetic skin response. Neurophysiol Clin 1995;25:146–57.

Pfannmöller JP, Schweizer R, Lotze M. Automated analysis protocol for high resolution BOLD-fMRI mapping of the fingertip somatotopy in brodmann area 3b. J Magn Reson Imaging 2015;43.

Prabhakaran S, Zarahn E, Riley C, Speizer A, Chong JY, Lazar RM, et al. Inter-individual Variability in the Capacity for Motor Recovery After Ischemic Stroke. Neurorehabil Neural Repair 2008;22:64–71.

Pustina D, Coslett HB, Turkeltaub PE, Tustison N, Schwartz MF, Avants B. Automated segmentation of chronic stroke lesions using LINDA: Lesion identification with neighborhood data analysis. Hum Brain Mapp 2016;37:1405–21.

van Putten MJAM. The revised brain symmetry index. Clin Neurophysiol 2007;118:2362–7.

van Putten MJAM. Extended BSI for continuous EEG monitoring in carotid endarterectomy. Clin Neurophysiol 2006;117:2661–6.

van Putten MJAM, Hofmeijer J. Invited Review. EEG Monitoring in Cerebral Ischemia: Basic Concepts and Clinical Applications. J Clin Neurophysiol 2016;33:203–10.

van Putten MJAM, Tavy LJ. Continuous Quantitative EEG Monitoring in Hemispheric Stroke Patients Using the Brain Symmetry Index. Stroke 2004;35:2489–93.

Ramírez RR, Kopell BH, Butson CR, Hiner BC, Baillet S. Spectral signal space projection algorithm for frequency domain MEG and EEG denoising, whitening, and source imaging. Neuroimage 2011;56:78–92.

Roiha K, Kirveskari E, Kaste M, Mustanoja S, Mäkelä JP, Salonen O, et al. Reorganization of the primary somatosensory cortex during stroke recovery. Clin Neurophysiol 2011;122:339–45.

Rollnik JD. May clinical neurophysiology help to predict the recovery of neurological early rehabilitation patients? BMC Neurol 2015;15:1–7.

Roś BP, Bijma F, de Gunst MCM, de Munck JC. A three domain covariance framework for EEG/MEG data. Neuroimage 2015;119:305–15.

Rossini PM, Caltagirone C, Castriota-Scanderbeg A, Cicinelli P, Del Gratta C, Demartin M, et al. Hand motor cortical area reorganization in stroke: a study with fMRI, MEG and TCS maps. Neuroreport 1998a;9:2141–6.

Rossini PM, Tecchio F, Pizzella V, Lupoi D, Cassetta E, Pasqualetti P. Interhemispheric differences of sensory hand areas after monohemispheric stroke: MEG/MRI integrative study. Neuroimage 2001;14:474–85.

Rossini PM, Tecchio F, Pizzella V, Lupoi D, Cassetta E, Pasqualetti P, et al. On the reorganization of sensory hand areas after mono-hemispheric lesion: a functional (MEG) / anatomical (MRI) integrative study. Brain Res 1998b;782:153–66.

Schaefer M, Mühlnickel W, Grüsser SM, Flor H. Reproducibility and stability of neuroelectric source imaging in primary somatosensory cortex. Brain Topogr 2002;14:179–89.

Schubert R, Ritter P, Wüstenberg T, Preuschhof C, Curio G, Sommer W, et al. Spatial attention related SEP amplitude modulations covary with BOLD signal in S1-a simultaneous EEG-fMRI study. Cereb Cortex 2008;18:2686–700.

Schulz R, Braass H, Liuzzi G, Gerloff C, Hummel FC, Hoerniss V, et al. White matter integrity of premotor – motor connections is associated with motor output in chronic stroke patients. Neuroimage 2015;7:82–6.

Shahbazi F, Ewald A, Nolte G. Self-Consistent MUSIC: An approach to the localization of true brain interactions from EEG/MEG data. Neuroimage 2015;112:299–309.

Sheorajpanday RVA, Nagels G, Weeren AJTM, van Putten MJAM, De Deyn PP. Quantitative EEG in ischemic stroke: Correlation with functional status after 6months. Clin Neurophysiol 2011;122:874–83.

Sheorajpanday RVA, Nagels G, Weeren AJTM, van Putten MJAM, de Deyn PP. Reproducibility and clinical relevance of quantitative EEG parameters in cerebral ischemia: A basic approach. Clin Neurophysiol 2009;120:845–55.

Singer OC, Sitzer M, du Mesnil de Rochemont R, Neumann-Haefelin T. Practical limitations of acute stroke MRI due to patient-related problems. Neurology 2004;62:1848–9.

Stinear C. Prediction of recovery of motor function after stroke. Lancet Neurol 2010;9:1228–32.

Stinear CM. Prediction of motor recovery after stroke: advances in biomarkers. Lancet Neurol 2017;16:826–36.

Stojanović B, Djurasić L. Brain Symmetry Index in Healthy and Stroke Patients for Assessment and Prognosis. Acta Chir Iugosl 2013;60:101–4.

Stolk-Hornsveld F, Crow JL, Hendriks EP, van Der Baan R, Harmeling-Van der Wel BC. The Erasmus MC modifications to the (revised) Nottingham Sensory Assessment: a reliable somatosensory assessment measure for patients with intracranial disorders. Clin Rehabil 2006;20:160–72.

Tecchio F, Oliviero A, Pasqualetti P, Lupoi D, Orlacchio A, Pizzella V, et al. Somatosensory evoked fields in acute stroke. 12th Int. Conf Biomagn., 2001, p. 443–6.

Tecchio F, Pasqualetti P, Zappasodi F, Tombini M, Lupoi D, Vernieri F, et al. Outcome prediction in acute monohemispheric stroke via magnetoencephalography. J Neurol 2007a;254:296–305.

Tecchio F, Zappasodi F, Tombini M, Caulo M, Vernieri F, Rossini PM. Interhemispheric asymmetry of primary hand representation and recovery after stroke : A MEG study. Neuroimage 2007b;36:1057–64.

Tecchio F, Zappasodi F, Tombini M, Oliviero A, Pasqualetti P, Vernieri F, et al. Brain plasticity in recovery from stroke: An MEG assessment. Neuroimage 2006;32:1326–34.

Theuvenet PJ, Dijk BW Van, Peters MJ, Ree JM Van, Lopes FL, Chen ACN. Cortical Characterization and Inter-Dipole Distance Between Unilateral Median Versus Ulnar Nerve Stimulation of Both Hands in MEG. Brain Topogr 2006;19:29–42.

Timmerhuis TPJ, Hageman G, Oosterloo SJ, Rozeboom AR. The prognostic value of cortical magnetic stimulation in acute middle cerebral artery infarction compared to other parameters. Clin Neurol Neurosurg 1996;98:231–6.

Tzvetanov P, Rousseff RT. Median SSEP changes in hemiplegic stroke : Long-term predictive values regarding ADL recovery. NeuroRehabilitation 2003;18:317–24.

Tzvetanov P, Rousseff RT, Atanassova P. Prognostic value of median and tibial somatosensory evoked potentials in acute stroke. Neurosci Lett 2005;380:99–104.

de Vos CC, van Maarseveen SM, Brouwers PJAM, van Putten MJAM. Continuous EEG Monitoring During Thrombolysis in Acute. J Clin Neurophysiol 2008;25:77–82.

Vrba J. Magnetoencephalography: The art of finding a needle in a haystack. Phys. C, vol. 368, 2002, p. 1–9.

Vrba J, Robinson SE. SQUID sensor array con gurations for magnetoencephalography applications. Supercond Sci Technol 2002;15:51–89.

Wang L, Arendt-Nielsen L, Chen ACN. Scalp field potentials of human pain: Spatial effects and temporal relation in finger stimulation. Brain Topogr 2004;17:85–98.

Ward NS. Restoring brain function after stroke — bridging the gap between animals and humans. Nat Rev Neurol 2017;13:244–55.

Ward NS. Does neuroimaging help to deliver better recovery of movement after stroke ? 2015;44:323–9.

Ward NS, Brown MM, Thompson AJ, Frackowiak RSJ. Longitudinal changes in cerebral response to proprioceptive input in individual patients after stroke: An fMRI study. Neurorehabil Neural Repair 2006;20:398–405.

Ward NS, Brown MM, Thompson AJ, Frackowiak RSJ. Neural correlates of motor recovery after stroke : a longitudinal fMRI study 2003.

Ward NS, Cohen LG. Mechanisms underlying recovery of motor function after stroke. Arch Neurol 2004;61:1844–8.

van Westen D, Fransson P, Olsrud J, Rosén B, Lundborg G, Larsson E-M. Fingersomatotopy in area 3b: an fMRI-study. BMC Neurosci 2004;5.

WHO World Health Organization. Geneva Switzerland. World Health Report 2003. 2003.

Wikström H, Huttunen J, Korvenoja A, Virtanen J, Salonen O, Aronen H, et al. Effects of interstimulus interval on somatosensory evoked magnetic fields (SEFs) a hypothesis concerning SEF generation at the primary sensorimotor. Electroencephalogr Clin Neurophysiol 1996;100:479–87.

Wikström H, Roine RO, Aronen HJ, Salonen O, Sinkkonen J, Ilmoniemi RJ, et al. Specific Changes in Somatosensory Evoked Magnetic Fields during Recovery from Sensorimotor Stroke. Ann Neurol 2000;47:353–60.

Wikström H, Roine RO, Salonen O, Lund B, Salli E, Ilmoniemi RJ, et al. Somatosensory evoked magnetic fields from the primary somatosensory cortex (SI) in acute stroke. Clin Neurophysiol 1999;110:916–23.

Winters C, Heymans MW, van Wegen EEH, Kwakkel G. How to design clinical rehabilitation trials for the upper paretic limb early post stroke? Trials 2016a;17:1–9.

Winters C, Kwakkel G, Nijland R, Wegen E Van. When Does Return of Voluntary Finger Extension Occur Post-Stroke ? A Prospective Cohort Study. PLoS One 2016b:1–12.

Winters C, van Wegen EEH, Daffertshofer A, Kwakkel G. Generalizability of the Maximum Proportional Recovery Rule to Visuospatial Neglect Early Poststroke. Neurorehabil Neural Repair 2016c.

Winters C, van Wegen EEH, Daffertshofer A, Kwakkel G. Generalizability of the Proportional Recovery Model for the Upper Extremity After an Ischemic Stroke. Neurorehabil Neural Repair 2015;29:614–22.

Winward CE, Halligan PW, Wade DT. Current practice and clinical relevance of somatosensory assessment after stroke. Clin Rehabil 1999;13:48–55.

Xiang J, Hoshiyama M, Koyama S, Kaneoke Y, Suzuki H, Watanabe S, et al. Somatosensory evoked magnetic fields following passive finger movement. Cogn Brain Res 1997;6:73–82.

Yao J, Dewald JPA. Evaluation of different cortical source localization methods using simulated and experimental EEG data. Neuroimage 2005;25:369–82.

Zappasodi F, Tombini M, Milazzo D, Rossini PM, Tecchio F. Delta dipole density and strength in acute monohemispheric stroke. Neurosci Lett 2007;416:310–4.

Zarahn E, Alon L, Ryan SL, Lazar RM, Vry M, Weiller C, et al. Prediction of Motor Recovery Using Initial Impairment and fMRI 48 h Poststroke. Cereb Cortex 2011;21:2712–21.

Summary

Somatosensory cortex plays an important role in motor planning and execution. After ischemic stroke, both afferent projections to sensory cortices (S1/2) and sensory projections to motor cortices are often affected. Changes in S1 are particularly interesting for our understanding of stroke recovery and rehabilitation strategies. The assessment of sensory impairment after stroke can certainly benefit from affordable and ambulant imaging modalities, like electroencephalography (EEG). Somatosensory evoked potentials (SEPs) recorded with EEG may be used to follow stroke patients longitudinally. In order to detect changes occurring in S1, precise measurements and with high spatial resolution are obligatory. In the present thesis, I first evaluated the capacity of SEPs for tracking longitudinal stroke recovery. Subsequently, I explored the potential benefits and pitfalls of EEG-based monitoring of stroke patients.

SEPs evoked by electrical stimulation of the upper limb and especially after median nerve stimulation is a method widely used in the literature when searching for predictors for post stroke recovery. It was unclear, however, if the EEG recordings after finger stimulation are reproducible within the same subject. I assessed different stimulation amplitudes and durations. Using a stimulation with maximum response, I tested the consistency and reproducibility of responses through bootstrapping as well as test-retest recordings in five healthy controls (**Chapter 2**). I further evaluated the possibility to discriminate activity of different fingers both at electrode and at source level. The lack of consistency and reproducibility suggested responses to finger stimulation to be unreliable, even for reasonably high signal-to-noise ratios (SNR) and large numbers of trials. After source reconstruction, the anatomically expected somatotopic arrangement of the fingers representation was only found in one of the subjects. Although I could identify distinct locations of activation of the different fingers, the optimized protocol did not allow for non-overlapping finger representations by current dipoles. These findings urged for reconsidering the notion of EEG's 'spatial resolution' and the

resulting limitations in disentangling sources in proximity (as those found within the S1 area of the somatosensory cortex).

Accuracy of source reconstruction depends on the spatial configuration of the neural sources underlying encephalographic signals, the temporal distance of the source activity, the level and structure of noise in the recordings, and – of course – on the employed inverse method. This plenitude of factors renders a definition of 'spatial resolution' of EEG a challenge. In **Chapter 3**, I addressed this by examining factors that may affect the separation of sources. In principle, a proper definition of spatial resolution requires a ground truth. Hence, I employed data from numerical simulations, in which two dipoles changed in time with waveforms resembling SEPs with peaks at moments: 20, 50 and 100 ms. Inter-dipole distances were varied and Gaussian white or realistic EEG noise was added to the simulated scalp recordings with distinct signal-to-noise ratios (SNRs). Prior to inverse modelling, pre-whitening was applied to both the simulated data and the leadfield. I explored three algorithms for source reconstruction: two-dipole fit, the sc-MUSIC, and the sc-eLORETA. Accuracy of source localization was assessed via the distance between the true, simulated point sources and the estimated ones. To quantify the resulting "spatial resolution" of EEG, we introduced the notion of separability, i.e. the separation of two dipolar sources with a certain inter-dipole distance. The results indicated separability of two sources in the presence of realistic noise with SNR up to 3 if they are 11 mm or further apart. In the presence of realistic noise, spatial pre-whitening appears a mandatory pre-processing step irrespective of the inverse method employed. Taken together the findings indicate that stroke-related changes within the S1 cortex can be identified.

To explore the use of SEP biomarkers for prediction of stroke recovery, 16 first ever stroke patients and 6 healthy controls were studied (**Chapter 4**). SEPs induced by electrical stimulation of the median nerve were recorded at three time points post stroke (T0, T1, T2) using high-density EEG. To facilitate participation, assessment was realized in a van at the patient's location. Using the proportional recovery model (based on Fugl-Meyer assessments), patients were considered either fitters or non-fitters and the two groups were correlated with normalized SEP parameters using machine learning (linear support vector machine, SVM).

Features based on amplitude and latency of the SEP recordings five weeks post stroke (T1) were associated with the identification of non-fitters. The resulting SVM had an accuracy of 86% tested through a leave-one-out procedure. When the SVM was fed with the SEP features of the healthy controls, they were all classified in the same category as the fitters. The data suggested that normalized SEP parameters recorded five weeks post stroke have predictive capacity for stroke recovery.

Electrical afferent stimulation of the fingers during EEG recording eliciting SEPs can be used for assessment of stroke patients. In the study summarized in **Chapter 5**, I applied this protocol to a group of chronic stroke patients and determined stimulus-related responses and their asymmetries (based on spectral power). I also extracted asymmetry values during resting state. All outcome variables were compared to that of age-matched healthy controls and correlated with clinical motor and sensory scales. While stimulus-locked responses appeared not optimal for characterizing chronic stroke, the delta power asymmetries turned out to correlate with the Fugl-Meyer scale.

EEG is an adequate tool to monitor stroke recovery when electrical stimulation of the median nerve is applied and a combination of SEP-derived parameters are used to define a prognostic model. On the other hand, stimulus-locked responses after electrical stimulation of the different fingers show low reproducibility, large overlap of the dipole representations and appeared not optimal for characterizing chronic stroke. In typical clinical settings, EEG can serve as an imaging modality to study changes in the somatosensory cortex (due to ischemic stroke) in distances of about 1 cm, provided that the signal-to-noise ratio is sufficiently high and proper pre-processing steps are being applied.

Samenvatting

De somatosensorische cortex speelt een belangrijke rol bij het plannen en uitvoeren van bewegingen. Na een beroerte zijn vaak zowel de afferente projecties op sensorische cortex (S1/2) als de sensorische projecties op de motorische cortex aangedaan. Met name veranderingen in S1 zijn interessant om het herstel na een beroerte, en de effecten van revalidatie, beter te begrijpen. Monitoring van sensorische veranderingen kan profiteren van betaalbare en ambulante beeldvormingsmodaliteiten, zoals elektro-encefalografie (EEG). Somatosensory evoked potentials (SEPs) gemeten met EEG maken het mogelijk om patiënten na een beroerte longitudinaal te volgen. Om veranderingen in S1 te detecteren, zijn nauwkeurige metingen met een hoge spatiële resolutie nodig. In dit proefschrift heb ik eerst de geschiktheid van SEPs voor het longitudinaal volgen van herstel na een beroerte onderzocht. Vervolgens onderzocht ik de potentiële voordelen en valkuilen van EEG-gebaseerde monitoring van patiënten na een beroerte.

SEPs geïnduceerd door elektrische stimulatie van de arm, en dan met name de nervus medianus, is een veelgebruikte methode in de zoektocht naar een prognostisch parameter voor het herstel na een beroerte. Echter, het was nog onduidelijk of EEG-opnamen na stimulatie van de vinger te reproduceren zijn bij een proefpersoon. Ik heb verschillende stimulatieamplitudes en -duren vergeleken. Met de maximale-respons stimulatie testte ik de consistentie en reproduceerbaarheid van SEPs in vijf gezonde proefpersonen (**Hoofdstuk 2**). Verder evalueerde ik de mogelijkheid om de activiteit van verschillende vingers in EEG te onderscheiden, zowel op elektrode- als op bronniveau. Het gebrek aan consistentie en reproduceerbaarheid suggereert dat vingerstimulatie onbetrouwbaar is, zelfs bij een redelijk hoge signaal-ruisverhoudingen (SNR) en grote aantallen herhalingen. Na bronreconstructie werd de anatomisch verwachte somatotopische representatie van de vingers slechts bij een enkele proefpersoon gevonden. Hoewel ik verschillende locaties van de vingers kon identificeren, was het met het geoptimaliseerde protocol niet mogelijk om de vingers te representeren

in niet-overlappende dipolen. Deze bevindingen drongen aan op een heroverweging van de ‘spatiële resolutie' van EEG en de resulterende beperkingen in het onderscheiden van nabij gelegen bronnen (zoals die gevonden in het S1-gebied van de somatosensorische cortex).

De nauwkeurigheid van bronreconstructie hangt af van de spatiële configuratie van de neurale bronnen die ten grondslag liggen aan het EEG, de temporele afstand van de bronactiviteit, het niveau en de structuur van ruis in het EEG, en - uiteraard - van de gebruikte inverse methode. Deze overvloed aan factoren maakt een definitie van de ‘spatiële resolutie' van EEG een uitdaging. In **Hoofdstuk 3** heb ik dit aangepakt door factoren te onderzoeken die van invloed zijn op het kunnen onderscheiden van bronnen. In principe vereist een definitie van spatiële resolutie kennis van de onderliggende waarheid. Daarom heb ik data gebruikt uit numerieke simulaties waarin twee dipolen in de tijd veranderden, met golfvormen die lijken op SEPs met pieken op 20 ms, 50 ms, en 100 ms. De afstand tussen de gesimuleerde dipolen werd gevarieerd en witte Gaussische ruis of realistische EEG-ruis met verschillende signaal-ruisverhoudingen (SNRs) werden toegevoegd aan het gesimuleerde EEG. Voorafgaand aan de inverse modellering werd *pre-whitening* toegepast op zowel de gesimuleerde data als op het *leadfield*. Ik onderzocht drie algoritmen voor de bronreconstructie: twee-dipoolfit, de sc-MUSIC en de sc-eLORETA. De nauwkeurigheid van de bronlocalisatie werd beoordeeld op basis van de afstand tussen de originele, gesimuleerde (punt)bronnen en de afstand tussen de geschatte bronnen. Om de resulterende "spatiële resolutie" van EEG te kwantificeren, introduceerden we het begrip onderscheidbaarheid, i.e. het kunnen onderscheiden van twee dipool-bronnen met een bepaalde inter-dipoolafstand. De resultaten suggereren dat, in de aanwezigheid van realistische ruis met een SNR tot 3, een onderscheidbaarheid van twee bronnen als ze 11 mm of verder uit elkaar liggen. In aanwezigheid van realistische ruis lijkt spatiële pre-whitening een noodzakelijke voorbewerkingsstap, ongeacht welke inverse methode werd gebruikt. Alles bij elkaar geven de bevindingen aan dat beroerte-gerelateerde veranderingen binnen de S1-cortex kunnen worden geïdentificeerd.

Om het gebruik van SEP biomarkers voor de voorspelling van het herstel na een beroerte te onderzoeken, werden 16 patiënten die voor het eerst een beroerte

hadden gehad en 6 gezonde proefpersonen onderzocht (**Hoofdstuk 4**). SEPs geïnduceerd door elektrische stimulatie van de nervus medianus werden gemeten met behulp van hoge-resolutie EEG op drie tijdstippen na de beroerte (T0, T1, T2). Om deelname te vergemakkelijken, werden de metingen uitgevoerd in een meetbus op locatie bij de patiënt. Met behulp van het proportionele herstelmodel (gebaseerd op de Fugl-Meyer-schaal) werden patiënten verdeeld in fitters en niet-fitters. Deze twee groepen werden gecorreleerd met de genormaliseerde SEP-parameters met behulp van machine learning (linear support vector machine, SVM). Kenmerken op basis van amplitude en latentie van de SEPs vijf weken na de beroerte (T1) werden geassocieerd met de identificatie van de niet-fitters. De resulterende SVM had een nauwkeurigheid van 86% getest via een leave-one-out procedure. Wanneer de SEP kenmerken van de gezonde proefpersonen werden ingevoerd in de SVM, classificeerde de SVM deze allemaal in dezelfde categorie als de fitters. De resultaten suggereren dat genormaliseerde SEP-parameters die vijf weken na een beroerte zijn gemeten voorspellende capaciteit hebben voor het herstel na een beroerte.

SEPs gemeten in EEG na elektrische afferente stimulatie van de vingers kunnen worden gebruikt voor de beoordeling van patiënten na een beroerte. In de studie die is beschreven in **Hoofdstuk 5**, heb ik dit protocol toegepast op een groep patiënten in de chronische fase na een beroerte en heb ik de stimulus-gerelateerde reacties (op basis van spectrale dichtheid) en hun asymmetrie bepaald. Ik heb ook asymmetrische kenmerken gemeten tijdens rust (‘resting state’). Alle uitkomstvariabelen werden gecorreleerd met klinische motorische en sensorische schalen en vergeleken met die van gezonde proefpersonen met dezelfde leeftijd. Hoewel stimulus-gerelateerde reacties niet optimaal leken om beroerte in de chronische fase te karakteriseren, bleek de asymmetrie van het vermogen in de delta-band te correleren met de Fugl-Meyer schaal.

EEG is een geschikt hulpmiddel om herstel na een beroerte te monitoren wanneer elektrische stimulatie van de nervus medianus wordt toegepast en een combinatie van SEP-afgeleide parameters wordt gebruikt om een prognostisch model te definiëren. Aan de andere kant hebben de activiteiten na elektrische stimulatie van de verschillende vingers een lage reproduceerbaarheid en een grote overlap van

de dipoolrepresentaties, en bleken daarom niet optimaal voor het karakteriseren van beroerte in de chronische fase. In typische klinische omgevingen kan EEG dienen als een beeldvormende modaliteit om veranderingen in de somatosensorische cortex (als gevolg van een beroerte) te bestuderen bij afstanden van ongeveer 1 cm, op voorwaarde dat de signaal-ruisverhouding voldoende hoog is en de juiste voorbewerkingsstappen worden toegepast.

About the Author

Konstantina (Nadia) Kalogianni was born in Thessaloniki, Greece, on the 15th of March 1986. In 2004, she started studying Informatics at Aristotle University of Thessaloniki. In 2008, she was honored with the ERASMUS scholarship which brought her to Claude Bernard University in Lyon, France. In March 2009, she completed her bachelor studies and in September 2009 she was admitted to the master program "Medical Informatics" an inter-departmental program of the Medical Faculty and the Electrical Engineering Faculty of Aristotle University of Thessaloniki. During her master studies, she took the direction "Biomedical Signal Processing" and in February 2011 she went to the Faculty of Life Sciences at the University of Copenhagen for her master thesis project on olfactory perception using encephalography. After an internship at the Health on the Net foundation in Geneva, Switzerland, she received her master degree in April 2012 with excellent degrees. She then continued her stay in Geneva and worked as a research assistant at the University of Geneva at the Multimodal Interaction group of the Computer Science Department. In December 2012, she moved to the Netherlands to pursue a PhD on extraction of stroke diagnosis markers from electroencephalographic data at Delft University of Technology. Since June 2017, she is working as a post-doc researcher at the Brain and Spine Institute in Paris. Her research focuses on revealing brain-body interactions underlying consciousness.

List of publications

Journal Publications

Konstantina Kalogianni, Mique Saes, Martijn P. Vlaar, Erwin van Wegen, Gert Kwakkel, Alfred C. Schouten, Frans C.T. van der Helm, Andreas Daffertshofer, Jan C. de Munck, on behalf of the 4D-EEG consortium, *Are longitudinal SEP recordings a biomarker for proportional motor recovery post stroke?* Submitted

Konstantina Kalogianni, Andreas Daffertshofer, Frans C.T. van der Helm, Alfred C. Schouten, Jan C. de Munck, on behalf of the 4DEEG consortium. *Disentangling somatosensory evoked potentials of the fingers: limitations and clinical potential*, Brain Topography 2018;31(3):498-512.

Konstantina Kalogianni, Jan C. de Munck, Guido Nolte, Alistair N. Vardy, Frans C.T. van der Helm, Andreas Daffertshofer*, Spatial resolution for EEG source reconstruction—A simulation study on SEPs,* Journal of Neuroscience Methods 2018;301:9-17.

Juhani Dabek, **Konstantina Kalogianni**, Edwin Rotgans, Frans C.T. van der Helm, Gert Kwakkel, Erwin E.H. van Wegen, Andreas Daffertshofer, Jan C. de Munck. *Determination of head conductivity frequency response in vivo with optimized EIT-EEG*, NeuroImage 2016;127:484-495.

Alkinoos Athanasiou, Chrysa Lithari, **Konstantina Kalogianni**, Manousos A. Klados, Panagiotis D. Bamidis, *Source Detection and Functional Connectivity of the Sensorimotor Cortex during Actual and Imaginary Limb Movement: A Preliminary Study on the Implementation of eConnectome in Motor Imagery Protocols*, Advances in Human-Computer Interaction, 2012.

Natalia Pletneva, Alejandro Vargas, **Konstantina Kalogianni**, Célia Boyer, *Online health information search: What struggles and empowers the users? Results of an online survey,* Studies in health technology and informatics, 2012.

Acknowledgements

What an adventure has been! Five years after my arrival in the Netherlands, I successfully finished this thesis. During this journey, I have learnt a lot, I failed and I succeeded but I always kept my passion for research.

First, I would like to thank Frans and Alfred who gave me the opportunity to work on this exciting project. Thank you for believing in me and challenging me along the way to keep on trying harder and find my scientific self. Thank you, Frans for asking me questions I couldn't easily answer and for pushing me harder to find scientific arguments to convince you. Thanks Alfred for being there whenever I needed you either for scientific advice or moral support.

Next, I would like to thank Andreas and Jan. Our joined meetings, in Amsterdam, at the end of my project have helped me enormously, inspired me and kept me going through times of demotivation and lack of inspiration. I would like to thank Andreas for his help in all chapters of the present thesis and especially for making chapter 3 possible. Thank you, Andreas, for always being patient with me and my writing skills, thank you for inspiring me, making me work harder and always giving me practical advice. Thanks a lot Jan for devoting a lot of time for me every Tuesday. I will never forget our endless discussions on somatosensory evoked potentials and EEG processing. You have helped me in every step of this thesis not only scientifically but also morally. Without your good words and your patience this project wouldn't be successful.

I would like to thank the rest of the 4D-EEG PhD, post-doc family. First, Martijn, thanks for always being one door away (mentally and physically) and being available to discuss with me all my scientific thoughts and doubts about my thesis or EEG processing in general. I hope our discussions were of help for you too. Next, I would like to thank Teodoro, Lena Yuan, Mark and my colleagues from Amsterdam, Mique, Sarah, Aukje, Caroline. I feel grateful that I had such nice co-PhD students, post-docs that shared with me all scientific challenges of this project.

Dear fellow BME PhD students: Annetje, Eline, Bram, Frederique, Ingrid, Peter, Awaz, Jeroen, Paul, Ewout, Tricia without our parties and gatherings during the weekends the PhD life would have been unbearable! Thank you for listening to all my problems and trying to help along the way even though my thesis was not a typical BME project and our topics were completely different. Special thanks to my two paranymps: Teun and Marta. There are no words to describe how grateful I am to you two especially at the end of my thesis. You were always there to listen to me, help me and more importantly drink a beer with me when absolutely necessary.

My friends for life and forever: Peny, Maria, Nata, Io, Vivian (the order is random, you have equal position in my heart). Being far away from each other and yet so close. You were my support and also my inspiration through my PhD life and not only. Thank you for reminding me every day how grateful I am to have you as friends.

A special thanks to Peny for listening all my monologues about my struggles and frustrations during my PhD thesis, even though you were far away and you couldn't really understand the topic of my thesis. Your patience and kindness have always inspired me.

I am very lucky to had you, Maria, there in The Hague only a bike ride away! Thank you for all those Monday nights at the Paap, all those weekends we spent together and thank you for trying to always be there all along my PhD journey and for believing in me.

I also would like to thank Marina who has the natural gift of listening to people and giving them (and me) endless support.

Jill, became my friend during the last bits of my PhD thesis. Thank you, Jill, for understanding my struggles and for being my running buddy in Malieveld.

I would like to thank my parents, Prokopis and Maria, who have supported me throughout my life. Thank you for always being there, for believing in all the qualities in me, for loving me and for teaching me that I can do everything with hard work and patience. A special thank you for all your moral support throughout this PhD journey. I couldn't have asked for better parents.

A big thanks to my sister, Eleni. Your scientific career and your strong and loving character has always been an inspiration for me. Thank you for being a phone call away and always trying to understand me.
Also, I would like to thank my extended family, my aunt Danai and my cousins Fenia and Sotiris for always believing in me.
Last but not least I would like to thank Anikitos who appeared in my life the last 3 years of my thesis. Even though you lived in Paris you provided endless support for me. I am extremely grateful for your practical and moral support, for always listening to me, believing in me and reminding me that I am a good scientist. Without your unrestrained love, I would not have been able to finish this project. Thank you for loving the real me, the one that gets frustrated and demotivated easily but also gets excited and tries very hard to reach her goal.